(NASA-CR-158837) BASIC RESEARCH RELEVANT TO CW-NUCLEAR PUMPED LASERS Final Report (Florida Univ.) 135 p HC A07/MF A01
CSCL 20E
N79-28533
Unclas
G3/36 29381

Basic Research Relevant to CW-Nuclear Pumped Lasers

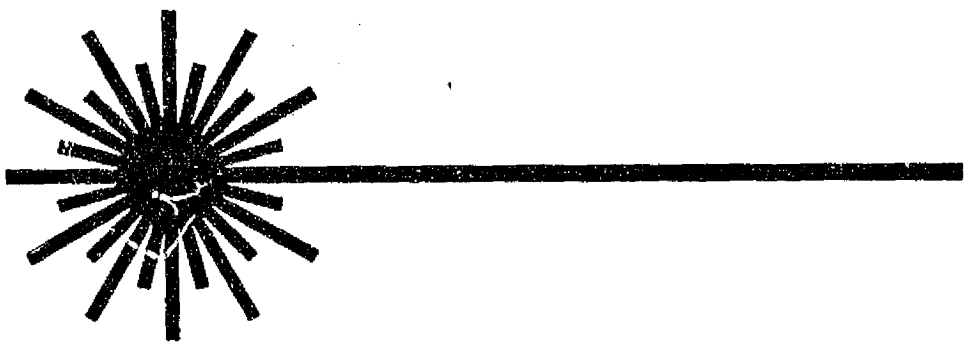

FINAL REPORT

Grant Nos. NGL 10-005-089 and NSG 7299
For

National Aeronautical and Space Administration

By

Dr. Richard T. Schneider
Department of Nuclear Engineering Sciences
University of Florida
Gainesville, Florida

June, 1979

BASIC RESEARCH RELEVANT

TO

CW-NUCLEAR PUMPED LASERS

Final Report

Grant Nos. NGL 10-005-089 and NSG 7299

for

National Aeronautical and Space Administration

by

Dr. Richard T. Schneider
Department of Nuclear Engineering Sciences
University of Florida
Gainesville, Florida

June, 1979

ACKNOWLEDGMENTS

The authors of this report and the numerous students supported under the two NASA grants would like to express their gratitude to the National Aeronautics and Space Administration for giving them the opportunities to work in this exciting field and gain this very valuable educational experience. Especially, we would like to express our thanks to Carl Schwenk, Karlheinz Thom and Frank Hohl for their patience in giving advice and contributing to the research effort.

The people supported in the form of salaries or equipment were: G. Albrecht, J. Balaguero, D. Baker, R. Borland, D. Carter, J. Cox, R. Davie, J. Davis, J. Fuller, T. Griffin, R. Hansen, E. Holtzclaw, R. Lee, D. Luker, J. Mack, J. Malloy, B. Miller, R. Paternoster, R. Randol, H. Rhoads, M. Rowe, T. Roxey, R. Schneider, B. Schnitzler, C. Seeger, G. Shipman, C. Skottegard, F. Southworth, J. Spector, D. Sterritt, G. Trummer, J. Usher, R. Walters and C. Winship.

TABLE OF CONTENTS

	Page
ACKNOWLEDGMENTS	ii
LIST OF TABLES	v
LIST OF FIGURES	vi
PREFACE	ix
I. NUCLEAR PUMPING OF LASERS AND THE GASEOUS CORE REACTOR	1
A. The Concept	1
B. Physics of Nuclear Pumping	2
C. Gaseous Core Reactors	3
D. Problems Connected with the Laser-Reactor Concept	3
II. HIGHLIGHTS OF RESULTS GENERATED UNDER NASA GRANTS NGL 10-005-089 and NSG 7299	5
A. Definition of Objectives	5
B. Optical Properties of Uranium Plasmas	7
C. Thermodynamic Properties of UF_6	9
D. Nuclear Enhancement of CO_2 Lasers	16
E. Mechanism of Excitation of Gases by Fission Fragments	20
F. Direct Nuclear Pumped Laser	22
G. Application of Gaseous Core Reactors for Transmutation of Nuclear Waste	30
H. Boiling Point of Uranium	41
III. UNPUBLISHED MATERIAL	46
A. Survey	46
B. Electronic State Populations of (n,p) Excited He^3	47
1. Purpose of Experiments	47
2. Experimental System	47
3. Experimental Results	53
a. Relative Line Intensities	53
b. Electron Temperatures	53
c. Non-Equilibrium Effects	63

		Page
C.	Lifetime System	63
	1. Purpose of Experiments	63
	2. Experimental Device	66
	3. Experimental Procedure	68
	4. Experimental Results	69
	a. Pure Gas Studies	69
	(1) Nitrogen	69
	(2) Neon/Nitrogen Mixtures	69
	(3) Helium/Nitrogen Mixtures	83
	(4) Argon/Nitrogen	86
	(5) Carbon Tetrafluoride	86
	b. UF_6 Additive Studies (Low Concentrations)	88
	(1) Nitrogen	88
	(2) Argon	88
	(3) Xenon	92
	Summary of UF_6 Admixture Results	92
	c. UF_6 Additive Studies (High Concentrations)	96
	(1) Nitrogen	97
	(2) Argon	97
D.	UF_6-CO_2 Laser-Reactor Studies	97
E.	Nuclear Pumped CW-Laser	101a
	1. Introduction	101a
	2. Gain Measurements	104
	a. Medium Flux Reactor Gain Measurements	104
	b. Low Flux Reactor Gain Measurements	107
	3. Laser Experiment	112
	4. Checks for Lasing	112
IV.	SURVEY OF ACCOMPLISHMENTS	117
A.	Ph.D Degrees Generated Under Both Grants	117
B.	Masters Degrees Generated Under Both Grants	117
C.	High Honors Projects	118
D.	Publications Generated Under Both Grants	119
	1. Book Edited	119
	2. Periodicals	119
	3. Invited Papers	121
	4. International Conferences	122
	5. National Meetings	123
REFERENCES		126

LIST OF TABLES

	Page
TABLE I: TRANSMUTATION FIGURE SYMBOL KEY	35
TABLE II: URANIUM ARC VOLTAGE -- CURRENT MODEL	45
TABLE III: CRITICALITY CALCULATIONS FOR UF_6/CO_2 LASER-REACTOR	101b

LIST OF FIGURES

		Page
Fig. 1.	Uranium Plasma Composition at Pressure of 500 Atmospheres	6
Fig. 2.	Uranium Arc Device	8
Fig. 3.	Radiation from Non-Fissioning Uranium Plasmas Normalized to 8000K	10
Fig. 4.	Schematic diagram of Ballistic Piston Compressor and Schematic Diagram of the Piston and Cup Seals	12
Fig. 5.	Measured Values of the Specific Heat Ratio of UF_6 as a Function of Temperature	15
Fig. 6.	I-V Characteristic of Laser with and without Neutron Irradiation	18
Fig. 7.	Laser Power Enhancement with Neutron Irradiation	19
Fig. 8.	Excitation Ratio versus Pressure	24
Fig. 9.	Basic Configuration for Nuclear Pumped Lasers	24
Fig. 10.	Oscilloscope Traces of Neutron Flux and Laser Output	28
Fig. 11.	Laser Output vs. Energy Input	29
Fig. 12.	Typical Fission Product Decay Chains	33
Fig. 13.	Iodine-129 Transmutation Reaction Paths	33
Fig. 14.	Iodine-129 Transmutation versus Irradiation Time	37
Fig. 15.	Americium Transmutation versus Irradiation Time	37
Fig. 16.	Americium-243 Transmutation versus Irradiation Time	37
Fig. 17.	Curium Transmutation versus Irradiation Time	38
Fig. 18.	Higher Actinide Build-up versus Irradiation Time	38
Fig. 19.	Relative Ingestion Hazard (RIGH) of Americium and Curium Wastes	40
Fig. 20.	High Pressure Uranium Plasma Device	44
Fig. 21.	High Pressure Uranium Arc Voltage-current Characteristics	44
Fig. 22.	Total System Pressure versus Apparent Anode Boiling Temperature. Broken Curves are Extrapolated from Empirical Data	44
Fig. 23.	Overall Layout for MCFIG Gas Irradiation Studies	48
Fig. 24.	All Welded MCFIG	50
Fig. 25.	Optical System	51
Fig. 26.	Electronic System	52
Fig. 27.	(n,p) Excited ^3He - Observed Lines	54

		Page
Fig. 28a.	Pressure Dependence of (n,p) Excited ^{3}He Line Intensities	55
Fig. 28b.	Pressure Dependence of (n,p) Excited ^{3}He Line Intensities	56
Fig. 29.	Comparison of Relative Spectral Line Intensities for F.F. and (n,p) Excited He	57
Fig. 30.	Method of Boltzmann Plots	58
Fig. 31.	Boltzman Plot - Species-Helium I Pressure-100 torr	59
Fig. 32.	Boltzman Plot - Species-Helium I Pressure-200 torr	60
Fig. 33.	Boltzman Plot - Species-Helium I Pressure-400 torr	61
Fig. 34.	Boltzman Plot - Species-Helium I Pressure-760 torr	
Fig. 35.	Relative Population of Upper and Lower States Giving Rise to the 18.62 m Transition	64
Fig. 36.	Radiation Induced Population Inversions In Helium	65
Fig. 37.	System for Lifetime Measurement	67
Fig. 38.	Decay Curves for Nitrogen $C^3\pi_u$ State	70
Fig. 39.	Inverse Decay Time vs. Pressure for 337.1 nm (Pure N_2)	71
Fig. 40.	Decay Time vs. Pressure for 585.2 nm (Pure Ne)	73
Fig. 41.	Decay Time vs. Pressure for 585.2 nm (Ne/N_2,100/1)	74
Fig. 42.	Decay Time vs. Pressure for 585.2 nm (Ne/N_2,10/1)	75
Fig. 43.	Decay Time vs. Pressure for 585.2 nm (Ne/N_2,1/1)	76
Fig. 44.	Decay Time vs. Pressure for 337.1 nm (Ne/N_2,100/1)	77
Fig. 45.	Decay Time vs. Pressure for 337.1 nm (Ne/N_2,10/1)	78
Fig. 46.	Decay Time vs. Pressure for 337.1 nm (Ne/N_2,1/10)	79
Fig. 47.	Decay Time vs. Pressure for 337.1 nm (Ne/N_2,1/100)	80
Fig. 48.	Decay Time vs. Pressure for 391.4 nm (Ne/N_2,10/1)	81
Fig. 49.	Decay Time vs. Pressure for 391.4 nm (Ne/N_2,1/1)	82
Fig. 50a.	Relative Intensity vs. Pressure for 391.4 nm (He/N_2)	84
50b.	Metastable Transfer in He/N_2	84a
Fig. 51.	Decay Time vs. Pressure for 391.4 nm (He/N_2)	85
Fig. 52.	Fast and Slow Decay in Ar/N_2 (10/1)	87
Fig. 53.	N_2 Impurity in CF_4	89
Fig. 54.	Results for 337.1 nm N_2 Line (N_2+UF_6)	90
Fig. 55.	Results for 810.3 nm ArI Line (Ar+UF_6)	91
Fig. 56.	Results for 828.0 nm XeI Line (Xe+UF_6)	93
Fig. 57.	Results for 337.1 nm N_2 Line	95
Fig. 58.	Effect of UF_6 Additive on N_2 Excited State Lifetime (337.1 nm)	98
Fig. 59.	Effect of UF_6 Additive on ArI Excited State Lifetime (810.3 nm)	99

		Page
Fig. 60.	Laser Output vs. UF_6 Concentration	102
Fig. 61.	Gas-Core Reactor Pressure vs. Concentration of Laser Gas	103
Fig. 62.	Experimental Arrangement	105
Fig. 63.	Results of Gain Measurements	106
Fig. 64.	Horizontal Throughport at UFTR	108
Fig. 65.	Results of Measurements at UFTR	111
Fig. 66.	Determination of Small Signal Gain	113
Fig. 67.	Laser Experiment	114
Fig. 68.	Laser Output versus Reactor Power	115

PREFACE

The two grants, NGL10-005-089 and NSG 7299 were so closely related in the subject matter that it seemed advantageous for the sake of clarity and coherence to write a combined final report.

Most of the material generated under these grants was published previously and, therefore, a list of the publications generated is included in this report.

However, there is yet some unpublished material which is reported here.

Also, for the convenience of a reader unfamiliar with the field of gaseous core reactors and nuclear pumped lasers, a short introduction into the field and a short review of the highlights of the material covered by the two grants is given.

I. NUCLEAR PUMPING OF LASERS AND THE GASEOUS CORE REACTOR

A. The Concept

During the fission process, about 200 MeV per reaction is released. Most of this energy appears as kinetic energy of the fission fragments. In a nuclear reactor using solid or liquid fuel, this energy is converted to heat and extracted from the core by conventional heat transfer means. This heat is consequently converted into useful energy (electricity) in a steam cycle.

Considering that the individual fission fragment may have an energy of 50 MeV and more while the steam ends up having only a few hundredths of an eV, which is consequently used to produce electricity having a few hundred kilovolts, one can certainly say that there is room for improvement.

The new concept consists of the idea to use the kinetic energy of the fission fragments directly to excite gas atoms into optical radiation, preferably light. This means a direct conversion of nuclear energy into light. In order to make this possible, the fission fragment must be given the opportunity to interact with the gas atoms, which requires that either the fission fragments are born in the gas (which calls for a gaseous fuel reactor) or the fission fragment comes out of the solid fuel, (which can only be achieved with thin coatings). Considering that the maximum coating thickness can only be 7 μm, it is more reasonable to expect to realize a gaseous core reactor, with the gas to be excited mixed right into the gaseous fuel. The only practical gaseous form of uranium seems to be UF_6. This calls now for a reactor where all the fuel (one critical mass) is in the form of UF_6 and a gas added for fluorescence.

There is also one further consideration. If this fluorescence can be made to lase, a nuclear pumped laser could be built. The cavity of the laser would then act as an energy trap. The reason is that the energy passing through the two states for which the cavity is tuned will be coupled out in the form of stimulated radiation, an output which would not have taken place in this magnitude, if stimulation would not have taken place.

B. Physics of Nuclear Pumping

Fission fragments are heavy ions possessing a large charge (up to 22). If injected into a gas, they will undergo collision with the gas atoms. Due to the mismatch in energy, only about 50 eV are exchanged at each collision. This energy is typically used to ionize the atom and provide the electron liberated with some kinetic energy. These electrons are, consequently, slowed down by collisions with the gas atoms--exciting or ionizing these atoms--until their kinetic energy is too low to provide for more excitation. The electrons are now subexcitation electrons and form a relatively cold electron gas. The majority of the electrons in a fission fragment excited gas are these subexcitation electrons and only a small fraction of the steady state electron population are electrons being currently slowed down. However, this small fraction carries the majority of the energy being transported.

While it is straight forward to see how--as described above--the fission energy is transferred into potential energy in the form of excitation or ionization, it is more difficult to see how any population inversion can take place.

Most nuclear pumped lasers demonstrated to date are recombination lasers. Depending on the gas, the inversion is created by dissociative recombination or 3-body recombination. So far, there are only a few

cases (CO, He-Ne) where this might not be the case. However, definitely more work is needed to explore other mechanisms for population inversion. Of special interest is the formation of excimers (XeF, Xe_2). Work on this subject is carried out at present at various laboratories.

C. Gaseous Core Reactors

Previous concepts of gaseous core reactors envisioned the nuclear fuel in the plasma state at temperatures up to 40,000°K. Some of the work under both grants was related to this concept. One reason for the high temperature was the desire to accomplish heat extraction out of the reactor core by radiative transfer.

Of course with a laser concept for energy extraction, the high temperature is no longer required, since there is no relation between temperature and population inversion. If anything, a high temperature is counterproductive to population inversion. Therefore, the gaseous core reactor envisioned for the laser-reactor concept will operate at low temperatures--as low as feasible. Excitation and ionization is not done thermally, but by collisions with nonrandomized electrons--nonequilibrium excitation and ionization.

Therefore, in order to have the nuclear fuel in the gaseous state, UF_6 has to be used. The radius of such a gaseous core reactor may be rather substantial (~2 meters); the critical mass will be around 20 Kg. Since this reactor can be continuously refueled, there is only one critical mass required. The UF_6 pressure, depending on the actual operation temperature will be between 1 and 4 atmospheres. Moderation has to be done externally by a moderator-reflector.

D. Problems Connected with the Laser-Reactor Concept

Obviously, the intent is to convert an appreciable fraction of the fission energy into laser light, otherwise a nuclear reactor system

cannot be justified in the proposed configuration. If a low power laser were desired to be operated "piggyback" on a regular reactor system, it would be probably less trouble to use the electricity which the conventional reactor is generating to power the laser.

Therefore, obviously any direct nuclear pumped laser has to be a high power laser in order to be viable.

This limits the choice of candidate laser gases drastically. There is, of course, always the possibility that certain gases will lase by nuclear excitation only and will be capable of high power.

Another problem is the required compatibility with UF_6. Since it is necessary to mix the laser gas with UF_6, it is possible that the UF_6 will destroy the population inversion by deexcitation by collision (quenching).

The quenching certainly is a serious problem, however, there are indications that certain gases are not affected. In conclusion, one can state, that it is, in principle, certainly possible to build a laser-reactor, however, what cannot be predicted yet is what the efficiency of conversion of nuclear energy into laser light will be. The possible benefits of having such a laser-reactor system are however substantial, so that further research in the area is certainly justifiable.

II. HIGHLIGHTS OF RESULTS GENERATED UNDER NASA GRANTS NGL 10-005-089 AND NSG 7299

A. Definition of Objectives

The objectives of the initial Grant (NGL 10-005-089) was to measure the optical properties of a uranium plasma. This was required in order to design the high temperature plasma core reactor and determine its operation conditions.

The optical constants would determine the expected radiative transfer, and this, in turn, would determine the operation temperature.

Once the operation temperature was established, the composition of the plasma could be determined. Since uranium has a very low ionization energy (~6eV) the plasma will be fully ionized at a reasonably low temperature. A computer model was developed to compute the constituents of a uranium plasma. Fig. 1 shows a typical result for 500 atm, which would be about the operation pressure of a plasma core reactor with 40,000°K core temperature. As can be seen from Fig. 1, the major species would be U^{3+} at 40,000°K. The partial pressure of U^{3+} would be less than 10% of the total pressure, the major contributor to the total pressure, being the electron pressure. Since only the uranium partial pressure enters in the criticality calculations, the knowledge of the exact composition of the uranium plasma is vital.

The temperature distribution across the reactor core would have the shape of a Bessel function, or a parabola with the center of the core being at 40,000°K and the edge around 8000°K. One important question would be how transparent this core is for optical radiation.

In 1971, a change in direction of the research took place. The plasma core reactor (high temperature) was deemphasized and the gaseous

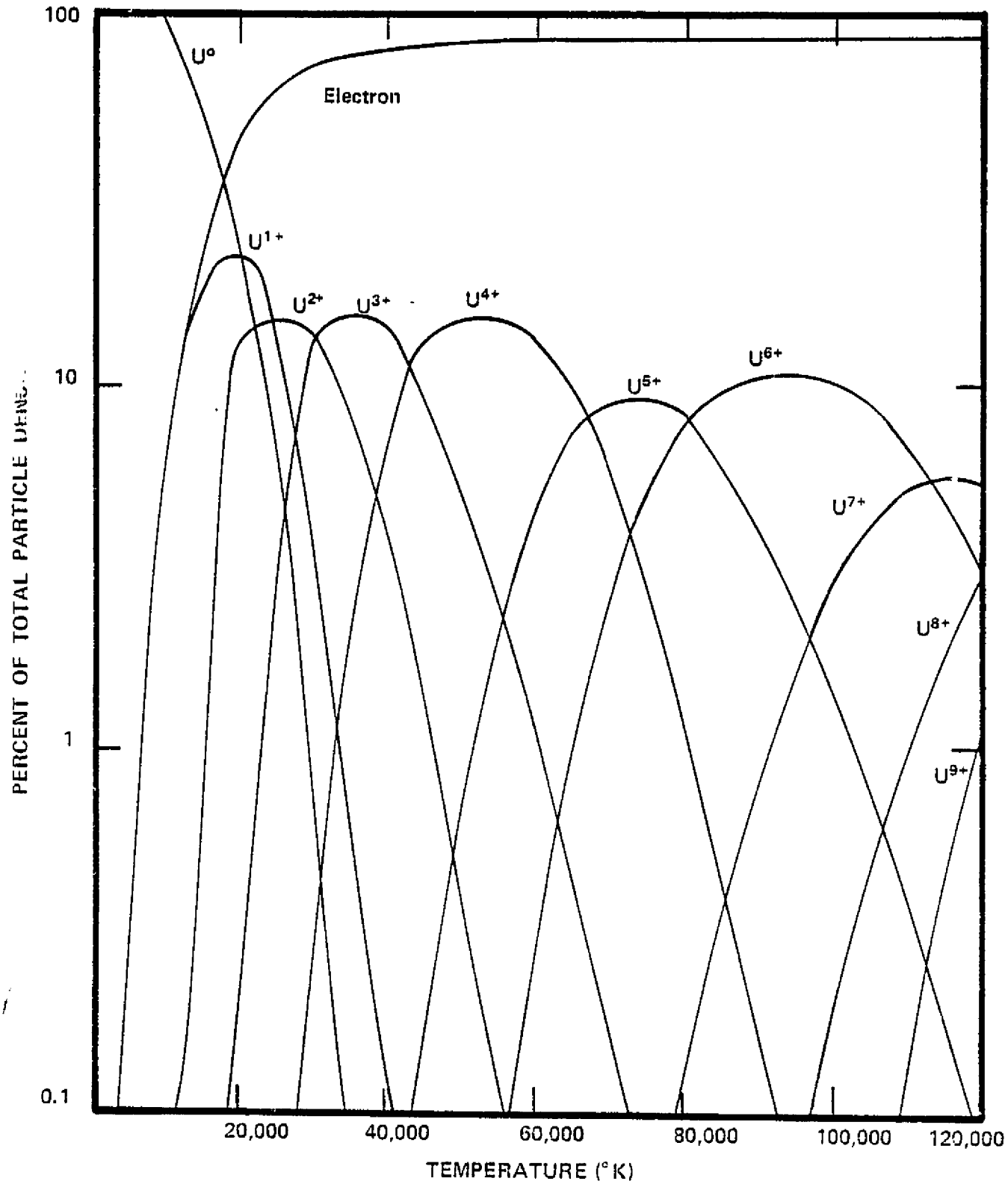

Fig. 1. URANIUM PLASMA COMPOSITION AT PRESSURE OF 500 ATMOSPHERES

core (low temperature) reactor was emphasized instead. Again, it was the objective to study the material properties under the grants. The thermodynamic properties were studied first; optical and chemical properties are still under investigation.

Another change in emphasis, which grew out of the UF_6 work was towards research of the nuclear pumped laser. The first effort resulted in results leading to nuclear enhancement of an electrical discharge CO_2 laser. Later on, feasibility of direct nuclear pumping was demonstrated for a He-Xe infrared laser. Naturally this shifted the emphasis away from UF_6 material properties toward research into the excitation mechanism of gases bombarded by fission fragments, which is still the major concern of the University of Florida research group in direct nuclear pumped lasers.

B. Optical Properties of Uranium Plasmas

Since the edge temperature of the plasma core reactor was expected to be around 8000°K, the plasma properties at this temperature were of most interest.

In order to determine the optical properties of such a plasma experimentally, a small model of a plasma core was developed, constructed and operated. It consisted of a uranium arc operating at 1 atm pressure and higher. See Figure 2. The anode consisted of a tungsten crucible filled with uranium metal. When operating the arc, the uranium metal melts and forms a liquid anode. Since uranium has a low ionization energy, it is, in this configuration, the only source for ions, no other material takes part in the electrical conduction phenomena in the arc. Spectroscopic analysis shows that a clean uranium plasma is obtained in the interelectrode space.

Insulator Order

(Inside-out)

1. Boron Nitride
2. O-ring
3. Phenollic (G-10)
4. Collant
5. Phenollic
6. O-ring
7. Phenollic

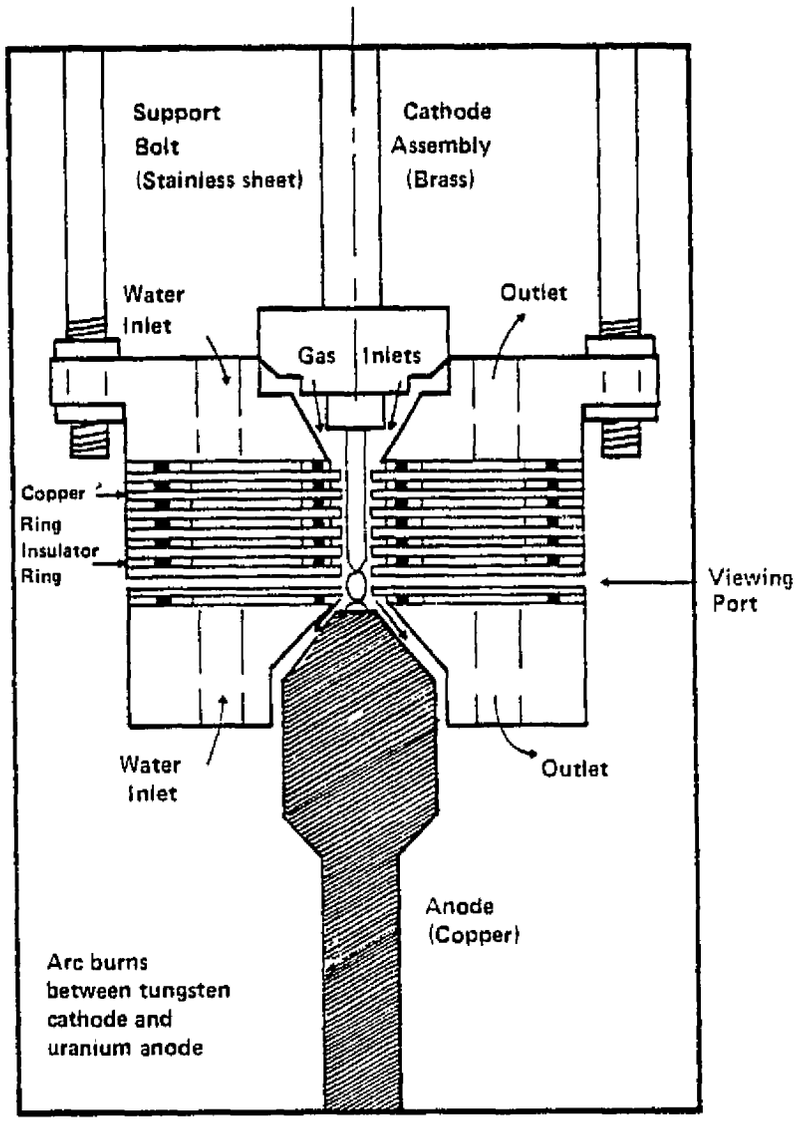

Fig. 2 URANIUM ARC DEVICE

The temperature of this uranium plasma was measured by spectroscopic techniques and a plot temperature vs. core radius was obtained and subsequently modeled using standard heat transfer theory. The main result, however, was the measurement of the emission coefficient of an 8000°K uranium plasma.

Figure 3 shows these results and as they compare to theory and other measurements. As can be seen, our measurements compare quite well with theory. The two peaks predicted by theory were actually found. Fig. 3 also contains for comparison an 8000°K Planck function. The way the graph is constructed insures that the numerical value of Planck function and emission coefficient are identical for the case of a geometrical depth of 1 cm for the plasma under consideration. The diameter of the arc was about that and, therefore, Fig. 3 gives an indication of the absorption coefficient and an indication at which part of the spectrum the plasma is close to being optically thick.

C. Thermodynamic Properties of UF_6

Experiments with a ballistic piston compressor were made to investigate certain thermodynamic properties of gaseous UF_6. Measured gas pressures, volumes, and temperatures were analyzed with a computer program employing a numerical optimization scheme to arrive at the desired properties. The thermodynamic properties deduced include the UF_6 constant volume specific heat, specific heat ratio, and the viscous coupling constant for UF_6/He mixtures at temperatures up to 1500°K.

Determination of basic data of this type for UF_6 is necessary for the successful design of advanced concepts such as the nuclear piston engine which employs gaseous UF_6 as the energy source. In addition to their usefulness in determining the thermodynamic properties of UF_6 and other gases

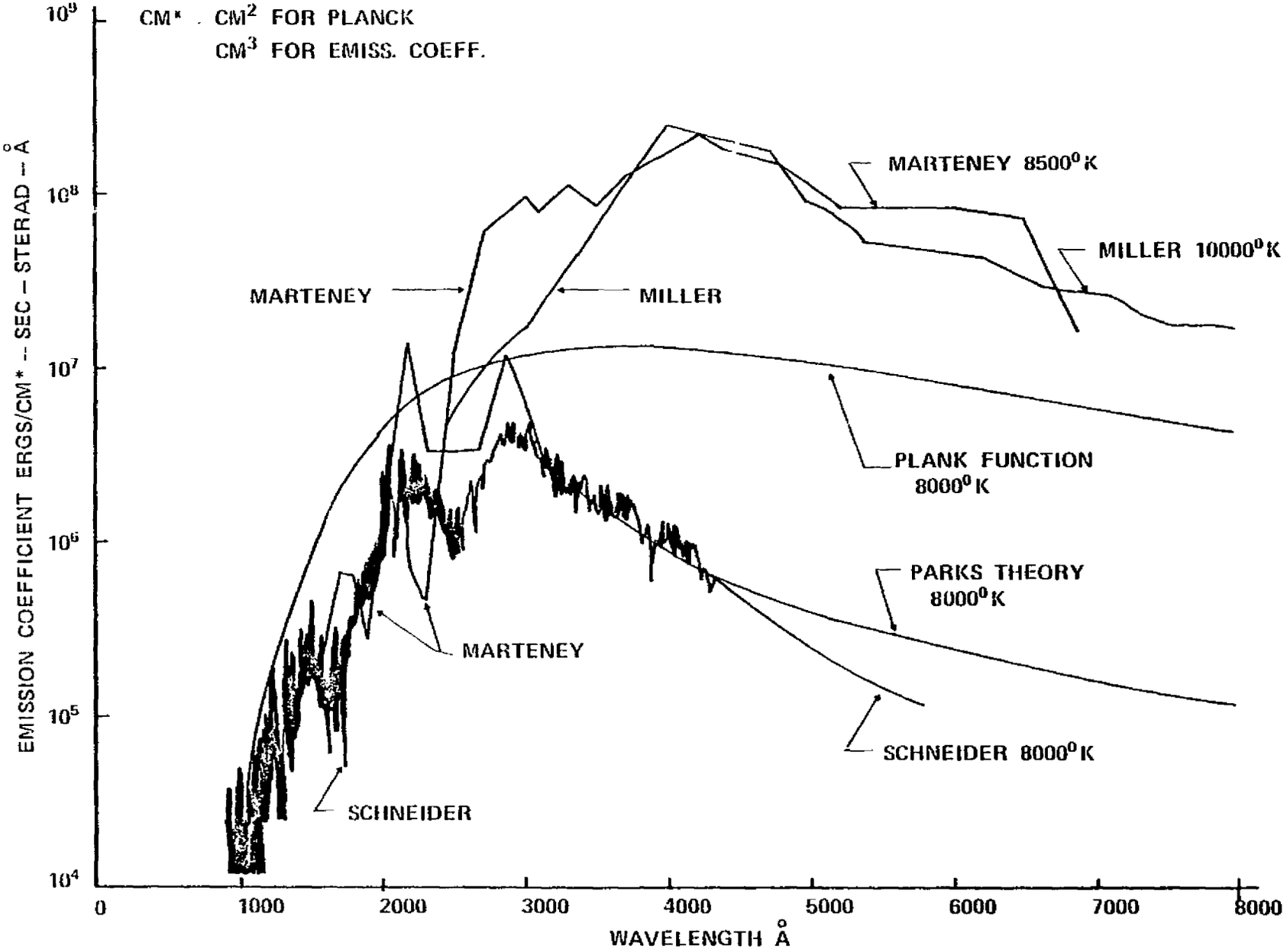

Fig. 3 RADIATION FROM NON-FISSIONING URANIUM PLASMAS NORMALIZED TO 8000 K

at high pressures and temperatures, ballistic compressors can provide information required in other fields of technology. The ballistic compressor simulates the rapid compression and expansion of a UF_6/He mixture in a nuclear piston engine and can provide much of the basic information such as size, moderator thickness, gas mixture ratios, and compression rate required for the design of a prototype critical-mass device.

The ballistic compressor shown schematically in Fig. 4 consists of four main parts: the reservoir, the piston release section, the tube, and the high pressure section.

The reservoir was designed for a maximum operating pressure of 136 atm and was statically tested to 200 atm. The reservoir is sufficiently large that the driver gas pressure remains essentially constant during the entire piston stroke. The tube is 3.89m long and has a 5-cm bore. The 5-cm bore high pressure section is 17.78 cm long, has a wall thickness of 2.57 cm, and contains diametrically opposite windows for absorption and emission measurements. The high pressure section is designed for pressures up to 5000 atm. Since the high temperatures generated in the high pressure section cause a slight vaporization of the inner walls, resulting in emission from impurities, the inner bore is plated with chromium. To minimize gas leakage around the piston, two cup seals are employed. The gases before and behind the piston expand these seals against the bore thus minimizing gas leakage past the piston. The steel piston body contains two phosphor bronze bearings that provide the surface upon which the piston moves and a molybdenum piston head to prevent ablation by the hot gas. The radial clearance between the bearing surface and the tube bore is 50 μm.

In operation the chamber behind the plunger of the piston release section is pressurized so that the plunger moves to the forward (left) position and seals the reservoir from the tube. The tube is then filled

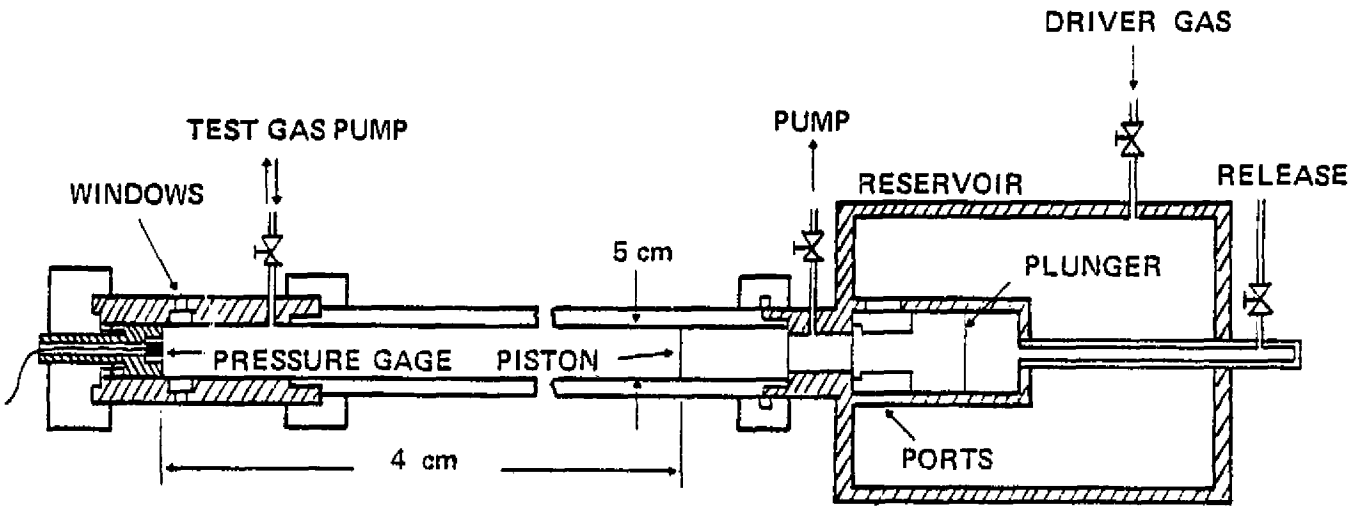

Schematic diagram of ballistic piston compressor.

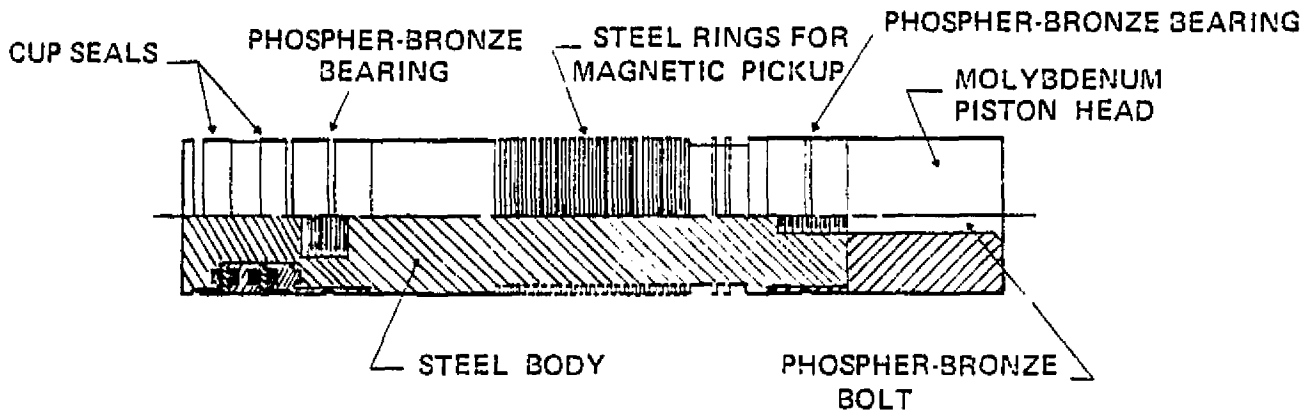

Schematic diagram of the piston and cup seals.

FIGURE 4

with the test gas or gas mixture, and its pressure and temperature are adjusted. Next, the reservoir is filled with driver gas to the pressure necessary to produce the desired maximum pressure in the test gas. The compressor is fired by releasing the pressure behind the plunger in the piston release section. The reservoir pressure acting on the front of the plunger moves it to its rear (right) position removing the seal between the reservoir and the tube. Reservoir gas rushes through the ports in the piston release section and impinges on the back of the piston driving it swiftly down the tube. The seals on the rear of the piston prevent all but a very small amount of reservoir gas from leaking into the tube and mixing with the test gas during a shot. Similarly, during the peak pressure part of the compression cycle, some test gas leaks across the piston and mixes with the reservoir gas. After the first compression cycle the piston oscillates back and forth until friction brings it to rest with equal gas pressure on its front and rear sides. The desired measurements are made during the peak pressure of the first compression stroke by the instrumentation located in the high pressure section.

A rough approximation of the variation of test gas density and temperature with test gas pressure can be obtained from the polytropic relations

$$\frac{P}{P_o} = \left(\frac{n}{n_o}\right)^{\gamma} = \left(\frac{T}{T_o}\right)^{\gamma/\gamma-1} \qquad (1)$$

where γ is the polytropic exponent, the ratio of specific heats. Equating the work done on the piston by the expanding reservoir gas to the work done by the piston on the test gas being compressed, assuming that the reservoir pressure, P_r, is constant, and substituting in above equation gives the following equation:

$$\frac{P_r}{P_o}(\gamma - 1) = \frac{\left(\frac{P_{max}}{P_o}\right)\left(\frac{P_{max}}{P_o}\right)^{1/\gamma}}{\left(\frac{P_{max}}{P_o}\right)^{1/\gamma} - 1}, \qquad (2)$$

which shows that P_{max} does not depend on the length of the tube or piston diameter, but is a function of only P_o, P_r, and γ. For $(P_{max}/P_o) \gg 1$, one obtains

$$\frac{P_{max}}{P_o} = \left[1 + (\gamma - 1)\frac{P_r}{P_o}\right]^{\gamma/\gamma-1}, \qquad (3)$$

which illustrates that the peak pressure generated in the test gas has a power law increase with reservoir pressure; i.e., a relatively low reservoir pressure generates a high test gas pressure, and that low γ-gases produce the highest peak test gas pressure for a given reservoir pressure. Typically, a reservoir pressure of 30 atm will generate a test gas pressure of 1000 atm in a monatomic gas.

A number of compressor firings were made and the results analyzed by a computer program (BCCC). All shots were made with an initial test gas pressure of 1 atm. Maximum test gas pressures and temperatures ranged from 175 to 350 atm, and from 750 to 1500 K. The UF_6 concentration in the UF_6/He test gas mixture was varied from 1.3 to 6.5%.

The value of $c_v(UF_6)$ was found to be the thermodynamic parameter most sensitive of all the parameters being optimized. This made it possible to determine the temperature dependence of $c_v(UF_6)$ with considerable accuracy throughout the complete temperature range of these experiments. Fig. 5 shows the measured value of the specific heat ratio of UF_6 as a function of temperature.

The principal goal of this investigation, the measurement of the specific heat ratio of gaseous UF_6 was achieved by determining the temperature dependence of the constant volume specific heat at high temperatures.

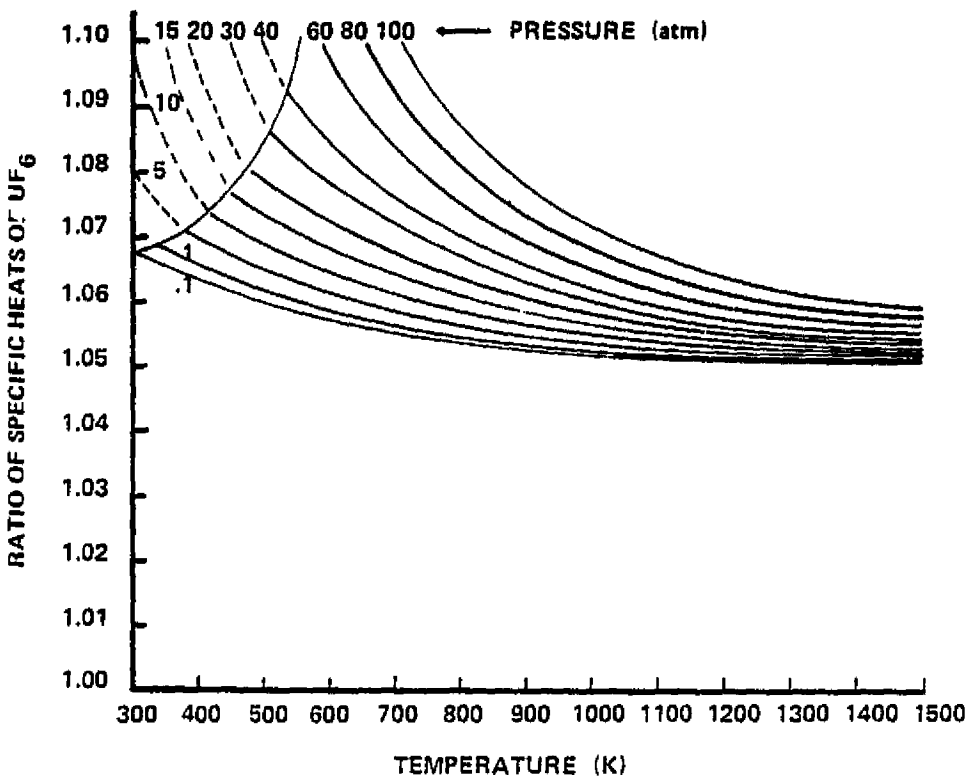

Fig. 5. Measured values of the specific heat ratio of UF_6 as a function of temperatures.

Analysis was accomplished by means of a computer program (BCCC) that is capable of determining thermodynamic properties of gases at pressure as high as 5000 atm, and at temperatures up to 5000 K. This program simulates the motion of the piston in a ballistic piston compressor (taking into account heat losses to the compressor walls and gas leakage past the piston), and derives the test gas thermodynamic properties that affect the compression process. The actual values of the thermodynamic properties are determined by a numerical optimization scheme that minimizes the error between calculated and experimental test gas pressures, volumes, and temperatures.

Analysis of the results showed that for UF_6/He mixtures the polytropic exponent (-lnP/lnV) can be approximated by the specific heat ratio. In addition, a rough estimate of the viscous coupling constant between UF_6 and He was determined, and it was established that no improvement could be made on the van der Waals constants derived from the UF_6 critical point.

The successful implementation of the BCCC as indicated by these studies has materially enhanced the usefulness of ballistic piston compressors for investigating the physical properties of gases at high pressures and temperatures.

D. Nuclear Enhancement of CO_2 Lasers

The potential and possible application of nuclear excitation of lasers was recognized by several investigators almost immediately after demonstration of the first gas laser.

However, early attempts to demonstrate nuclear pumping failed, and the matter was considered fairly hopeless around the early 1970's.

For this reason attention was given to nuclear augmentation of existing gas discharge lasers rather than attempting to build a direct nuclear pumped laser right away.

In a CO_2 laser (cavity length 1 m, electrode spacing 65 cm, total pressure 6 torr, 1:1:8 mixture), the ^4He isotope was replaced by ^3He. Due to the scarcity of ^3He the laser had to be operated in a sealed off condition. The laser was inserted in the University of Florida Training Reactor and exposed to a neutron flux of 10^{10} n/cm^2sec. Exploiting the very steep gradient of the neutron flux distribution, it was possible to expose only one half of the tube to the neutron flux. By reversing the electric polarity either cathode or anode could be in the high flux region.

Figure 6 shows the IV-characteristic of the laser with and without neutron irradiation. The experimental conditions are explained on the figure. Fig. 7 shows the enhancement obtained in output power due to the bombardment of the lasing gas by protons and tritons generated in the $^3He(n,p)T$ reaction.

The nuclear power input in this case was in the milliwatt region while the electrical power input was around 100 watts. Nuclear energy could not, therefore, possibly be the source for the increased laser power, but contributes only indirectly. An enhancement of the laser power was observed only when the cathode part of the laser was exposed to the neutron flux; indicating that the observed phenomenon is a cathode effect.

The change in the operating characteristics of the laser may be understood by examining the change in current at constant voltage with and without the neutron flux. When the anode end of the laser was in the high flux region, the change in current was a constant equal to 2.5 ma. An increase of 2.5 ma corresponds to an increase of about 1.5×10^{16} electrons per second. The number of $^3He(n,p)T$ reactions occurring

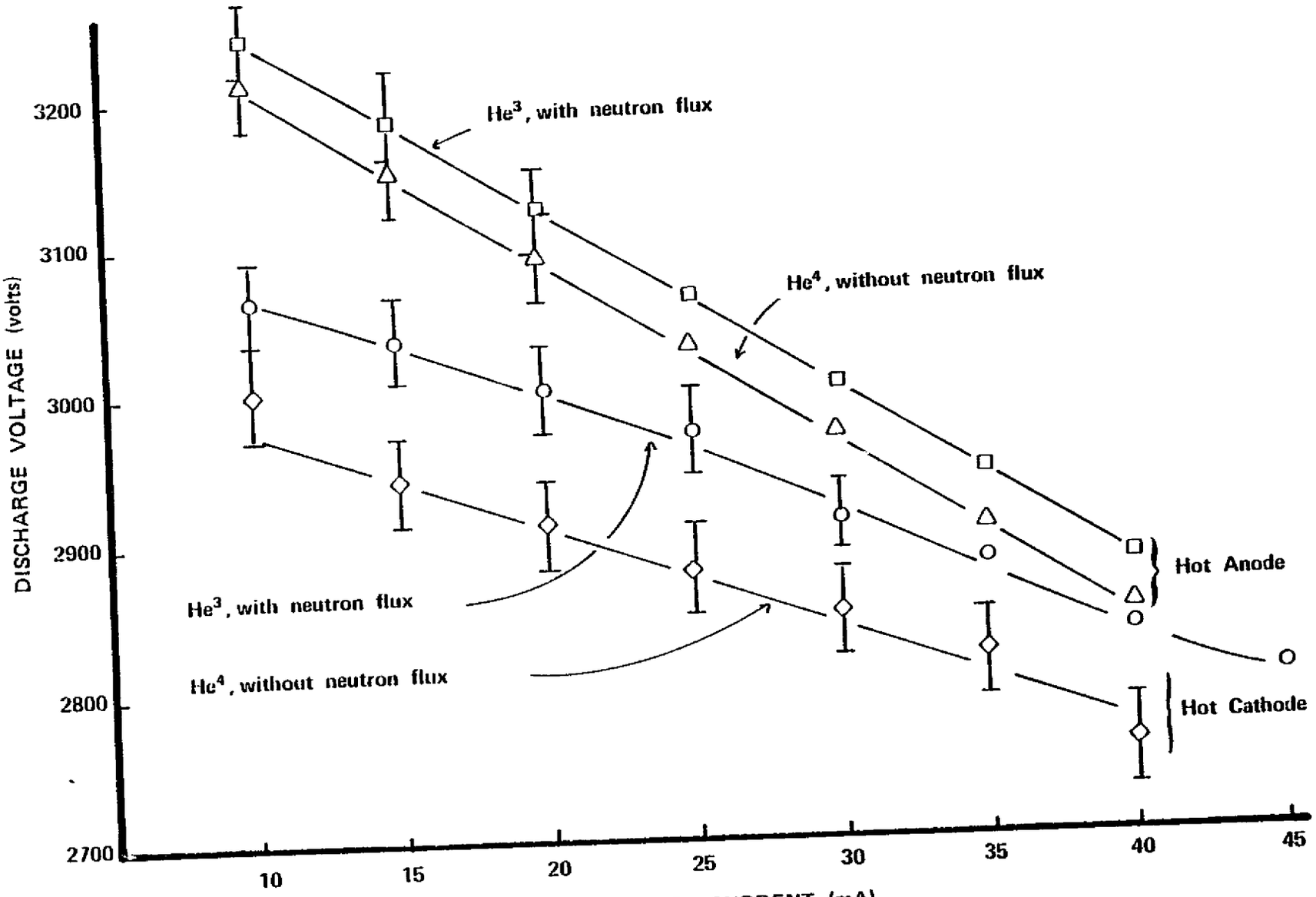

Fig. 6. I-V CHARACTERISTIC OF LASER WITH AND WITHOUT NEUTRON IRRADIATION

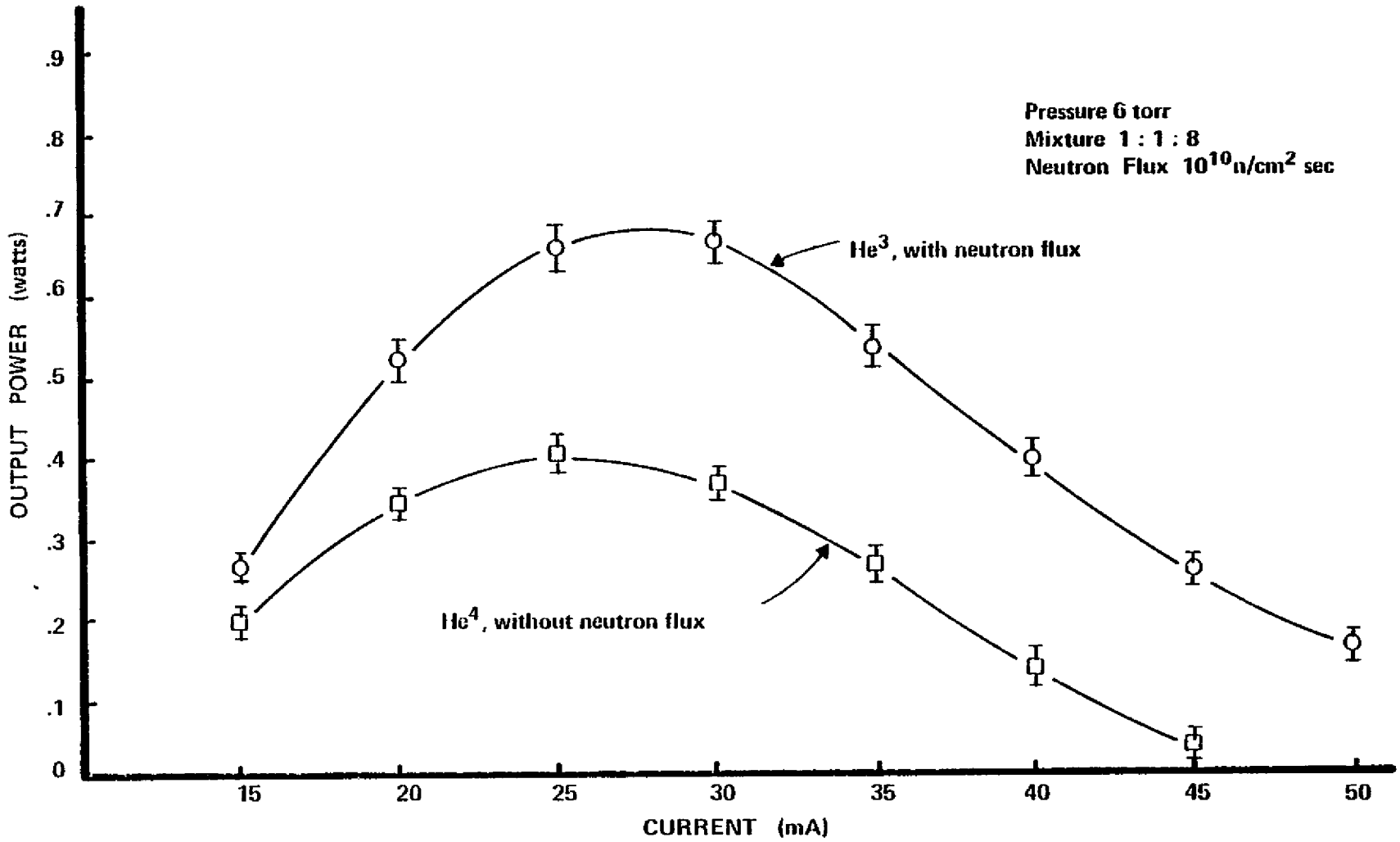

Fig. 7. LASER POWER ENHANCEMENT WITH NEUTRON IRRADIATION

within the plasma volume per second is 6.11×10^{12}. Each proton and triton creates about 10^3 ion pairs and since there are 2 particles per reaction, the number of electrons created is about 1.2×10^{16}. Thus, the increase in current for this case is due to the volume ionization of the plasma. Assuming that the volume effects are the same whichever electrode is in the high flux region, we may subtract the increase in current due to volume ionization from the curve for cathode irradiation. The resulting values represent an increase in electron density above that due to volume ionization.

The increase in electron current may be due to bombardment of the cathode by protons and tritons. In an ordinary glow discharge positive ions, accelerated by the cathode fall bombard the cathode in order to provide the electron emission current to sustain the discharge. The role of the positive ions is now taken over by the protons and tritons thus eliminating the need for a cathode fall. The voltage drop across the cathode fall is now available for the positive column, where the E/N ratio is increased due to this additional voltage, shifting the operation conditions to a more favorable region, resulting in enhanced laser output.

In general, nuclear enhancement of laser output has to be understood as a mechanism which changes the efficiency of the electrical gas discharge laser, rather than adding a significant amount of energy to it.

E. Mechanism of Excitation of Gases by Fission Fragments

The range of a fission fragment, α-particle, electron, or the stopping power of a given gas can be predicted fairly well. The same is true for the average energy transferred per collision in a fission fragment-gas interaction during the whole range of the fast particle. It is customary to designate these average energies as W-values. The

energy transferred (W-value) consists of different components, the energy used to excite the bombarded gas, to ionize it, and the energy carried away by the electrons. This means that a part of the nuclear energy is used to establish an electron population with an electron energy distribution peculiar to the nuclear source. These electrons are available for pumping of the laser gas. Direct excitation of the gas caused by the fission fragments is also a possibility.

In the special case of helium, it is possible to distinguish between these two effects. The two electrons of the helium atom give rise to a singlet and a triplet system of excited states. The ground state is a singlet state. The transition from all triplet states to the ground state is, therefore, a forbidden transition, since the electron spin has to be conserved. For the same reason, triplet states cannot be excited from the ground state. The reason that triplet excitation occurs is that a colliding electron, having the right spin, can be exchanged with an orbital electron. Thus, excitation of triplet states can only be caused by electrons. A measurement of the ratio of the intensities of helium lines originating from the singlet system versus those originating from the triplet system should clarify if electrons or fission fragments cause the observed excitation.

An experiment was performed to measure this ratio. For this purpose a quartz tube was coated at the inner surface with $^{235}U_3O_8$ and mounted in a vacuum chamber. The whole assembly was filled with helium to the desired pressure and inserted in the University of Florida Training Reactor. The neutron bombardment of the coating initiates fission reactions in the coating. Some of the fission fragments generated close to the surface of the coating will leave the surface, having a wide spread in energy and direction and are available for interaction with the gas.

The line intensities generated by these interactions were measured for several pressures. Analysis of the obtained ratio is shown in Fig. 8. The ratio of excitation caused by fission fragment versus the number of excitations caused by electrons is plotted versus pressure. As can be seen, the fission fragments participate only at low pressures appreciably in the excitation mechanism. With this result, it was recognized that the fission energy is transferred to the electrons which, in turn, excite the atoms. This means that excitation mechanism of the direct nuclear pumped laser should be quite similar to the one of the electron beam pumped laser or a recombination laser.

F. Direct Nuclear Pumped Laser

Concepts of using nuclear energy directly to excite lasers have been described in the literature since about 1961. A major distinction exists between the excitation of atomic and molecular states and the excitation of nuclear states. Only the former is worked on under the present research program. Furthermore, the described research is restricted to gas lasers. Attempts to pump crystalline materials or liquids by nuclear radiation have been made by several researchers with varying success.

The major difference of nuclear pumping of a gas laser from other methods of pumping is the very high energy of the energizing particles (fission fragments). Although gamma rays from nuclear reactions have the potential of inducing population inversions in gases, they are not considered here for nuclear pumping, since in a nuclear reactor most of the energy released by the fission reaction appears in the form of kinetic energy of fission fragments.

For research purposes, several methods are available for providing a flux of fission fragments or other high energy nuclear particles and

for study of their interactions with a test gas as depicted in Fig. 9. All depend on an external source of moderated neutrons. One group of experimental setups requires that the inside of the laser tube be coated with boron 10 or enriched uranium (U_3O_8). The following reactions produce energetic particles:

$$B^{10} + n \rightarrow \alpha(1.46\ MeV) + Li^{7}\ (0.84\ MeV)$$

and

$$U^{235} + n \rightarrow ff_h\ (\sim 65\ MeV) + ff_\ell\ (\sim 97\ MeV)$$

where n = neutron, α = alpha particle, ff_h = heavy fission fragment, and ff_ℓ = light fission fragment.

Only the latter reaction provides a fission fragment flux, while the α-particle flux of the first reaction can be considered only for simulation of nuclear pumping. In both cases, the particle flux has to emerge from the surface of the solid material which forms the coating in order to interact with the laser gas. Therefore, the coating needs to have the thickness of only one mean free path of the fission fragment (or α-particle) in the solid. Any increased thickness of the material will have the effect that additional fissions occurring in the coating will heat the solid material without contributing to the fission fragment flux emanating from the surface. This fact limits the achievable nuclear power input into the gas. This limitation disappears for a fissioning gas; as a matter of fact, the achievable power density should far exceed that density obtainable by electrical or chemical power input. The coated tube technique, however, has the advantage of relative experimental ease and of allowing the testing of various undiluted gas mixtures.

A volume source of energizing particles is achieved when, instead of coating the walls, the laser tube is filled with He^3 and an additional (laser) gas mixture. The He^3 isotope has a large cross section for the

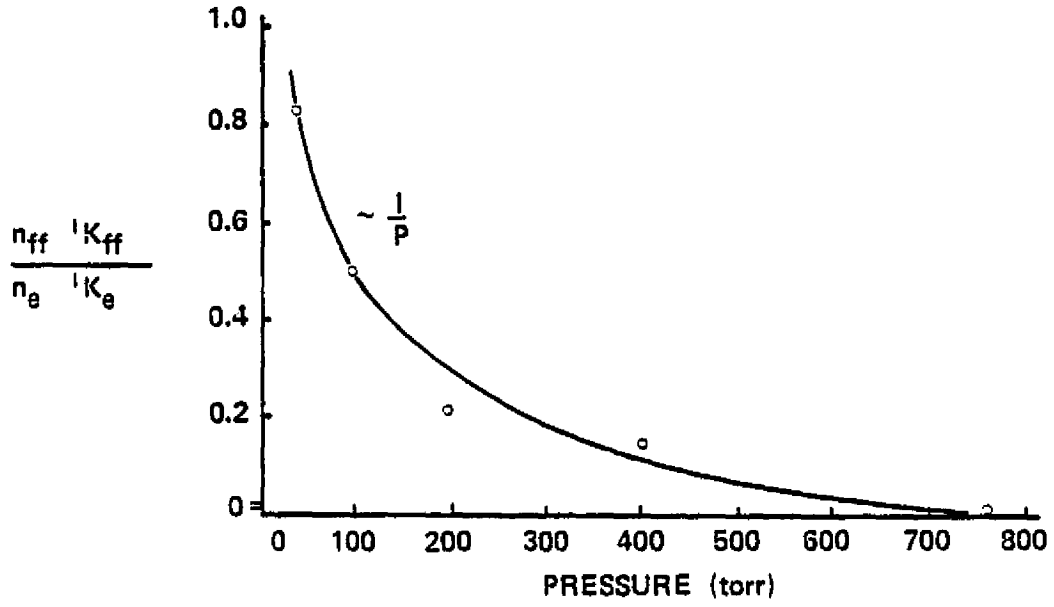

Fig. 8. EXCITATION RATIO VERSUS PRESSURE

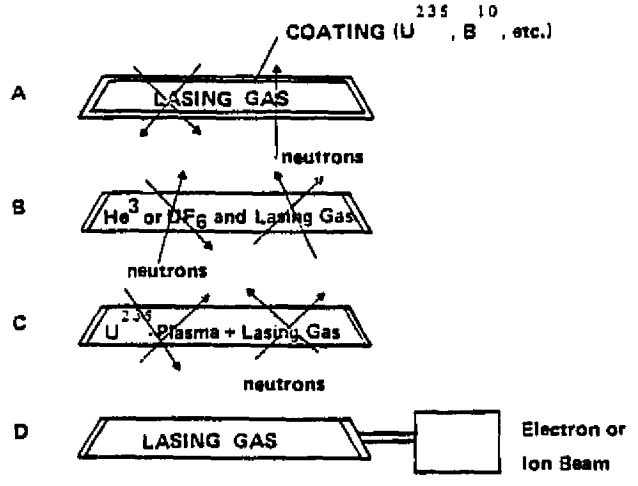

Fig. 9. BASIC CONFIGURATION FOR NUCLEAR PUMPED LASERS.

capture of neutrons. The reaction

$$He^3 + n \rightarrow p(0.57\ MeV) + T(0.19\ MeV)$$

provides a particle flux of fast protons (p) and fast tritons (T). Such a volume source has the advantage that at constant neutron flux the nuclear power in the laser tube increases with He^3 partial pressure. Of course, this reaction, again, can only be considered as a simulation, albeit a very convenient one, of a fissioning gas.

All these methods have been tried. The coated tube technique has been successfully employed in experiments independently conducted by three different groups of researchers. The He^3 volume source method has so far yielded only partial success in experiments where nuclear excitation doubled the efficiency of an electrically pumped CO_2 laser. It is now believed that at pressures of 1 atm and higher, excimer laser systems are promising candidates for the He^3 volume source excitation.

Nuclear pumping of a laser is now understood to be the direct conversion of the kinetic energy of fission fragments into coherent electromagnetic radiation. It is, therefore, a process of energy conversion that does not involve thermodynamical efficiency limitations. In principle, nuclear pumped lasers could become a means of utilizing fission power at energy levels (and at equivalent temperatures) greatly exceeding those of conventional nuclear power generation. This may result in significantly improved efficiency and power density, apart from other benefits that can be derived from the monochromaticity and coherence of laser energy. In the recent past, a major motivation for relevant research has been the needs of the space program. The energy sources for the nuclear pumping of lasers are conceived to be gaseous core reactors, similar to those which for many years have been investigated under NASA programs. The possibility of non-equilibrium radiation from such reactors with its concomitant fission

induced population inversion, is an area of major concern in this research. This has been intensively investigated primarily by use of the previously described coated-tube technique in combination with research reactors as neutron sources. While the main objective was to demonstrate non-equilibrium distributions of ionized and excited states in fission-fragment energized gases and plasmas, nuclear pumping of lasers was also attempted. The experimental work was supplemented by theoretical research, which, however, is still greatly hampered by the lack of data, such as cross sections and transition probabilities. In this earlier work, the existence of non-equilibrium radiation from fission fragment excited gases was clearly demonstrated by spectroscopically measured deviations of energy levels from Boltzmann distributions.

For initial demonstration of nuclear pumping of lasers, owing to the incidental limitations of the coated tube technique, extremely high neutron flux densities were needed in order to deliver sufficient fission power for the laser gas to surpass threshold conditions.

The largest neutron flux density from an experimental reactor can be obtained from a fast burst reactor, such as was developed for example at the Los Alamos Scientific Laboratory. Such a reactor consists of a cylinder, control and safety rods all manufactured of highly enriched uranium 235 metal totaling a weight of 65 kg. It is unshielded and unmoderated, so to speak bare, and because of this fact is named GODIVA. By pneumatic means the control rod is quickly inserted into a position within the cylinder to form a supercritical mass and a pulse in excess of 100,000 MW of power is obtained for 100 μsec, during which time a neutron flux of a peak value of about $10^{18}/cm^2$ sec is emitted.

The laser consisted of a 2.2-cm-diameter tube lined with a ^{235}U foil of 33 cm length. The tube, fitted with potassium chloride Brewster windows,

was sited within a resonant optical cavity. The optical path led through a 0.2-cm-diameter output aperture in one of the mirrors to a heavily shielded, liquid-nitrogen-cooled, gold-doped germanium detector. The detector was located in an adjacent laboratory room 18 m from the laser. The light path had four 90° bends for adequate shielding of the detector against streaming γ and neutron radiation from the reactor. The laser tube was surrounded by a 8.5-cm thick polyethelene sleeve, serving as a neutron moderator. An ion chamber probe inserted in the cadmium covered polyethelene moderator monitored the fission rate near the uranium foil to determine the fission power input into the laser.

With this arrangement, nuclear pumping of a He-Xe laser was achieved. By use of three Corning glass color-filters, the observed wavelength was established to be around 3.5μm. It is assumed that the strong Xe $5d\ [7/2]^{\circ}_{3}$ - $6p\ [5/2]_2$ transition was produced.

Figure 10 shows typical signals of the laser output and the fast neutron pulse versus time. The laser pulse was delayed by approximately 50 μsec in respect to the fast neutron pulse. This effect was caused by the neutron thermalization time which was required for moderation of the fast neutrons, since the fission reactions in the U_3O_8 coating have to be induced by thermal neutrons. An analysis of the curves also exhibits a threshold for onset and termination of laser action which, in a different way, was confirmed by the variation of the GODIVA reactor power. This result is shown in Figure 11. Best results were obtained from a Xe/He mixture ratio of 1:4 at 350-Torr pressure. The measured laser intensity was at least 0.1 W. Fission fragments from the coating of the tube were found to be the only source of laser pumping, and actual lasing was confirmed by various conventional methods.

The work was conducted jointly by the University of Florida and the Los Alamos Scientific Laboratory personnel.

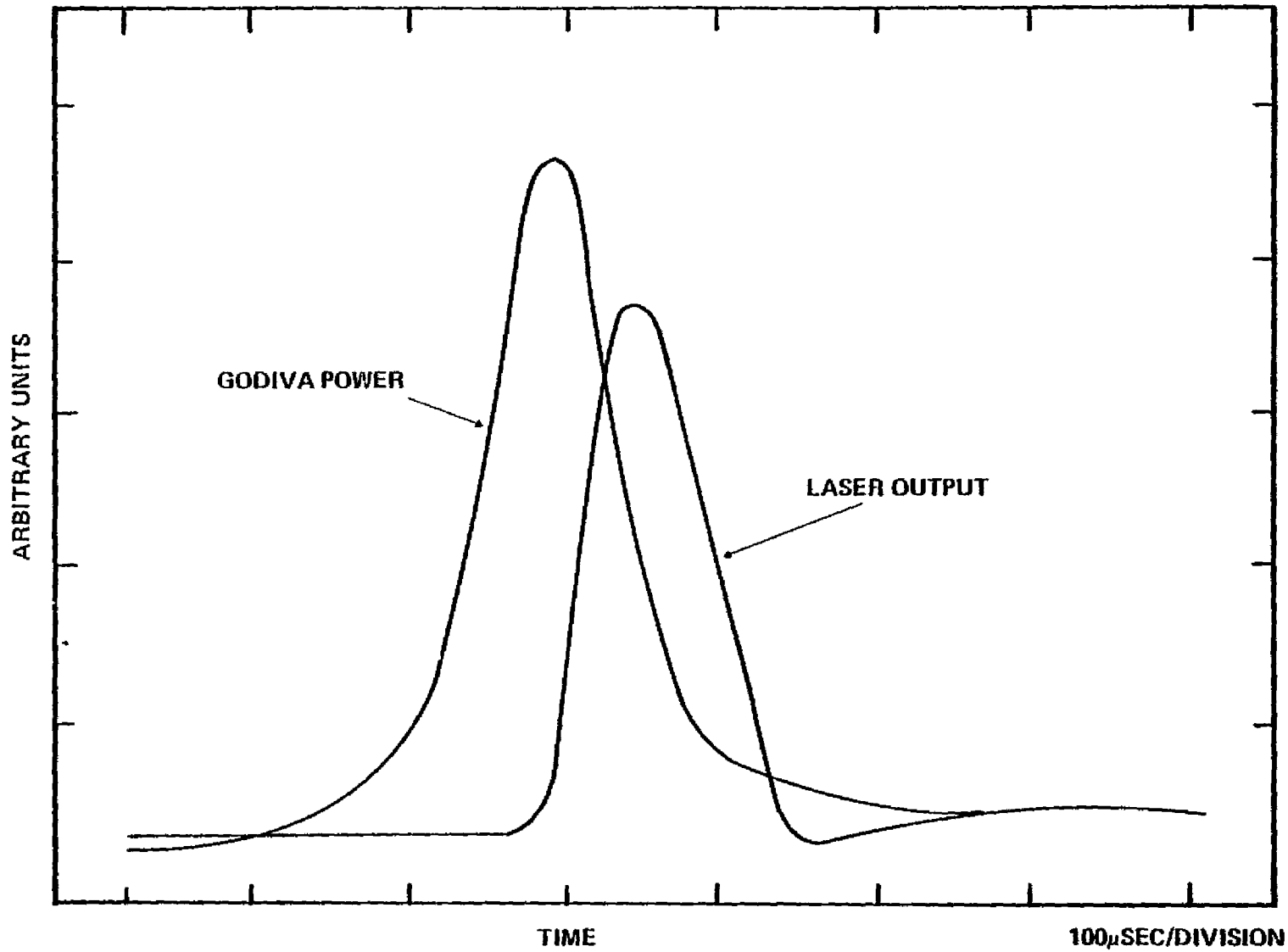

OSCILLOSCOPE TRACES OF NEUTRON FLUX AND LASER OUTPUT

Fig. 10

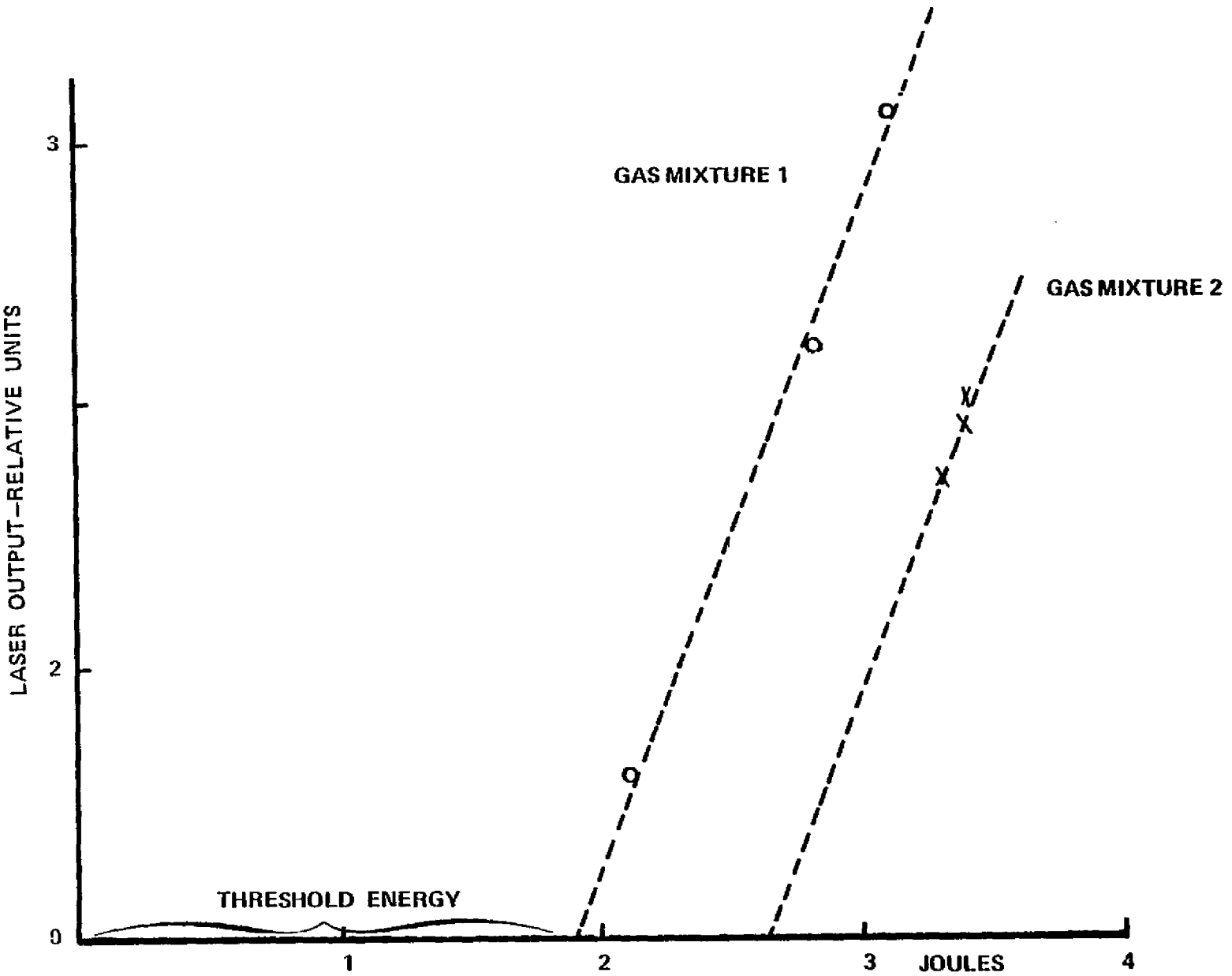

LASER OUTPUT VS ENERGY INPUT

FIG. 11

G. Application of Gaseous Core Reactors for Transmutation of Nuclear Waste

The effort under Grant NGL10-005-089 aimed at understanding the gaseous core reactor led to an interesting unexpected result. It turns out that a cavity reactor, like the gaseous core reactor, has a neutron spectrum which is very suitable to destroy nuclear waste by nuclear transmutation.

The proper management of high-level radioactive waste is an important issue with which the nuclear community must deal. In the face of rising social pressure, the identification of a satisfactory long-term management scheme is vital to the health of the industry.

A number of high-level, long-term waste management schemes have been proposed; none are entirely satisfactory. The ultimate standard against which any proposed scheme must be judged is whether or not it will prevent any nuclear waste material from ever posing a threat to man's well-being. Management schemes are invariably aimed at accomplishing this goal by isolation of the waste material from man and from the environment for whatever period of time it remains hazardous. Transmutation is the only exception to the isolation rationale. Transmutation is unique in that it offers the potential of converting hazardous nuclides into non-hazardous forms by the same nuclear processes responsible for their creation.

Until recently, spent fuel reprocessing had been directed toward recovery of most of the uranium and plutonium present. Recovery fractions were governed by trade-offs between the value of the recovered metal and sharply increasing costs with higher recovery fractions. The remaining high-level waste was treated collectively by storage until future implementation of a long-term management scheme. With this technique, the entire high-level waste mass must be treated as though it had the half-

life of the longest lived nuclide, the chemical toxicity of the most toxic nuclide, etc.

The fission products are characterized by high specific activity and relatively low neutron absorption cross sections. They are generally short-lived compared to the actinide elements. They are neutron rich and decay toward a stable neutron-proton ratio by successive beta decays. Typical decay chains are illustrated in Figure12. For thermal fission of U-235, there is slightly less than 1% fission yield into the 129 mass chain. There is negligible direct yield of xenon-129. The shorter-lived chain members rapidly decay into iodide-129 which has a half-life of 15.9 million years. Within the fission product group, a few long-lived nuclides, such as I-129, control the long-term waste hazard.

The trans-uranic actinides are formed by those neutron absorption reactions in the fuel which do not result in fission. The most common such reaction competing with fission is radiative capture. The newly formed nuclide may then undergo spontaneous or neutron induced fission, decay by particle emission, or another neutron absorption reaction such as radiative capture may take place. In this manner, higher and higher mass number trans-uranics are built up in the fuel.

The heavy metals present the most severe long-term management problems. They are characterized by high chemical toxicity and very long half-lives. The waste hazard associated with the heavy metals remains high for hundreds of thousands of years. In general, the actinides possess substantial neutron reaction cross sections.

Transmutation is any process by which a nuclide is changed into another nuclide. The decay of a radioactive nuclide is a natural transmutation process, but it may not occur on a sufficiently short time scale to be useful for waste management. Transmutation may also be artificially induced

by neutrons, photons, or charged particles. Of the known methods of artificially inducing transmutation, only neutron induced transmutation appears to offer near term technical and economic feasibility.

Transmutation of the long-lived waste fraction will involve treatment of the actinides and some key fission products. For the fission products, the motivation for treatment is illustrated by considering iodine-129. The I-129 decay bottleneck illustrated in Figure 13 may be relieved by irradiation. Radiative capture reactions in the I-129 will drive it to I-130. The short-lived (12.4 hours) I-130 will then beta decay to xenon-130 which is stable and non-hazardous. The very slowly decaying nuclides in a particular mass chain are shifted to a more rapidly decaying chain.

A number of competing reactions may also occur. The major reaction paths are indicated in Figure 13. Table 1 contains a symbol key for the figure. For I-130, radiative captures producing I-131 compete with the natural beta decay producing Xe-130. Similar competitive reaction paths may be readily observed for other nuclides. In general, the rate at which the transmutation proceeds will be governed by the magnitude of the neutron flux. The reaction rate may also be altered, sometimes substantially, by tailoring the neutron spectrum to exploit neutron absorption resonances. Particular reaction paths can be enhanced by altering the spectrum. The eventual distribution of nuclides is strongly dependent on the neutron spectrum.

The final nuclide distribution will be very significant from a waste management standpoint. The variety of possible reaction paths generally precludes prediction of the final distribution by observation. The effect of a spectral change must be evaluated by following the isotopic balance as a function of time during the irradiation and subsequent decay period. Nuclide concentrations, transmutation rates, and the waste hazard may then be calculated.

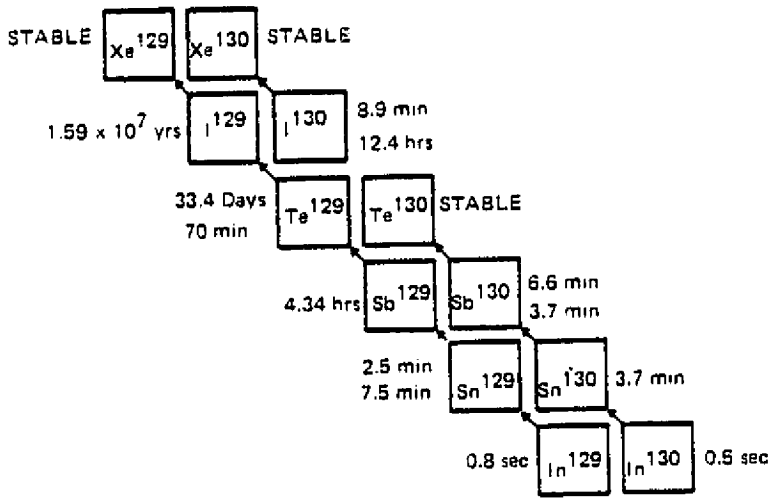

Fig. 12. TYPICAL FISSION PRODUCT DECAY CHAINS

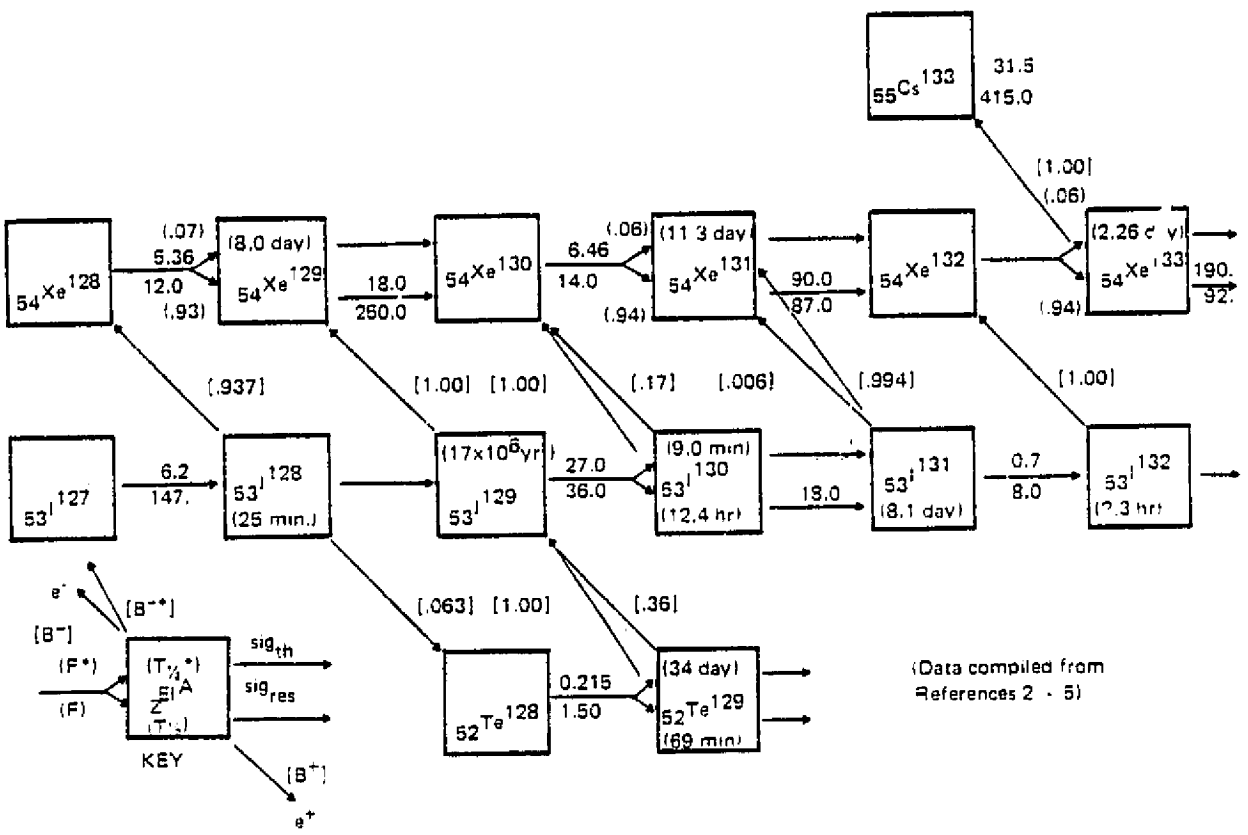

Fig. 13. IODINE-129 TRANSMUTATION REACTION PATHS

For the actinides, the transmutation rationale is different. Contrary to the fission products, there is little to be gained by radiative capture reactions in the actinides. To build even higher actinides from them is of questionable value. The ultimate objective is to induce fission. Actinide fission cross sections generally decrease with increasing energy, but at a faster rate for most actinides. Therefore, fission can be promoted over radiative capture by the employment of a harder neutron spectrum. As with the fission products, the optimum spectrum cannot be predicted by simple observation and detailed calculations must be performed.

The requirements for very high neutron fluxes and the desirability of spectrum tailoring make the cavity reactor a logical candidate for transmutation of both fission product and actinide wastes. A uranium hexafluoride fueled heavy water moderated cavity reactor was considered in initial studies. The reactor was assumed to operate at an average thermal flux of approximately 6.4×10^{14} neutrons/cm^2-sec for a five-year period. The assumed fuel enrichment was 5%. The transmutation rates of several waste isotopes present in the discharged fuel from currently operating light water reactors were studied using the isotopic generation and depletion code ORIGEN.

The isotopes selected for evaluation of the gas core transmutation potential were I-129, Am-241, Am-242m, Am-243, Cm-243, Cm-244, Cm-245, and Cm-246. Americium and curium were chosen since they control the actinide waste hazard for very long decay times. The fission product iodine-129 was chosen since it is a major contributor to the long-term waste hazard. The amounts of the initial waste loading were determined by the composition of 20 typical light water reactor fuel loads stored for a decay interval of ten years. The waste quantitites employed in the study are therefore approximately equivalent to that generated in 60 reactor years of operation.

TABLE 1: TRANSMUTATION FIGURE SYMBOL KEY

El	element symbol	(F*)	fraction of (n,γ) transitions to an excited state of the product nuclide
A	mass number		
Z	atomic number	(F)	fraction of (n,γ) transitions to a ground state of product nuclide
e^-	electron emission		
e^+	positron emission	$[B^+]$	fractional decay by positron emission
(Tl/2*)	excited state half-life	$[B^-]$	fractional decay by electron emission
(Tl/2)	ground state half-life		
sig_{th}	thermal cross section for (n,γ) absorption	$[B^-*]$	fractional decay by electron emission to an excited state of the product nuclide
sig_{res}	resonance integral for (n,γ) absorption		

NOTE: designates an isomeric transition; the fraction of excited state decays by isomeric transition is $1 - [B^+] - [B^-] - [B^-*]$

As previously indicated, the transmutation rates and the final isotopic balances are strong functions of the neutron spectrum. For this study, three reference spectra were employed. A relatively hard spectrum typical of that expected in the core and a thermal spectrum typical of that present in the heavy water moderator were used. In addition, an intermediate spectrum typical of that found in light water reactors was used for comparison purposes. It is emphasized that only the spectrumis typical of the LWR; the magnitude of the flux in the gas core is substantially higher than that attainable in the light water reactor.

The initial loading of I-129 was 400 kilograms. The mass of I-129 remaining as a function of irradiation time for the three reference spectra is shown in Figure 14. The curve labeled $\phi 3$ corresponds to irradiation in the core spectra and $\phi 1$ to irradiation in the moderator spectra.

Curves for the transmutation of the americium isotopes in the spectrum present in the reflector-moderator are shown in Figure 15. The initial loadings of the three americium isotopes considered are indicated. The Am-243 concentration approaches a steady state value after approximately two years. This behavior is due to Am-243 production by successive radiative captures and beta decays in the U^{238} present in the reactor fuel.

The effect of the neutron spectrum on the transmutation of Am-243 is illustrated in Figure 16. The reflector-moderator is indicated by the subscript 1 and the core by the subscript 3.

The curium transmutation calculations are illustrated in Figure 17. The significance of the neutron spectrum employed is most vividly illustrated in the case of curium-244. After an irradiation period of approximately six months, the Cm-244 waste masses differ by a factor of 30 depending on whether the core or moderator spectrum is employed.

Successive radiative captures and beta decays in both the reactor fuel and the isotopes to be transmuted can produce significant quantities of higher mass number actinides. The production curves for significant transmutation by-products are shown in Figure 18.

The success of a particular transmutation scheme can be judged in terms of the overall reduction in the waste hazard. The relative inhalation hazard (RIHH) is defined as the volume of air (cubic meters) required to dilute the radioactivity in the waste to the Radiation Concentration Guide levels listed in Title 10 of the Code of Federal Regulations. Similarly, the relative ingestion hazard (RIGH) is defined in terms of

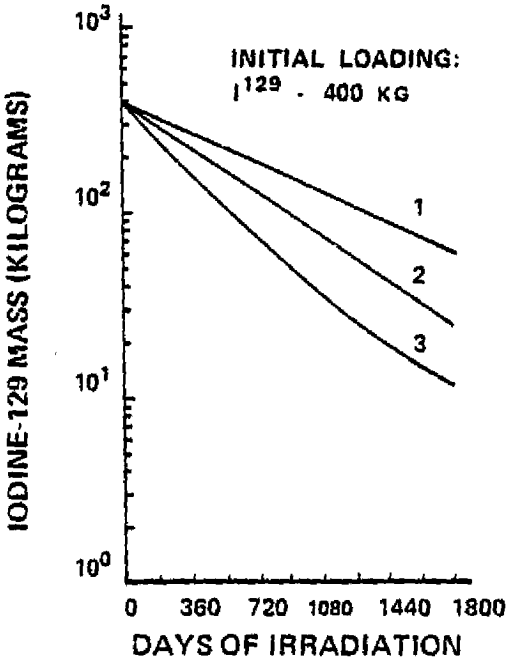

Fig. 14. Iodine-129 Transmutation versus Irradiation Time

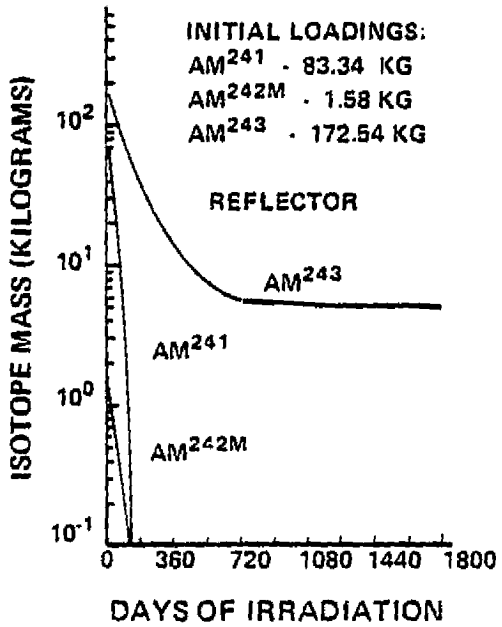

Fig. 15. Americium Transmution versus Irradiation Time

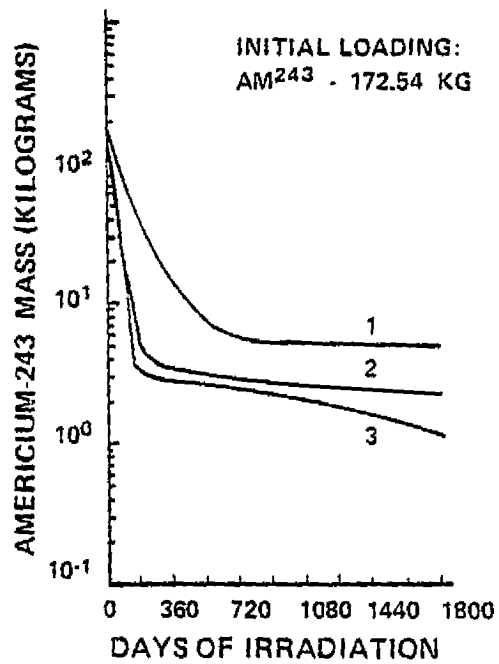

Fig. 16. Americium-243 Transmutation versus Irradiation Time

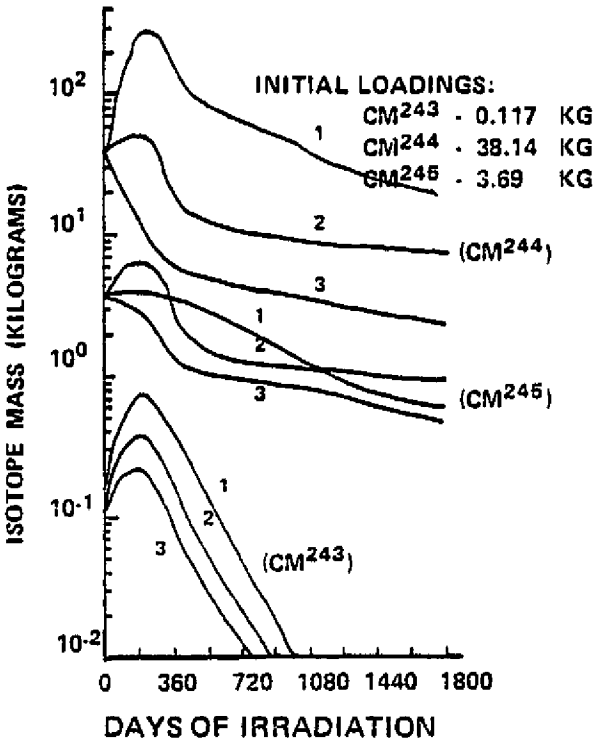

Fig. 17. Curium Transmutation versus Irradiation Time

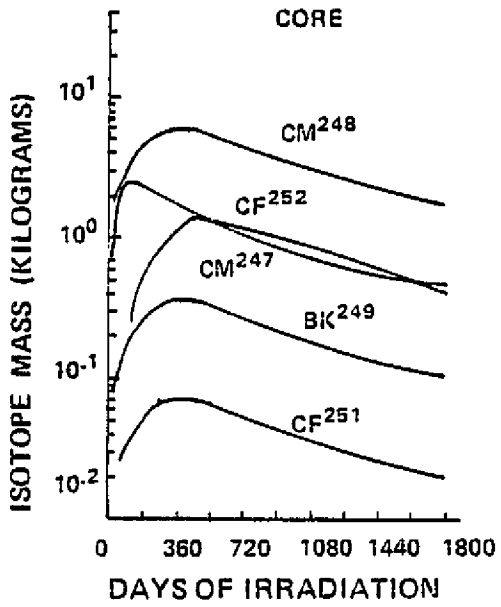

Fig. 18. Higher Actinide Build-up versus Irradiation Time

the volume of water required for dilution. The primary hazard associated with long-term waste disposal is the danger of dissolution in ground water or dispersal in the atmosphere and subsequent uptake by man. The quantity of air or water required to dilute the waste to a concentration low enough for unrestricted use can be used as a crude measure of the waste hazard.

The relative ingestion hazard associated with the americium and curium wastes is illustrated in Figure 19. The top curve represents the no irradiation case and the lower three curves, irradiation by the three reference spectra. The lower curves represent the hazard measure of the actinides to be transmuted, the by-products of the transmutation, and the new wastes generated by operation of the reactor for five years.

In conclusion, it can be said that transmutation of I-129 by a five-year exposure to a thermal neutron flux of $6.4 \times 10^{14} n/cm^2$-sec result in nearly order-of-magnitude reductions in the waste inventory of this nuclide. A five-year transmutation of americium and curium wastes produces order-of-magnitude decreases in the overall hazard potential of actinide wastes generated in 60 reactor years of LWR operation.

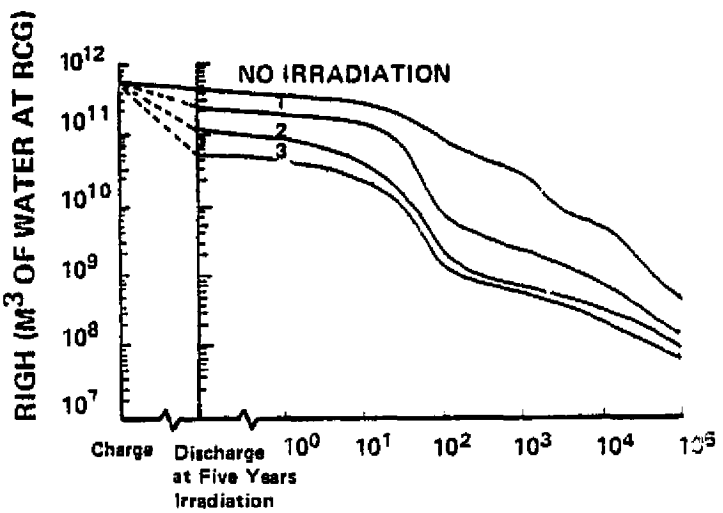

Fig. 19. Relative Ingestion Hazard (RIGH) of Americium and Curium Wastes

H. Boiling Point of Uranium

The experimental uranium plasma program at the University of Florida was initiated in 1966. The successful operation of the first plasma experiment pointed to the potential of further work. A dc arc struck between fixed tungsten and uranium electrodes in a subatmospheric helium environment generated the plasma. Experimental test times were typically of the order of 1 to 3 min and were limited by heat dissipation, graphite crucible sublimation, and uranium electrode losses.

The growing interest in the thermal characteristics of uranium in the plasma state prompted a continuation of the program. The extension of the experiment into the regime of gaseous-core feasibility resulted in the development of the device shown in Figure 20. As in the prototype, the uranium plasma was generated in a dc arc. The system improvements included internal electrode cooling, high-pressure capability, a method for arc stabilizing, and an adjustable electrode configuration.

The arc is struck between a tipped tungsten cathode pin and a ^{238}U anode pellet. The anode pellet sits in a tungsten crucible brazed into the copper anode pedestal. Both electrodes are internally cooled with a single-pass water flow. The pressure cell is designed for 200 atm at a wall temperature of 500°F. Cell wall temperatures are held below 150°F with the water-cooled, thermal shield.

The chamber pressure environment is derived from a bottled, high-pressure gas cylinder. The gas is injected into the chamber in a concentric sheath about the plasma column periphery. The axial downflow of the gas stabilizes the column during high-pressure, high-power operation.

Arc ignition is obtained with a pneumatic electrode drive. A manual control initiates the downward motion of the cathode and at the onset of current a sensing device triggers the extraction of the electrode.

Electric power is derived from a 40-kW dc generator with a maximum current rating of 160 A.

In addition to a complete program of plasma temperature and number density diagnostics, the relation between the plasma electrical characteristics and the ambient pressure and temperature was of interest. With an appropriate model, it is possible to predict gaseous-core engine start-up characteristics by assuming that the initial uranium core volume is to be supplied through a consumable electrode system.

Arc electrical characteristics were analyzed with a model based on

$$V_{arc} = V_{anode} + V_{cathode} = \frac{Cdp^m}{I^n} \tag{4}$$

The voltage drops across the sheath regions of each electrode are accounted for in V_{anode} and $V_{cathode}$. The term describing the positive column of the arc includes functional dependences on the electrode separation d, ambient chamber pressure p, and the arc current I. The model subjected to computer analysis was

$$V_{obs} = IR_{system} + V_{sheath} + \frac{Cdp^m}{I^n} \tag{5}$$

where an additional term IR_{system} accounts for voltage drop in the electrodes. The independent laboratory variables were d, p, and I.

A least-squares curve fitting routine was used to determine R_{system}, V_{sheath}, the constant C, the component m, and the exponent n.

Samples of the arc current-voltage characteristics analyzed are shown in Figure 21. The most important characteristic of these curves is the hyperbolic characteristic from which the exponent n of the current I can be evaluated.

The boiling-point parameter n is related to the boiling point of the anode material through the following expression:

$$n = 2.62 \times 10^{-3} T_{anode} \qquad (6)$$

This relationship was the result of work performed and compiled in 1924 by Nottingham. The experiment performed in 1924 was similar to the experiment under discussion.

There is evidence that the Nottingham relationship is reliable for uranium. In particular, Table II attests to the fact that a uranium arc in an inert helium atmosphere is well described by the empirical relationship. Table II lists the complement of pressures and electrode separations for which the uranium arc current-voltage model was analyzed. The gradual increase of the sheath voltage with increasing pressure is an expected trend and the magnitude indicates that the arc is supported by the uranium species rather than by the helium. The computed values of the Nottingham boiling-point parameter are listed together with the corresponding evaluation of the anode boiling point. The excellent agreement between the results of this experiment and accepted values for the vapor pressure of uranium is illustrated in Figure 22. The broken curves are two state-of-the-art extrapolations of vapor pressure measurements made at temperatures below 2100°K. These measurements were made under vapor pressure conditions three orders of magnitude lower than the pressures of interest.

It is important to note that the ordinate is total system pressure P_A, the sum of the uranium and helium partial pressures as measured external to the plasma chamber. The necessary correlation is that the vapor pressure measured in an equilibrium experiment, that is, effusion experiment, is equivalent to the ambient pressure in the quasi-equilibrium arc method. [Raug, E.G., and Thorn, R.J., "Vapor Pressure of Uranium," J. Chem Phys., Vol. 22, 1954, p. 1515; Drowart, J, Pattoret, A. and Smoes, S.J., Nucl. Mat., Vol 12, 1964, p. 312.]

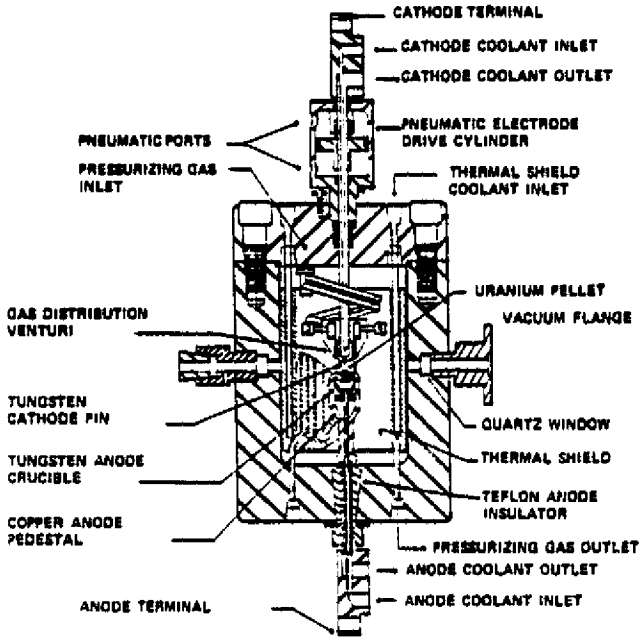

Fig. 20. HIGH PRESSURE URANIUM PLASMA DEVICE

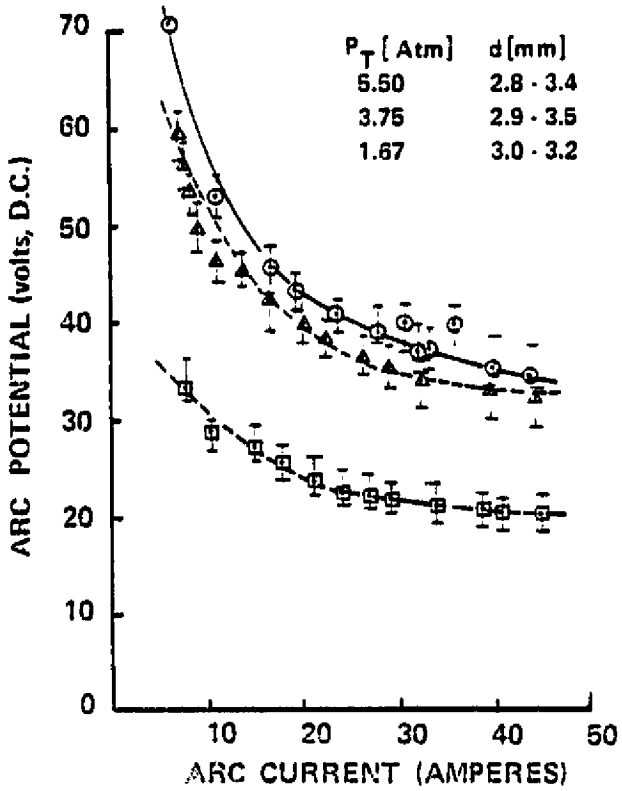

Fig. 21. High Pressure Uranium Arc Voltage-current Characteristics

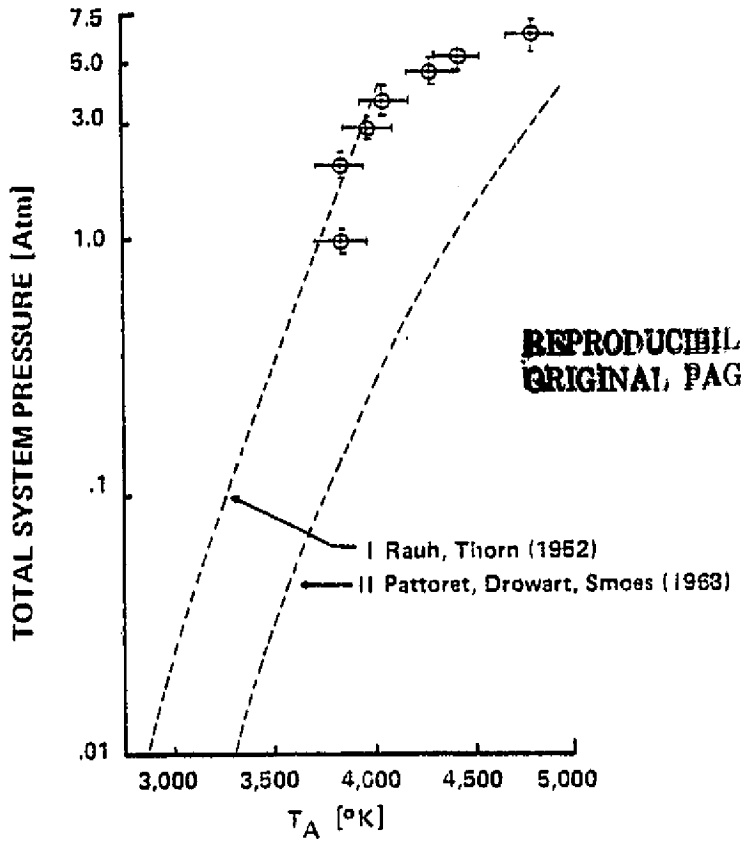

Fig. 22. Total System Pressure versus Apparent Anode Boiling Temperature. Broken Curves are Extrapolated from Empirical Data.

TABLE II. URANIUM ARC VOLTAGE -- CURRENT MODEL

Experimental parameter		Computer results		
Total pressure, p, atm	Electrode gap, d, mm	Sheath voltage, V	Nottingham parameter, n	Anode Boiling Point temperature, T, °K
1.0	4.07	14.28	1.008	3847
2.0	3.0 to 3.2	16.3	1.0056	3838
2.86	4.75	16.5	1.050	4007
3.72	2.9 to 3.5	17.9	1.068	4076
4.82	6.01	17.3	1.128	4305
5.6	2.8 to 3.4	23.06	1.170	4465
6.8	6.01	26.8	1.270	4847

III. UNPUBLISHED MATERIAL

A. Survey

At the time of this writing several papers have been submitted to scientific journals for publication. Some of the material generated under these grants is quite detailed and will be incorporated into publications only superficially.

For this reason, some of these details are reported here so that they can be referenced in later publication. These are:

Electronic State Populations of (n,p) Excited He^3

- Purpose of Experiments
- Experimental System
- Experimental Results
  - Relative Line Intensities
  - Electron Temperatures
  - Non-Equilibrium Effects

Lifetime System

- Purpose of Experiments
- Experimental Device
- Experimental Procedure
- Experimental Results
  - Pure Gas Studies
    - Nitrogen
    - Neon/Nitrogen Mixtures
    - Helium/Nitrogen Mixtures
    - Argon/Nitrogen
    - Carbon Tetrafluoride
  - UF_6 Additive Studies (Low Concentrations)
    - Nitrogen
    - Argon
    - Xenon
  - Summary of UF_6 Admixture Results
  - UF_6 Additive Studies (High Concentrations)
    - Nitrogen
    - Argon

UF_6-CO_2 Laser-Reactor Studies

Nuclear Pumped CW-Laser

- Introduction
- Gain Measurements
  - Medium Flux Reactor Gain Measurements
  - Low Flux Reactor Gain Measurements
- Laser Experiment
- Checks for Lasing

B. Electronic State Populations of (n,p) Excited He^3

1. Purpose of Experiments

To date, the two most viable modes of pumping in nuclear lasers are via a slab source (fission foil) or volume excitation ($^3He(n,p)T$). For this reason, it is desirable to have knowledge of the excitation spectrum produced by either technique.

It is well known that in charged particle pumping schemes, electronic excitation is accomplished with the secondary particles (delta rays) generated by the fission fragment. This being the case, one would expect electron temperatures present in a U-235 fission fragment excited plasma to greatly exceed those accompanying ^3He (n,p) volume excitation.

Previous experiments by Walters on U-235 fission fragment excited He^4 indicated electron temperatures ranging from 3400 to 4600°K for the He^4 pressures of 25 to 760 torr. At that time, an effort was made to perform the same experimental measurements on He^3. Low emission intensities and high noise levels, however, prevented measurements at that time.

Modification of the spectroscopic system and improvements in the electronics were made to enhance the sensitivity and signal to noise ratio allowing emission measurements to be performed with (n,p) excited He^3. The following paragraphs report on the experimental arrangement utilized and results of the He^3 emission studies.

2. Experimental System

An overall schematic of the ^3He neutron irradiation system appears in Figure 23. Gas irradiation was performed in the east-west horizontal throughport of the University of Florida Training Reactor. Peak thermal flux level was $2 \times 10^{12} n/cm^2$-sec. The east-west throughport is maintained at rough vacuum (10^{-2} torr) during measurements to provide for secondary gas containment and to prevent atmospheric absorption of the emitted optical

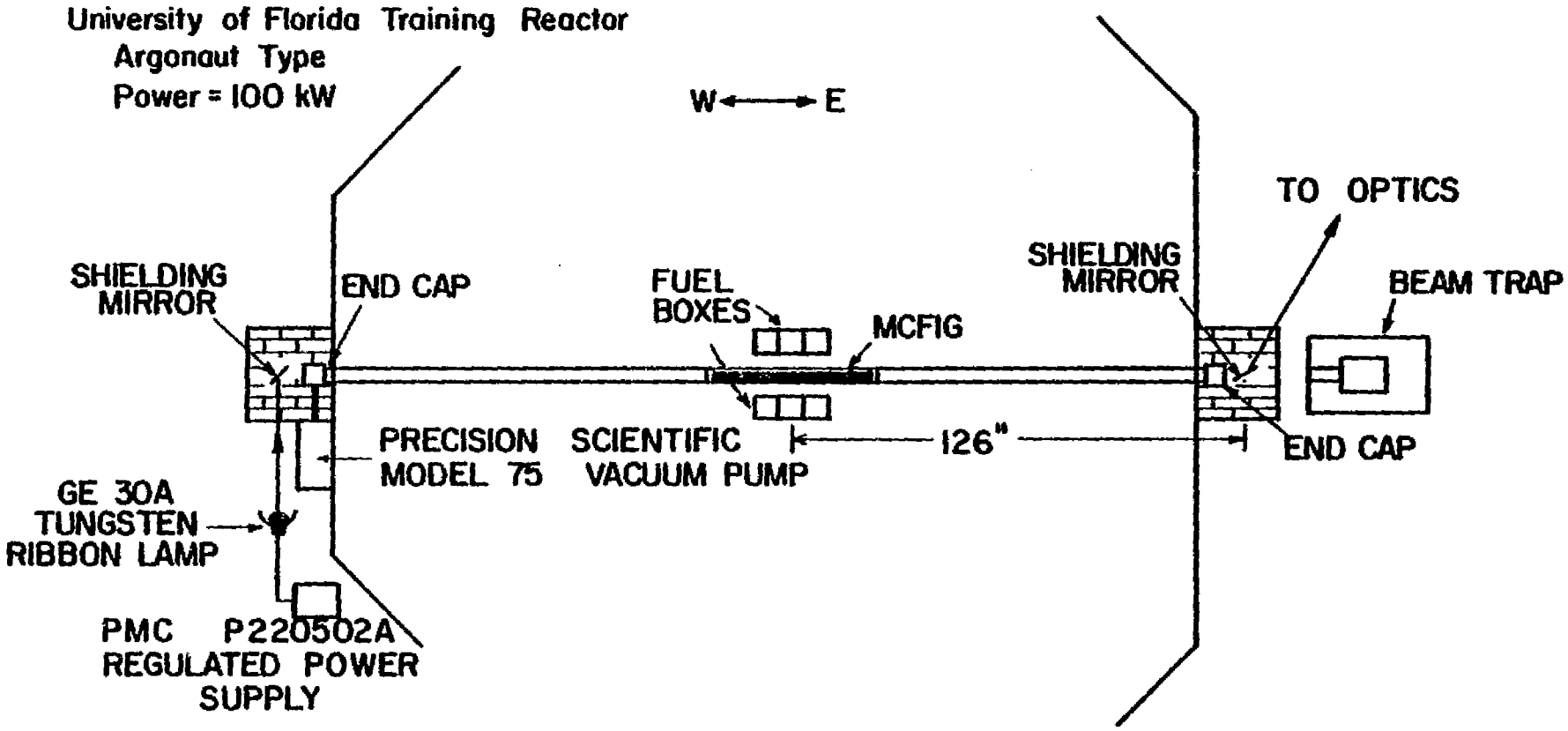

OVERALL LAYOUT FOR MCFIG GAS IRRADIATION STUDIES

Figure 23

radiation. This procedure also eliminates gamma excited N_2 fluorescence emission from the high flux region.

The ends of the throughport are terminated with sapphire windows allowing spectroscopic measurements over an extended wavelength span. This technique also facilitates relative intensity calibration and transmissivity measurements performed with a tungsten ribbon lamp situated at the opposite end of the throughport.

The gas capsule, termed a MCFIG (multipurpose capsule for irradiation of gases) appears schematically in Figure 24. Experiments were performed with two capsule types of identical diameter and length but with differing window mounting schemes. The flanged window system, however, was found to lose vacuum integrity after several irradiations and was replaced with the all welded design. Prior to filling, the capsule was evacuated to 10^{-5} torr. Fill pressures varied from 100 to 760 torr, the low limit being established by the acceptable signal to noise ratio.

A schematic of the optical system appears in Figure 25. The capsule emission was imaged onto the spectrometer entrance slit with a 48 inch focal length parabolic mirror. Optical alignment was performed with an internal spectrometer mounted He-Ne laser.

The spectrometer utilized was a 48 inch Czerny-Turner design modified for scanning monochromator operation. Slit width for all measurements was 300 μm. While this slit width limited spectral resolution, it was deemed necessary to provide sufficient signal level. The grating was lead screw driven via a stepping motor/driver arrangement.

A schematic of the detector/electronic/recording system appears in Figure 26. Signal detection was performed with a thermoelectrically cooled UV extended photomultiplier tube. The signal was voltage converted, filtered (for gamma noise), and finally recorded on an X-Y plotter.

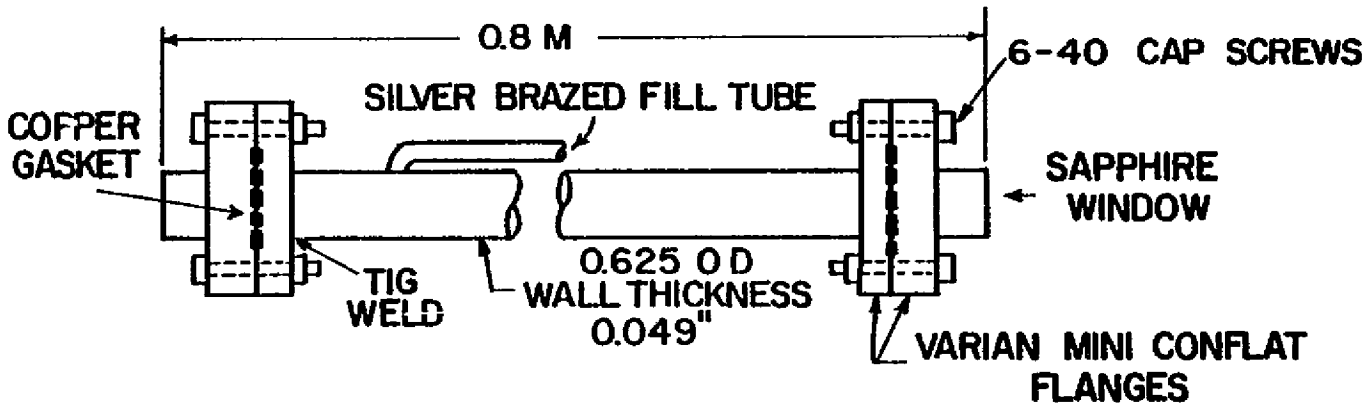

FLANGED TWO WINDOW MCFIG

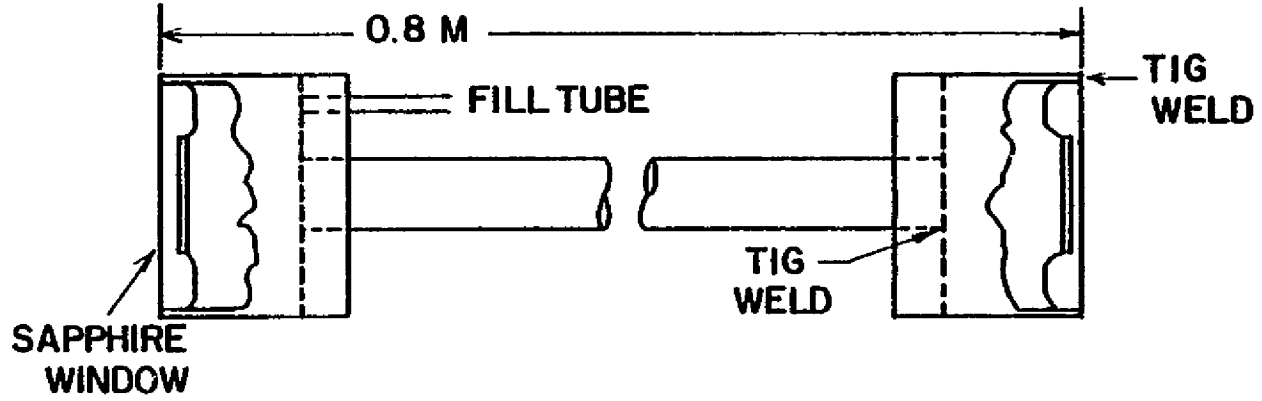

ALL WELDED MCFIG

Figure 24

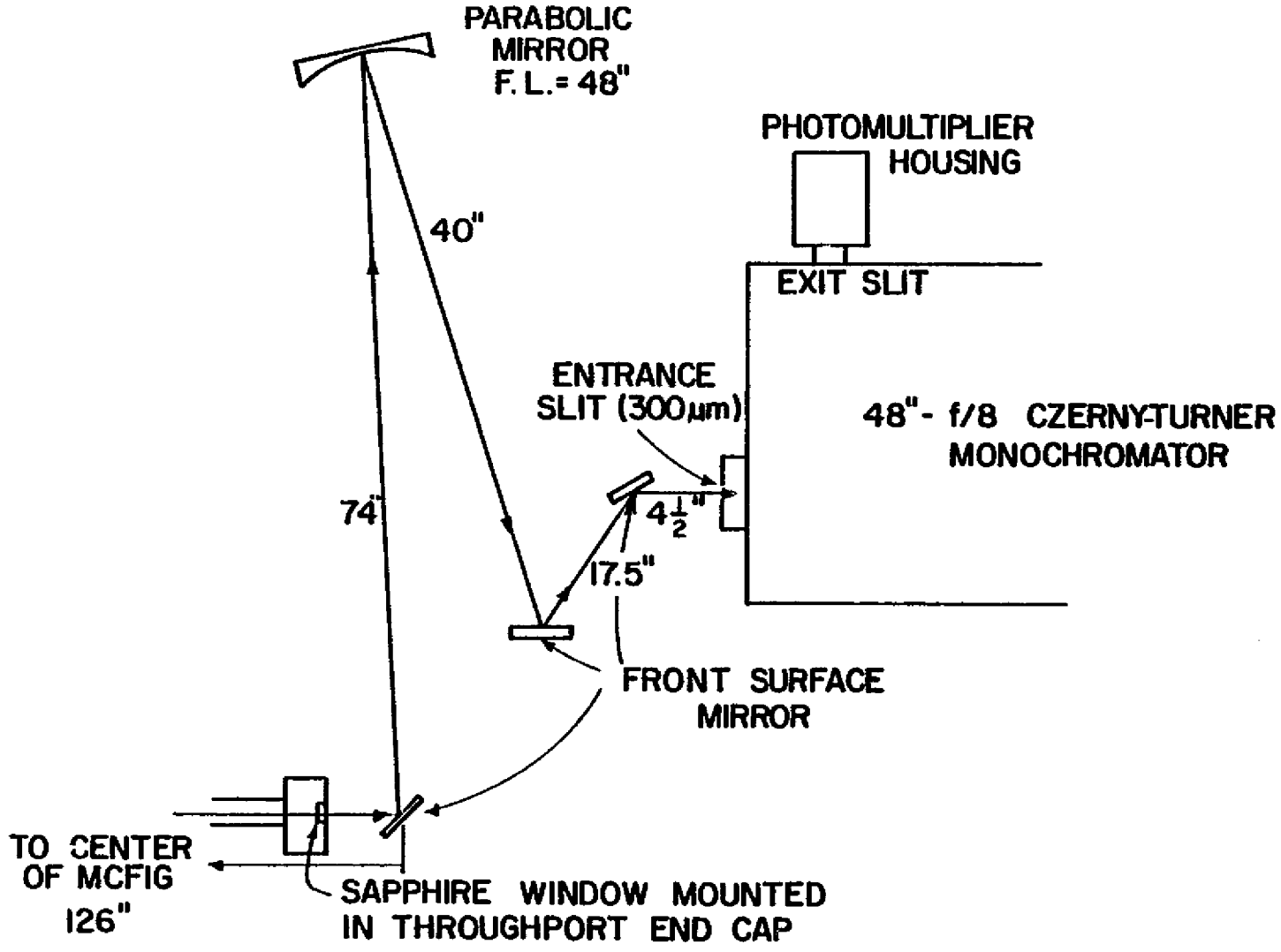

OPTICAL SYSTEM

Figure 25

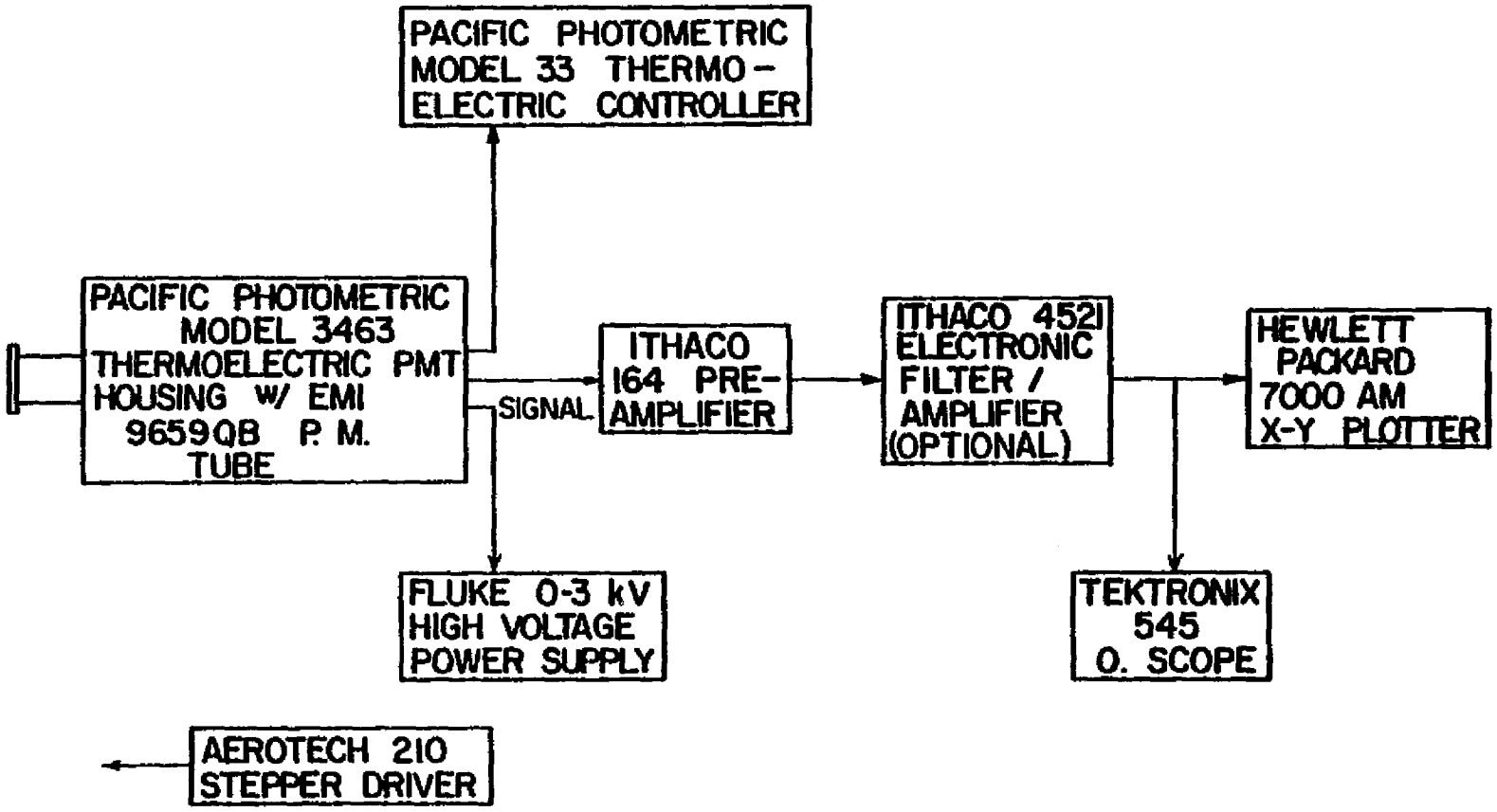

ELECTRONIC SYSTEM

Figure 26

3. Experimental Results

a. Relative Line Intensities:

The observed ^{3}He emission lines are tabulated in Figure 27. The relative intensities of these lines are plotted as a function of ^{3}He fill pressure in Figure 28, part a and b. There appears to be no consistent trend in emission intensity as a function of pressure. While maximum emission for some lines (notably 4471.5, 7065.3 and 7281Å) occurs at less than 760 torr, other lines indicate a monotonically increasing intensity function (3888.7, 4921.9, 5015.7, 5875.7 and 6678.2Å).

A comparison of two line intensities as a function of pressure with the corresponding fission fragment excited lines is depicted in Figure 29. Note that peak emission for the fission fragment case occurs at a much lower pressure than for ^{3}He(n,p)T excitation and, in general, is monotonically decreasing beyond this pressure.

b. Electron Temperatures:

Electron temperatures for the ^{3}He(n,p)T excited plasma were determined by the method of Boltzmann plots outlined in Figure 30. The technique requires the measurement of relative line emission intensities from the plasma. Results for four ^{3}He fill pressures (100,200,400,760 torr) appear in Figures 31, 32, 33, and 34, respectively. For comparison, the data for fission fragment excited ^{4}He emission are included in the figures. Note that the slope of each line is given by $-1/kT$ allowing assignment of electron temperatures. Results for fission fragment and ^{3}He excitation are comparable. This indicates that although the fission fragments produce higher intensity delta rays of higher energy, the excitation appears to be most effectively performed by lower energy (degraded) secondary electrons.

(n,p) Excited ^3He – Observed Lines

THERMAL FLUX - 2×10^{12} n/cm^2-sec
PRESSURE - 100–760 Torr

WAVELENGTH (A)	TRANSITION ARRAY	MULTIPLET
3705.0	1s2p - 1s7d	$^3P^0 - ^3D$
3888.7	1s2s - 1s3p	$^3S - ^3P^0$
4471.5	1s2p - 1s4d	$^3P^0 - ^3D$
4921.9	1s2p - 1s4d	$^1P^0 - ^1D$
5015.7	1s2s - 1s3p	$^1S - ^1P^0$
5047.7	1s2p - 1s4s	$^1P^0 - ^1S$
5875.7	1s2p - 1s3d	$^3P^0 - ^3D$
6678.2	1s2p - 1s3d	$^1P^0 - ^1D$
7065.3	1s2p - 1s3s	$^3P^0 - ^3S$
7281.4	1s2p - 1s3s	$^1P^0 - ^1S$

Figure 27

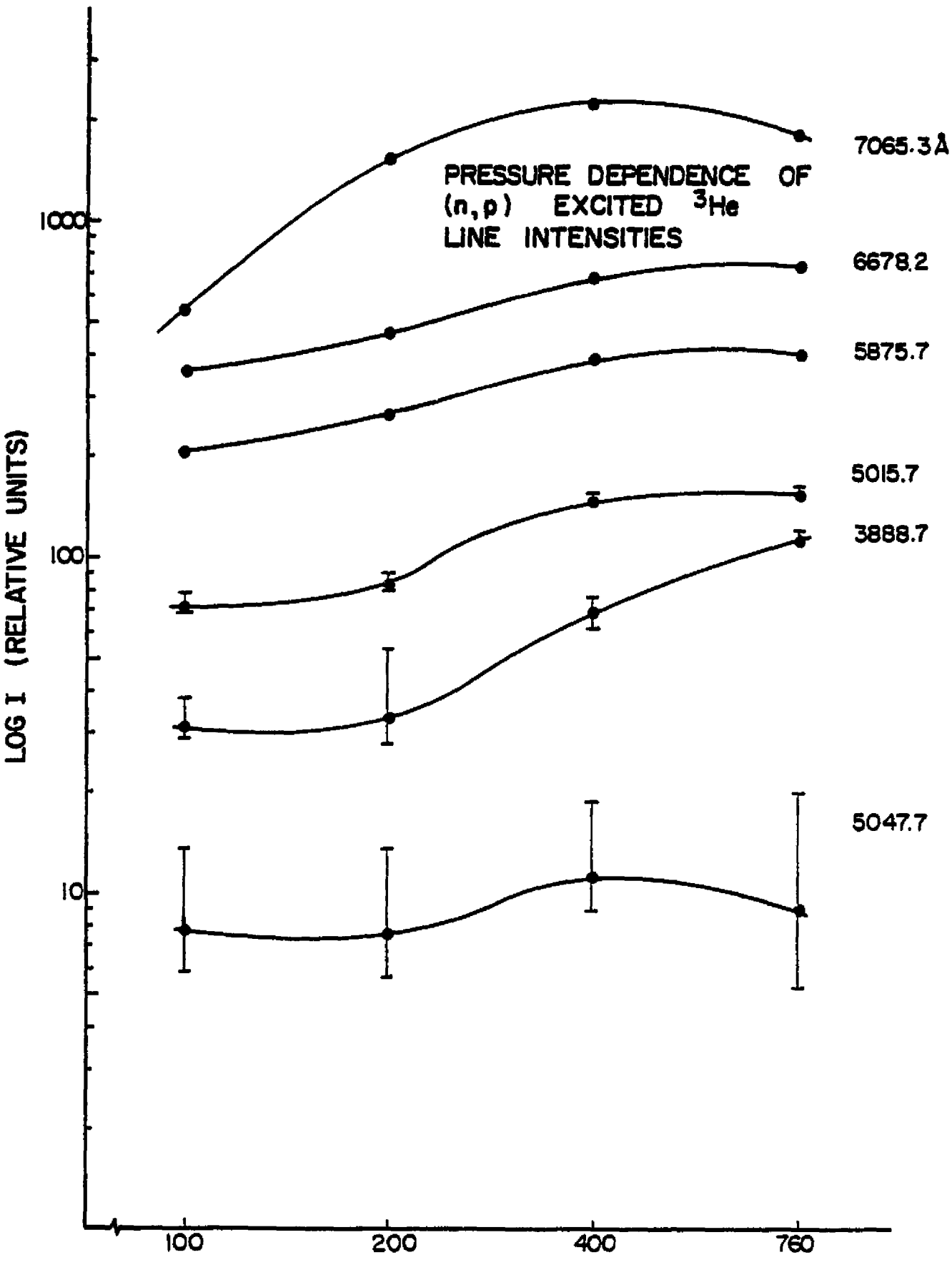
PRESSURE DEPENDENCE OF
(n,p) EXCITED ^{3}He
LINE INTENSITIES
7065.3 Å
6678.2
5875.7
5015.7
3888.7
5047.7
1000
100
10
LOG I (RELATIVE UNITS)
100
200
400
760
PRESSURE – Torr

Figure 28A

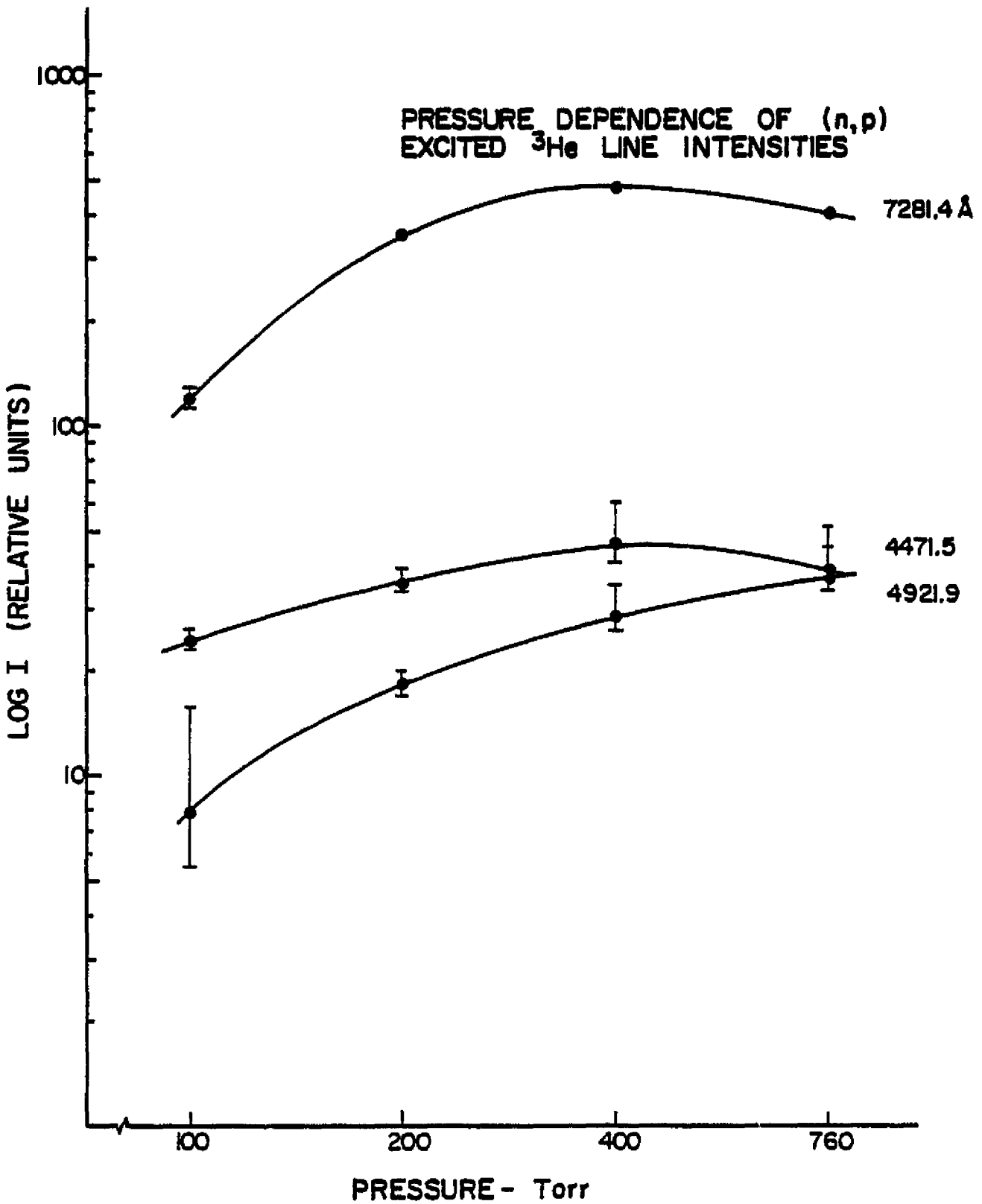
PRESSURE DEPENDENCE OF (n,p)
EXCITED ^{3}He LINE INTENSITIES
7281.4 Å
4471.5
4921.9
LOG I (RELATIVE UNITS)
1000
100
10
100
200
400
760
PRESSURE - Torr

Figure 28B

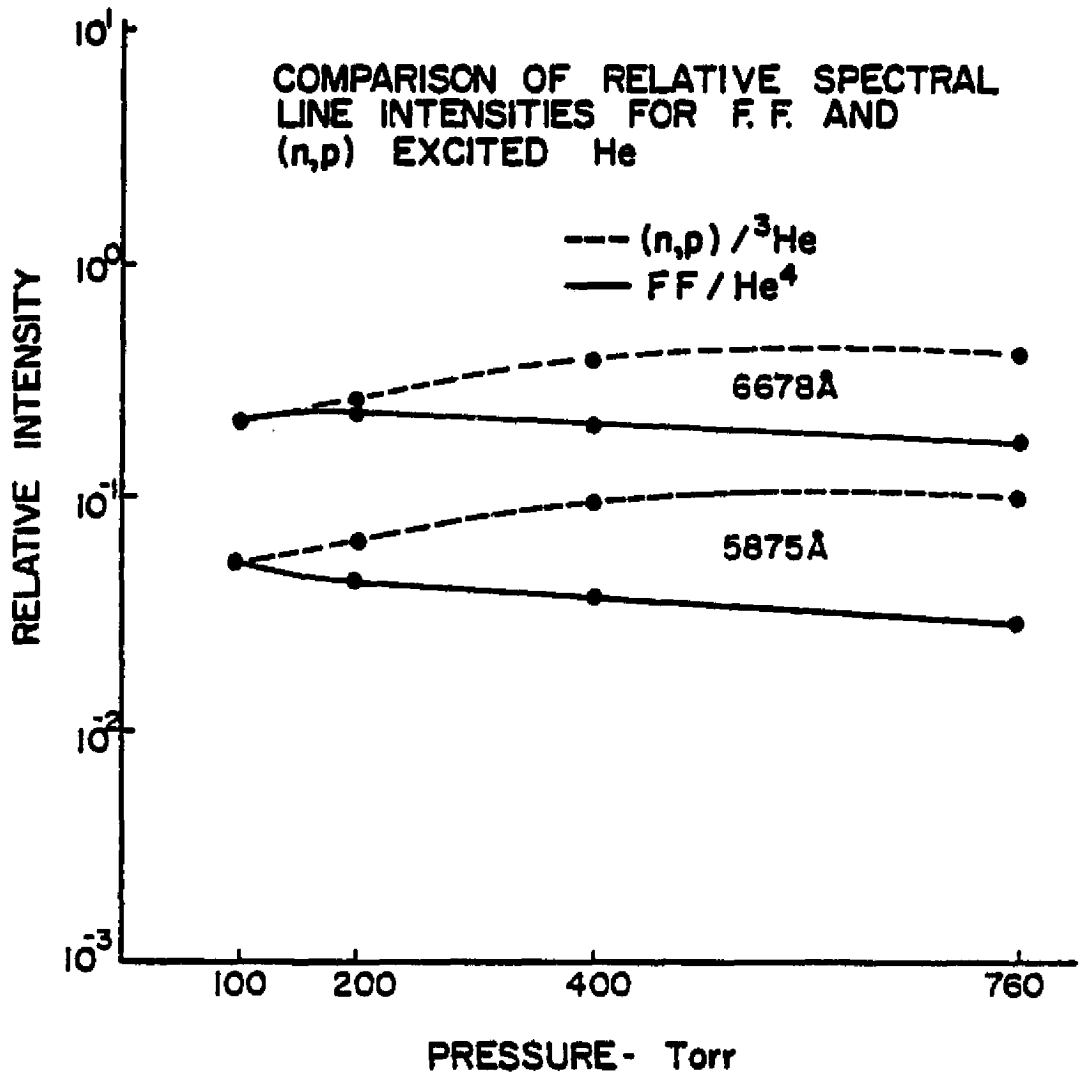
COMPARISON OF RELATIVE SPECTRAL LINE INTENSITIES FOR F. F. AND (n,p) EXCITED He
--- (n,p) / 3He
— FF / He4
6678Å
5875Å
RELATIVE INTENSITY
10^1
10^0
10^-1
10^-2
10^-3
100
200
400
760
PRESSURE - Torr

Figure 29

METHOD OF BOLTZMANN PLOTS

INTENSITY OF A SPECTRAL LINE

$$I = n^* A h\nu$$

FOR A BOLTZMANN ELECTRON ENERGY DISTRIBUTION

$$n^* = n_o \frac{g}{u} \exp(-E/kT)$$

WITH THE RESULT

$$I = n_o \frac{g}{u} \exp(-E/kT) A h\nu$$

WHICH MAY BE REARRANGED TO GIVE

$$\ln\left[\frac{I\lambda}{gA}\right] = \text{CONSTANT} - \frac{1}{kT}E$$

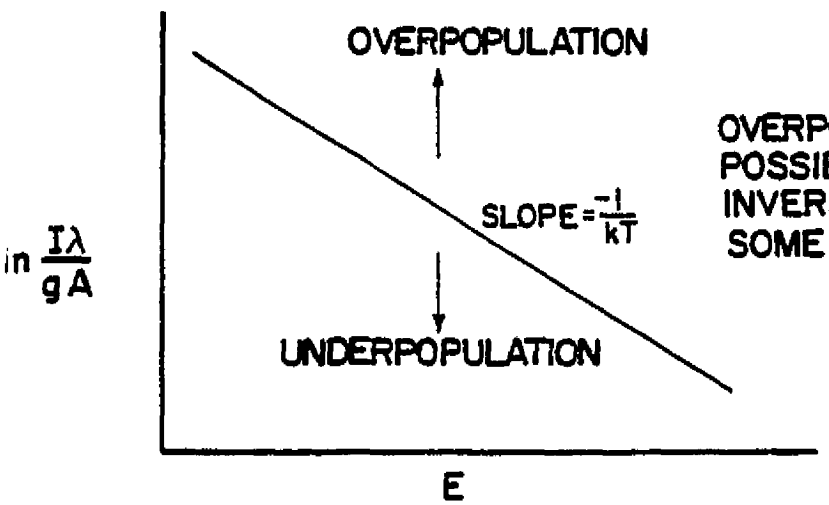

OVERPOPULATED STATES INDICATE POSSIBILITY OF A POPULATION INVERSION WITH RESPECT TO SOME LOWER LYING STATE

Figure 30

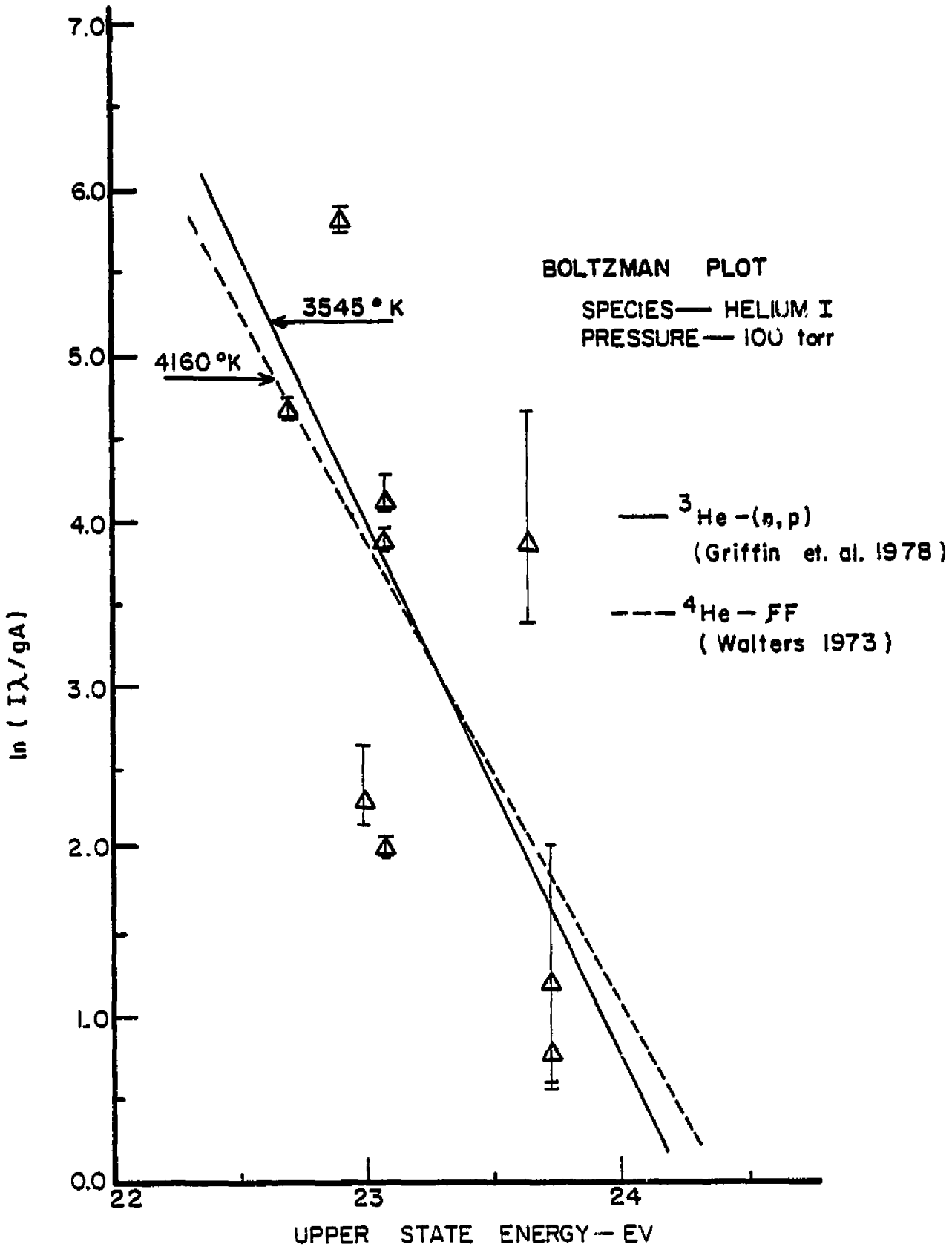
BOLTZMAN PLOT
SPECIES— HELIUM I
PRESSURE— 100 torr
3545 °K
4160 °K
— ^{3}He -(n, p)
(Griffin et. al. 1978)
--- ^{4}He – FF
(Walters 1973)
ln (Iλ/gA)
7.0
6.0
5.0
4.0
3.0
2.0
1.0
0.0
22
23
24
UPPER STATE ENERGY — EV

Figure 31

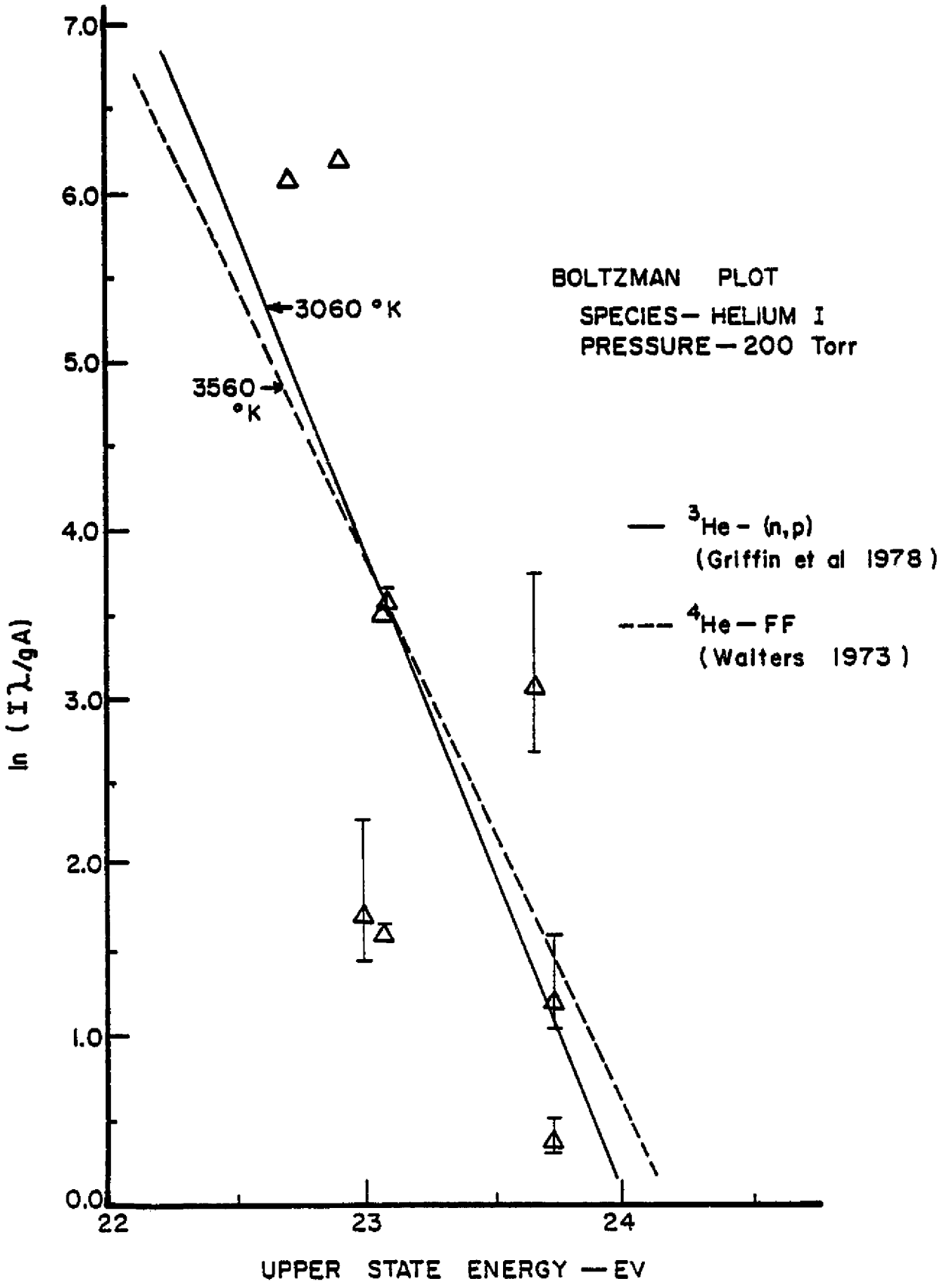
BOLTZMAN PLOT
SPECIES— HELIUM I
PRESSURE— 200 Torr
3060 °K
3560 °K
— ^{3}He - (n,p)
(Griffin et al 1978)
--- ^{4}He — FF
(Walters 1973)
ln (Iλ/gA)
UPPER STATE ENERGY — EV
7.0
6.0
5.0
4.0
3.0
2.0
1.0
0.0
22
23
24

Figure 32

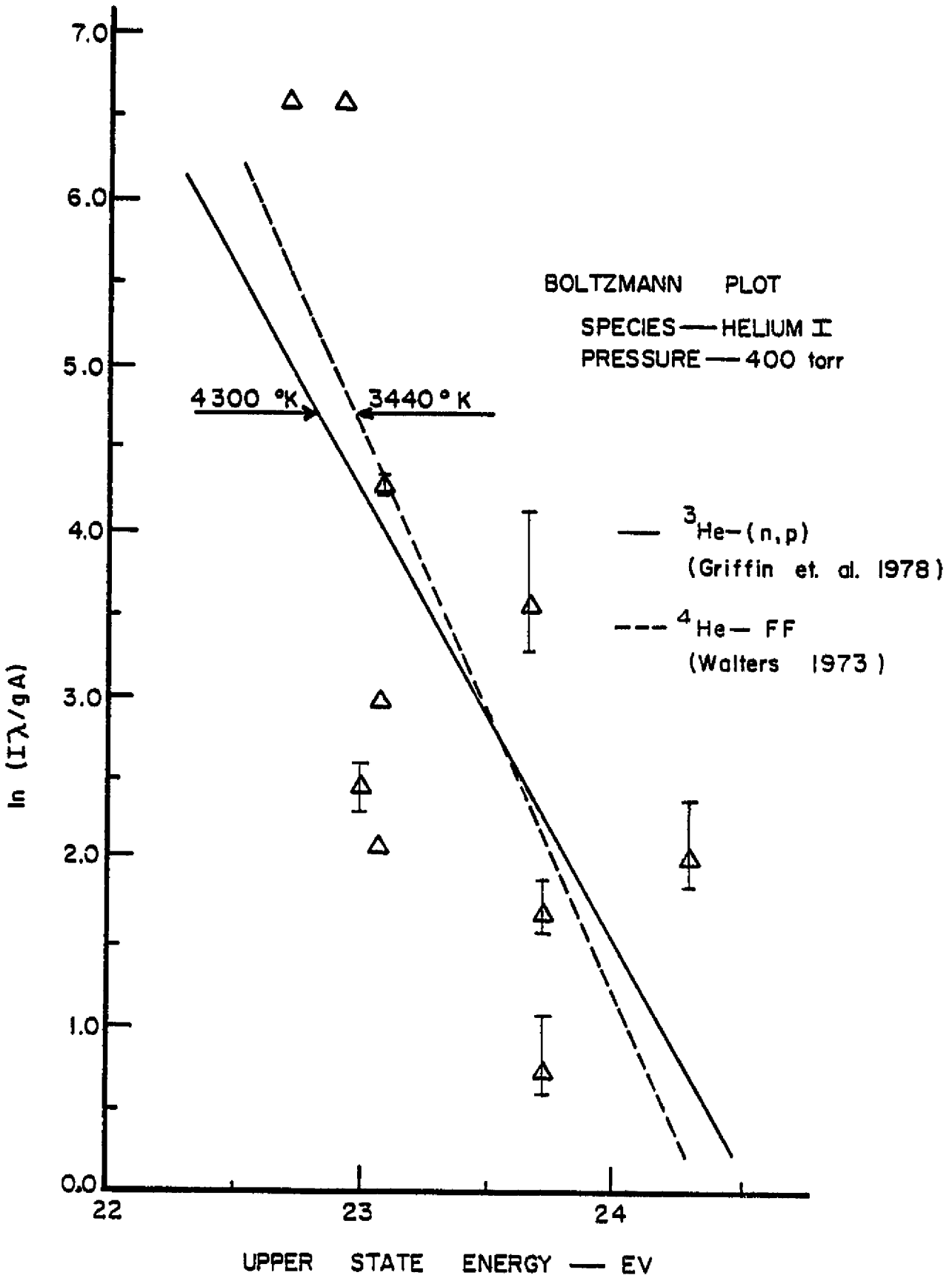
BOLTZMANN PLOT
SPECIES — HELIUM II
PRESSURE — 400 torr
4300 °K
3440 °K
— ^{3}He–(n,p)
(Griffin et. al. 1978)
--- ^{4}He— FF
(Walters 1973)
ln (Iλ/gA)
7.0
6.0
5.0
4.0
3.0
2.0
1.0
0.0
22
23
24
UPPER STATE ENERGY — EV

Figure 33

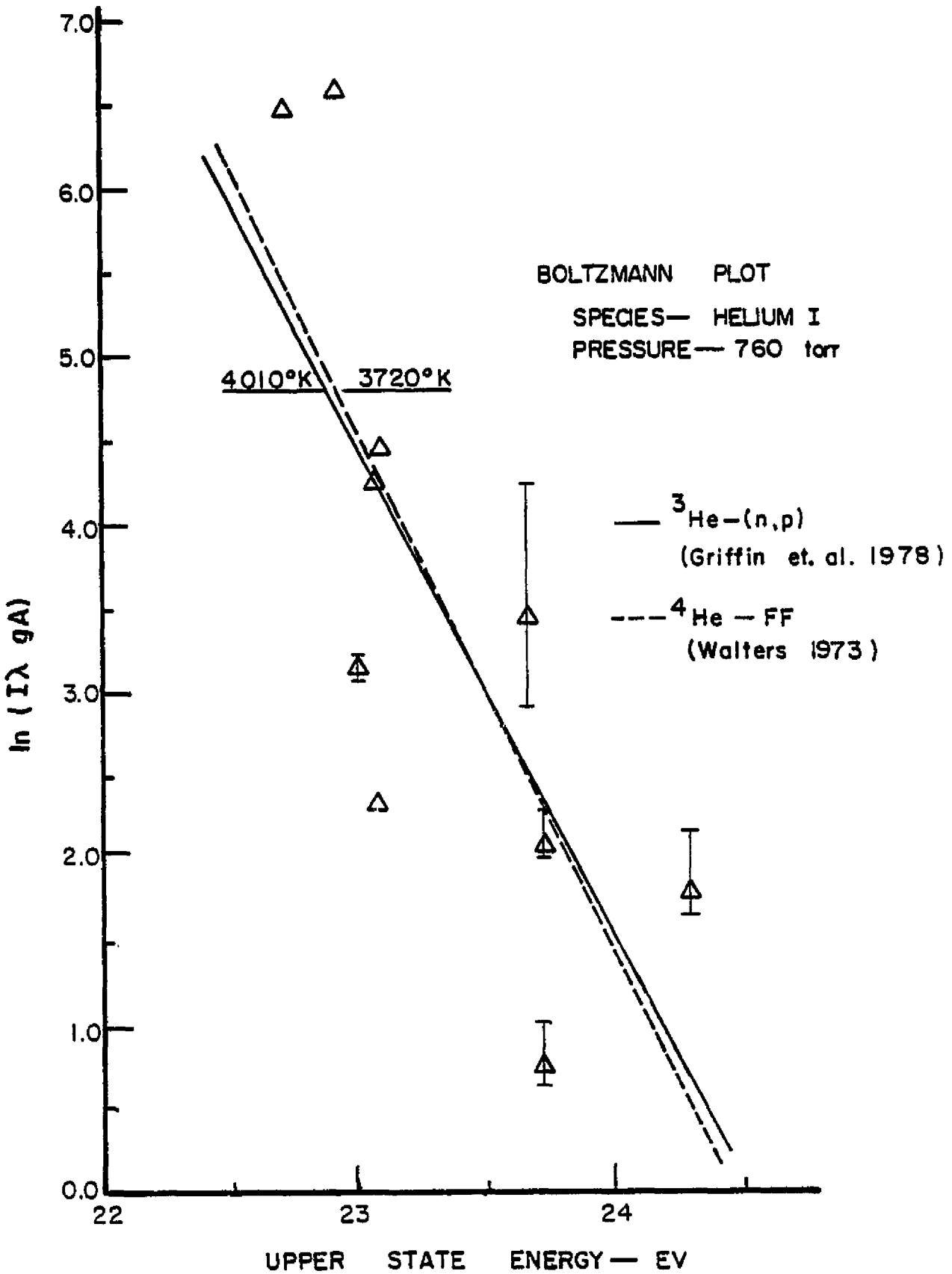
7.0
6.0
5.0
4.0
3.0
2.0
1.0
0.0
22
23
24
ln (Iλ gA)
UPPER STATE ENERGY — EV
BOLTZMANN PLOT
SPECIES— HELIUM I
PRESSURE— 760 torr
4010°K
3720°K
— 3He-(n,p)
(Griffin et. al. 1978)
---4He — FF
(Walters 1973)

Figure 34

c. Non-Equilibrium Effects:

Only one possible population inversion was observed between the 1s3p-1s3d states corresponding to a 18.62 μm transition. A plot of the n_{upper}/n_{lower} population ratio appears in Figure 35. Note that this population inversion is marginal and pressure dependent.

A single population inversion in the fission fragment excited case was observed by Walters. This inversion was observed between the 4^1P and 4^1D states corresponding to a 216 μm transition. A comparison of the n_{upper}/n_{lower} ratio for this case with that for the He^3 case appearsin Figure 36. Note that this inversion is also pressure dependent peaking at a lower pressure than for the ^3He case.

C. Lifetime System

1. Purpose of Experiments

The design of nuclear pumped laser systems requires the knowledge of excited state lifetimes for laser candidate gases. In the case of gas excitation by uranium foils or He^3 the transition probabilities are obtainable from absolute emission intensity measurements on neutron irradiated samples (e.g., in a nuclear reactor). The accompanying low emission intensities and high noise levels severely limit the accuracy of these measurements and, therefore, alternative techniques are desirable.

Such a technique is delayed coincidence spectroscopy. In this experimental technique, the use of a spontaneously fissioning source (Cf^{252}) allows fission fragment excitation data to be acquired without the use of a reactor. Since the spontaneous fission flux is necessarily low, a single photon counting technique is most suitable for the lifetime measurements.

Of primary interest are:

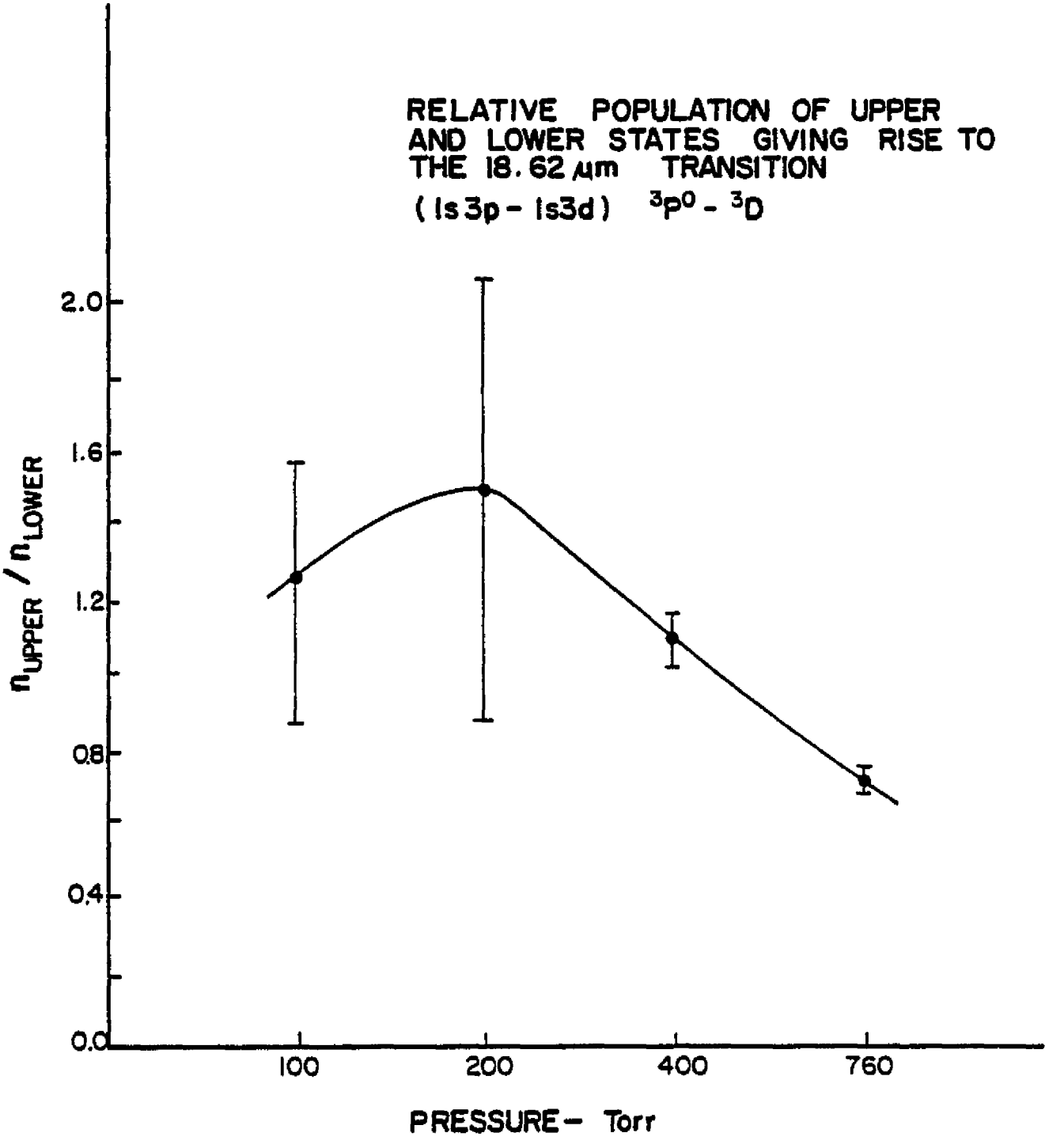
RELATIVE POPULATION OF UPPER AND LOWER STATES GIVING RISE TO THE 18.62 μm TRANSITION
(1s3p - 1s3d) $^3P^0 - ^3D$
n_{UPPER} / n_{LOWER}
2.0
1.6
1.2
0.8
0.4
0.0
100
200
400
760
PRESSURE - Torr

Figure 35

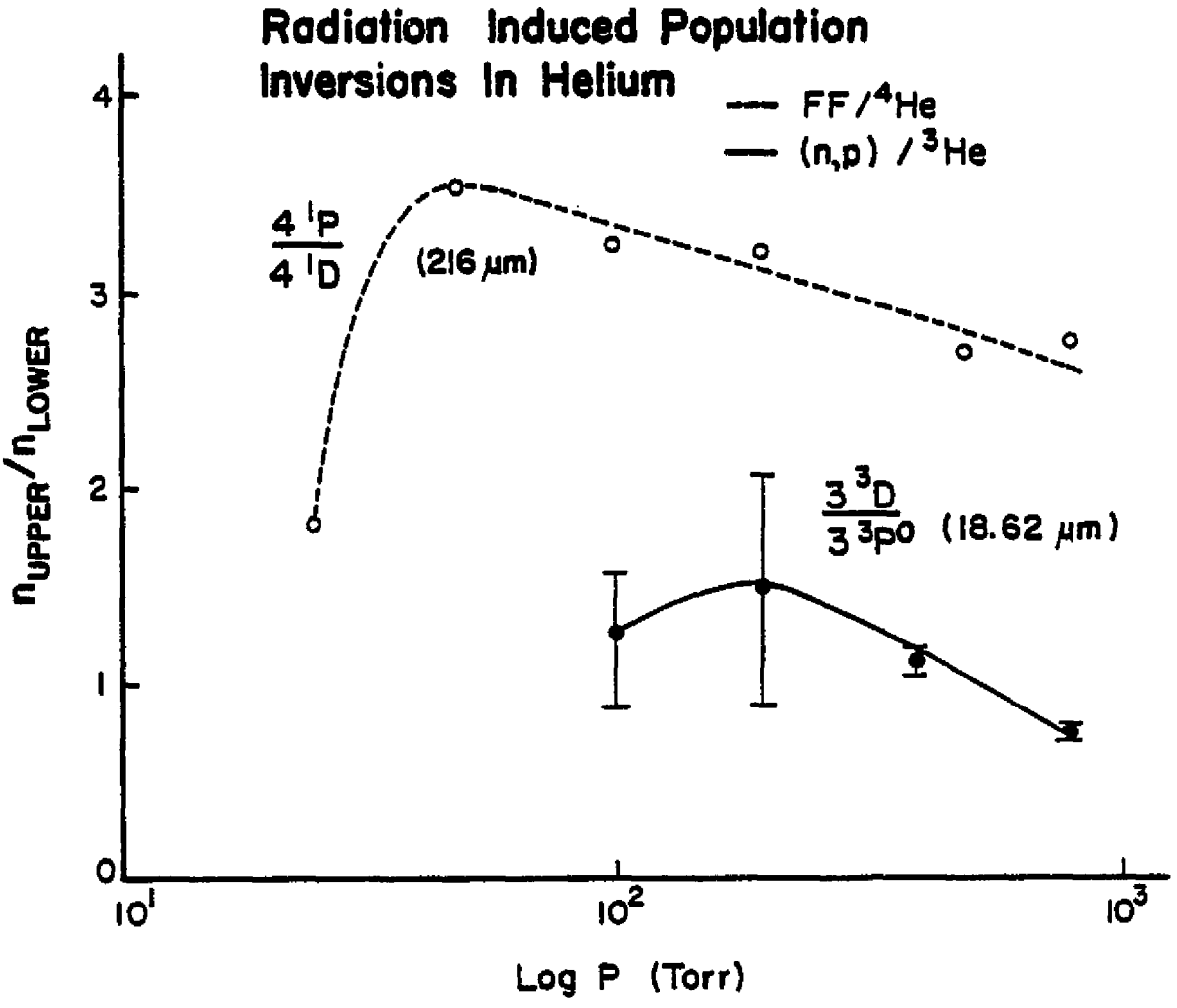
Radiation Induced Population Inversions In Helium
FF/4He
(n,p) /3He
4 1P / 4 1D
(216 μm)
3 3D / 3 3P0 (18.62 μm)
nUPPER/nLOWER
0
1
2
3
4
10^1
10^2
10^3
Log P (Torr)

Figure 36

1. the variation of the excited state lifetime with total pressure, and

2. the influence of additive gases (e.g., UF_6) upon state decay rates.

UF_6 is of particular interest as it appears to be the most viable option for volume excitation. While He^3 is the most amenable of the excitation gases (due to its high number of metastable states) its associated low decay energy severely limits the achievable power densities. The ensuing paragraphs discuss the delayed coincidence spectroscopy system, hereafter called the lifetime system, and the results of past and ongoing experiments. More detailed discussion is to be found in references 1, 2, and 3.

2. Experimental Device

A schematic of the delayed coincidence spectroscopy (lifetime) system appears in Figure 37. Briefly, it consists of a source chamber (containing the spontaneous fission source and the gas under test), a total luminosity channel (signals the occurrence of a fission event), a specific luminosity channel (signals the decay of an excited atomic/molecular state), a time to pulse height converter (measures the time increment between fission and state decay) and a multichannel analyzer for data accumulation over extended acquisition times.

The source/gas chamber consists of a modified stainless steel nipple with a quartz window affixed to one end for total luminosity transmission and a sapphire window on the other for extended optical transmission. Gas excitation was accomplished by a Cf^{252} source mounted on the chamber wall. Cf^{252} undergoes spontaneous fission and the source used emitted about 6×10^3 fission fragments per second.

The birth of a fission fragment is signaled by a high luminosity photon burst detected by PM1. This photon emission is a result of gas excitation

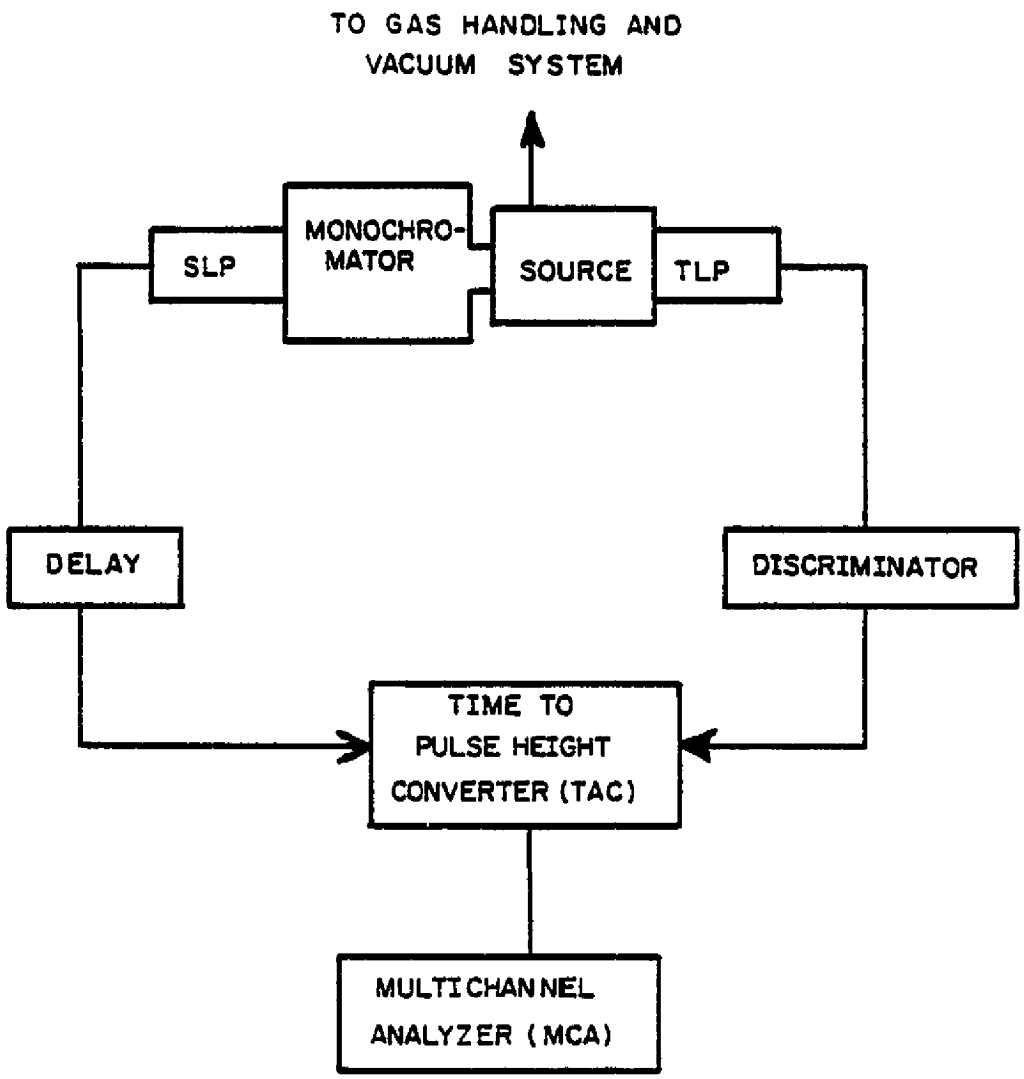

Figure 37. SYSTEM for LIFETIME MEASUREMENT

by the fission fragment and the generated delta rays followed by the subsequent decay of all short lifetime states and ion-electron recombination. The total luminosity photomultiplier output (PM1) is passed through a discriminator which effectively eliminated false starts due to the lower amplitude gamma emission. The discriminator output starts the time to pulse height converter. Decay of the excited state level of interest is accompanied by photon emission of known wavelength for which the spectrometer is tuned. This decay photon is detected by PM2, the output of which is delayed and passed to the stop input of the time to pulse height converter (TPHC).

The output of the TPHC is a series of voltage pulses of amplitude proportional to the excited state lifetime. These are accumulated in the MCA over a time interval determined by the desired statistical accuracy of the lifetime measurement.

3. Experimental Procedure

Prior to all experimental measurements, the test chamber was evacuated via a combination of roughing, diffusion and ion pumps to a hard vacuum of 5×10^{-9} torr. (Note that in the case of the UF_6 additive experiments, the use of the ion pump was deemed unadvisable so that the ultimate vacuum was approximately 10^{-5} torr for these experiments.) The chamber was then filled with research grade gas and the pressure measured to within 1 torr with a Wallace and Tiernan diaphragm type gauge. Due to chamber wall outgassing, data acquisition times were limited to a maximum of 72 hours in order to maintain a tolerable gas purity.

The resulting distribution of observed pulses is an exponential decay as a function of channel numbers. The decay constant gives the collisional lifetime of the state. The radiative lifetime (or transition probability) can be obtained by measuring the collisional lifetime as a function of

pressure and extrapolating back to zero pressure. All lifetime determinations were made by applying a least error curve fitting scheme to the data. This algorithm is discussed in the references.

4. Experimental Results

The experimental results based on the use of the delayed coincidence spectroscopy system can be grouped into three areas: 1) pure gas studies, 2) UF_6 additive studies, and 3) electric field augmentation/perturbation studies. These three areas are now discussed in detail.

a. Pure Gas Studies

In this study, the variation of excited state lifetimes for pure nitrogen, carbon tetrafluoride, and mixtures of neon/nitrogen, helium/nitrogen, and argon/nitrogen at various total pressures and mixture ratios were investigated.

(1) Nitrogen

A sample data set for the $C^3\pi_u$ state lifetime of nitrogen for two pressures appears in Figure 38. Note that increased pressure decreases the upper state lifetime, a result attributable to two-body collisional deexcitation. Indeed, the upper state inverse decay time is a highly linear function of pressure up to pressures of 800 torr as evidenced by Figure 39. The departure from linearity at greater pressures is a result of the increasing influence of three body deexcitation mechanisms.

(2) Neon/Nitrogen Mixtures

An extensive study was made of neon and neon/nitrogen mixtures. Using this mixture provided the opportunity of viewing, simultaneously, three lines from three different species; atomic neon, molecular nitrogen, and the nitrogen molecular ion. The experimental results for pure neon utilizing the 585.2 nm line

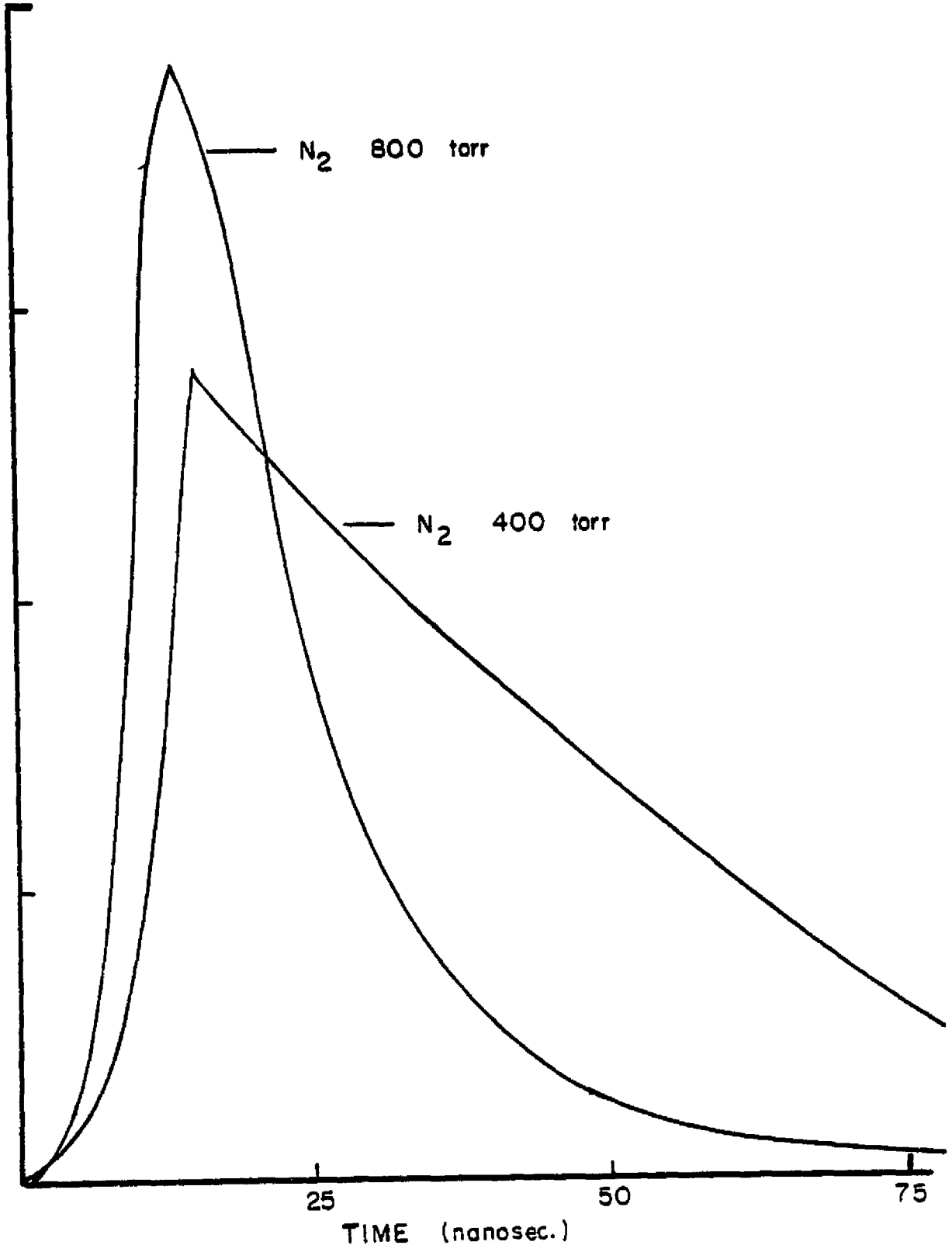

Figure 38. Decay Curves for Nitrogen $C^3\Pi_u$ State

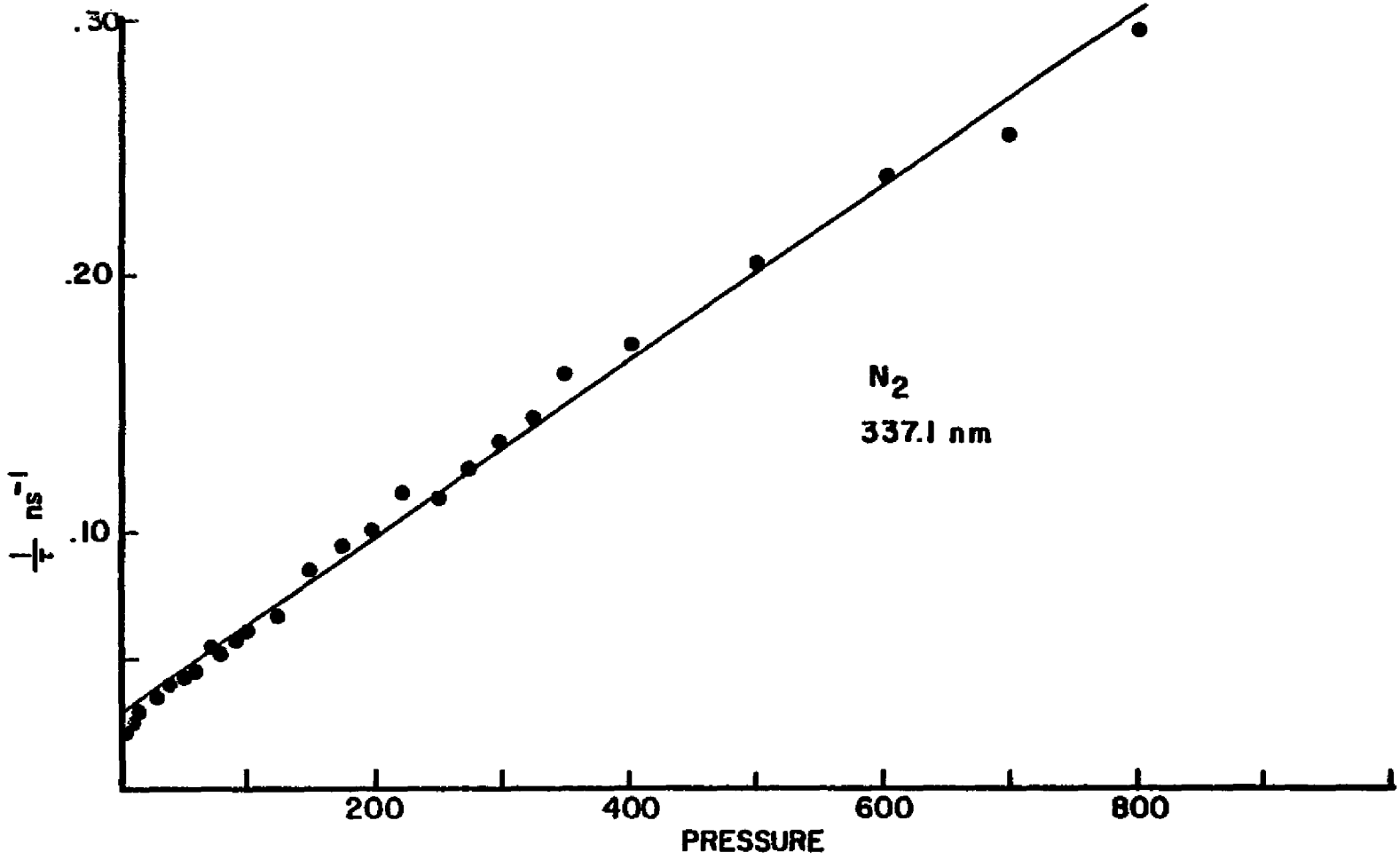

Figure 39. Inverse Decay Time Versus Pressure for 337.1 nm.

appear in Figure 40 and the results for various mixture ratios of neon/nitrogen appear in Figures 41, 42, and 43. Note that k_1 is the sum of all transition probabilities from the upper excited states of the observed line, k_2 is the two-body collisional quenching rate, and τ_r is the radiative lifetime of the upper excited state ($k_1=1/\tau_r$). All values are calculated based on the observed data. Looking first at the 585.2 nm line in pure neon, we find a radiative lifetime of 16.6 ± 0.7 ns. As the nitrogen impurity concentration increased from 1% to 10% to 50% there was no significant change in the lifetime of the neon excited state. This might be expected since there was a very poor energy match between the levels of neon and those of nitrogen. Calculated values for the collisional transfer coefficient, appeared to show a systematic decrease with nitrogen concentration. If this trend is real, it means that the nitrogen is less effective than the neon in quenching the level that gives rise to the 585.2 nm line. The effect of the neon admixture on the $C^3\pi_u$ state of N_2 was also investigated and the experimental results appear in Figures 44, 45, 46, and 47. It is seen that when the nitrogen was the dominant gas, the lifetime varied strongly with pressure; whereas, when the neon was dominant, there was very little change. This again indicates that there was not much interaction between the levels of the two gases. Analysis was also made of the 391.4 nm emission due to the N_2^+ molecular ion. These results appear in Figures 48 and 49. This line is reported to have a radiative lifetime of about 65 ns and the experimental results are contradictory to this. In pure neon, the first negative band due to nitrogen impurities within the gas had a lifetime of 90,000 ± 3500 ns. As the nitrogen concentrations increased to 10% and 50%, the lifetime dropped to 10,000 ± 400 and finally, to 3800 ± 150 ns.

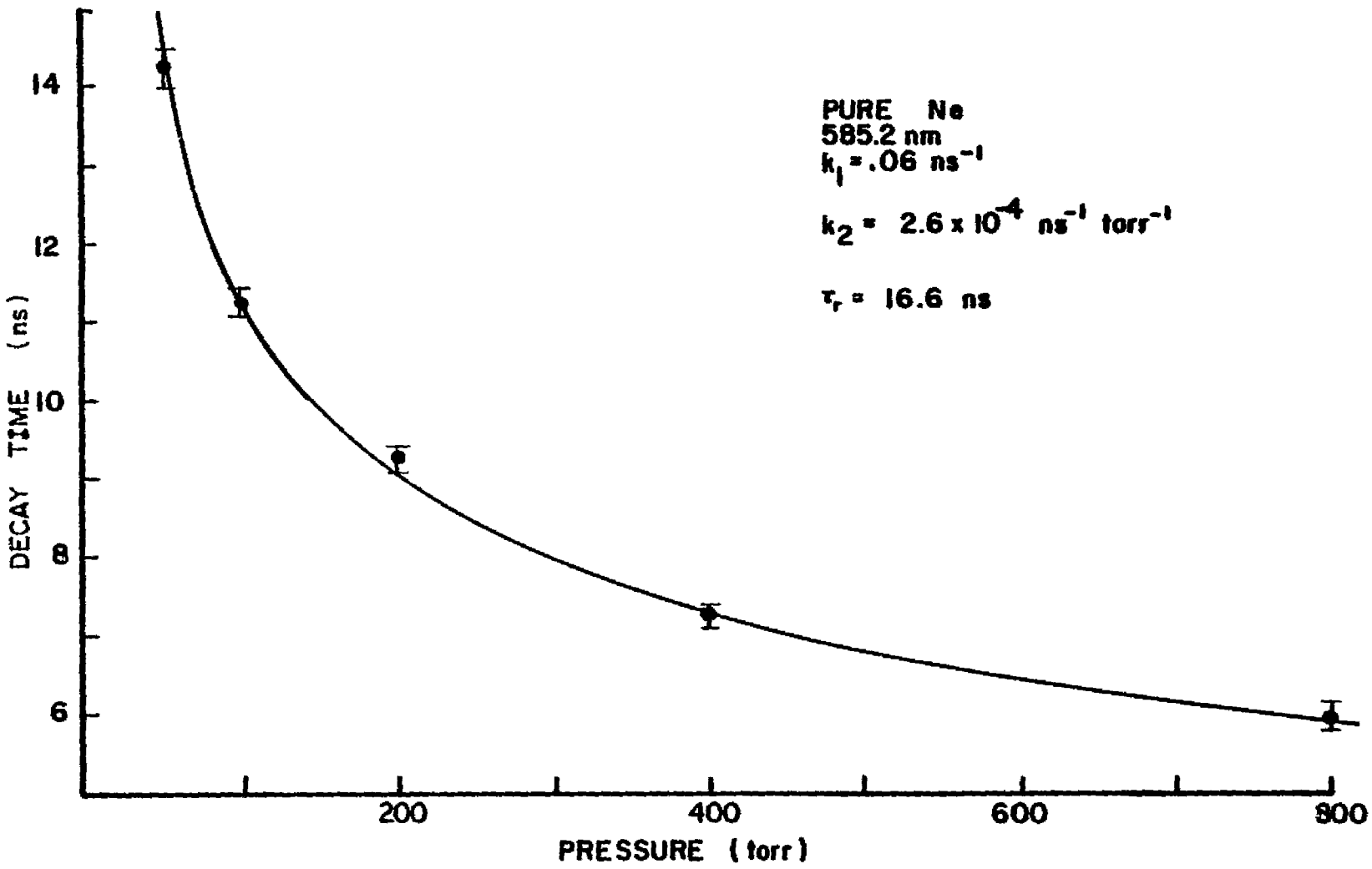

Figure 40. Decay Time Versus Pressure for 585.2 nm

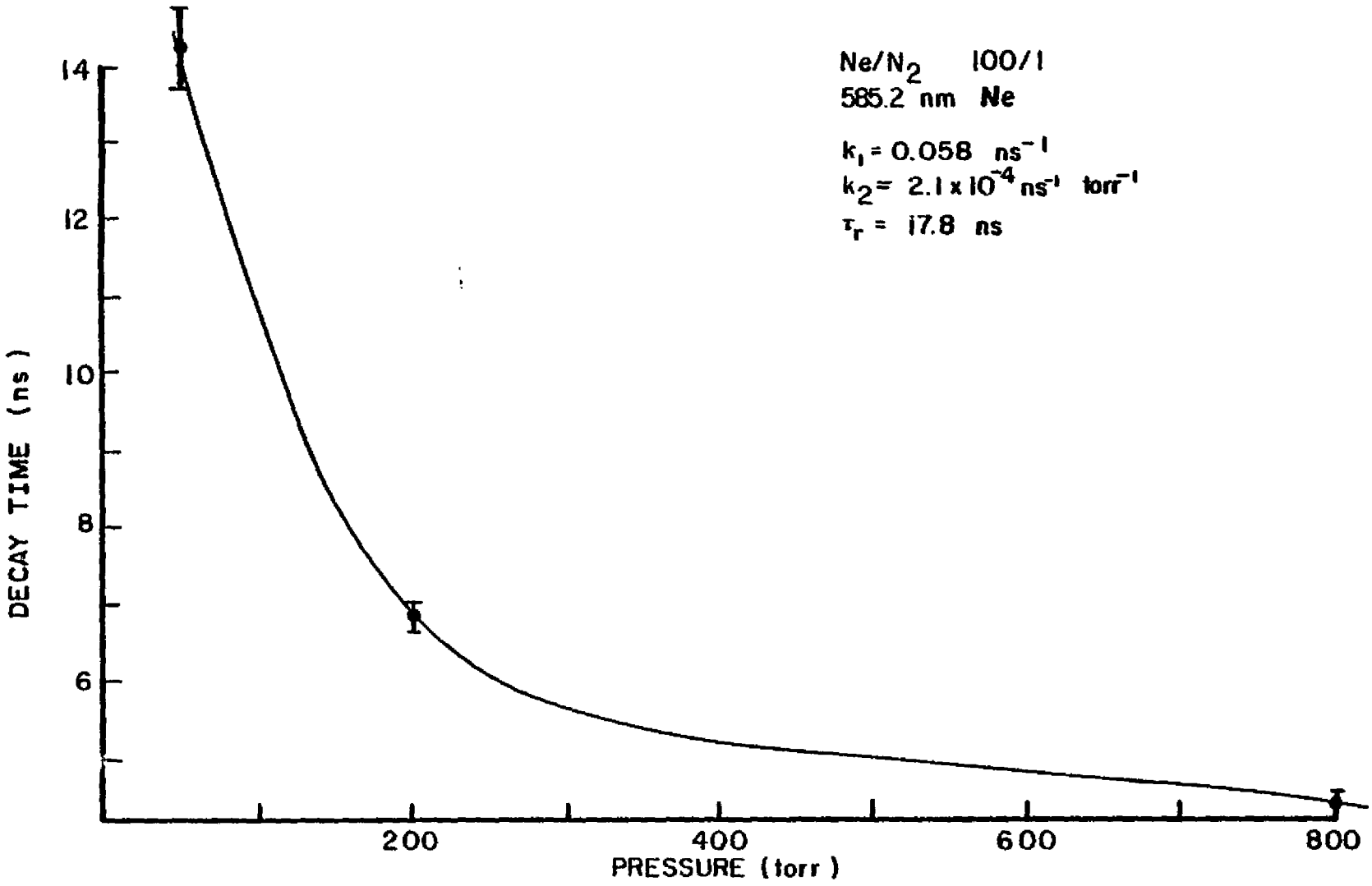

Figure 41. Decay Time Versus Pressure for 585.2 nm

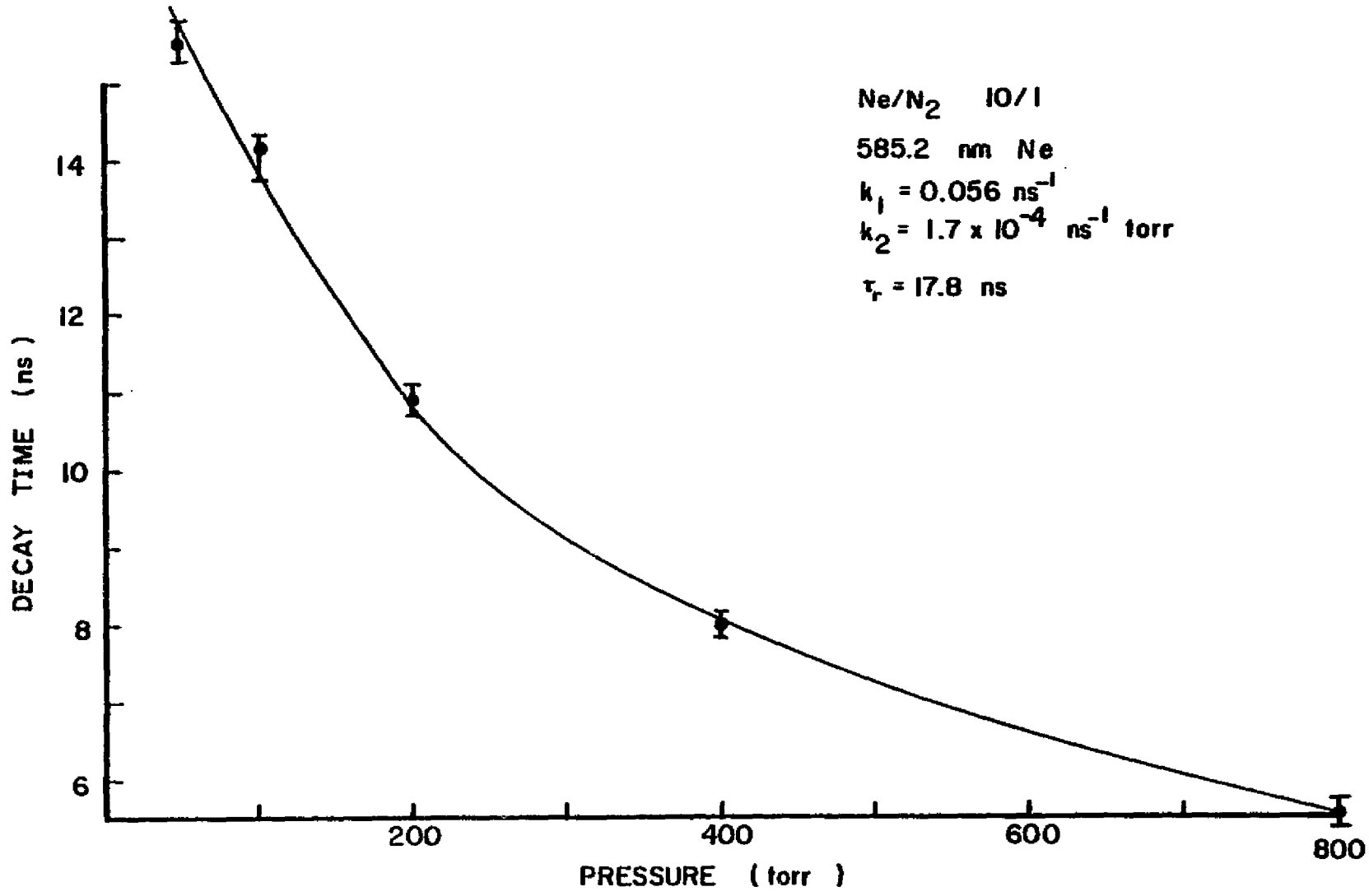

Figure 42. Decay Time Versus Pressure for 585.2 nm

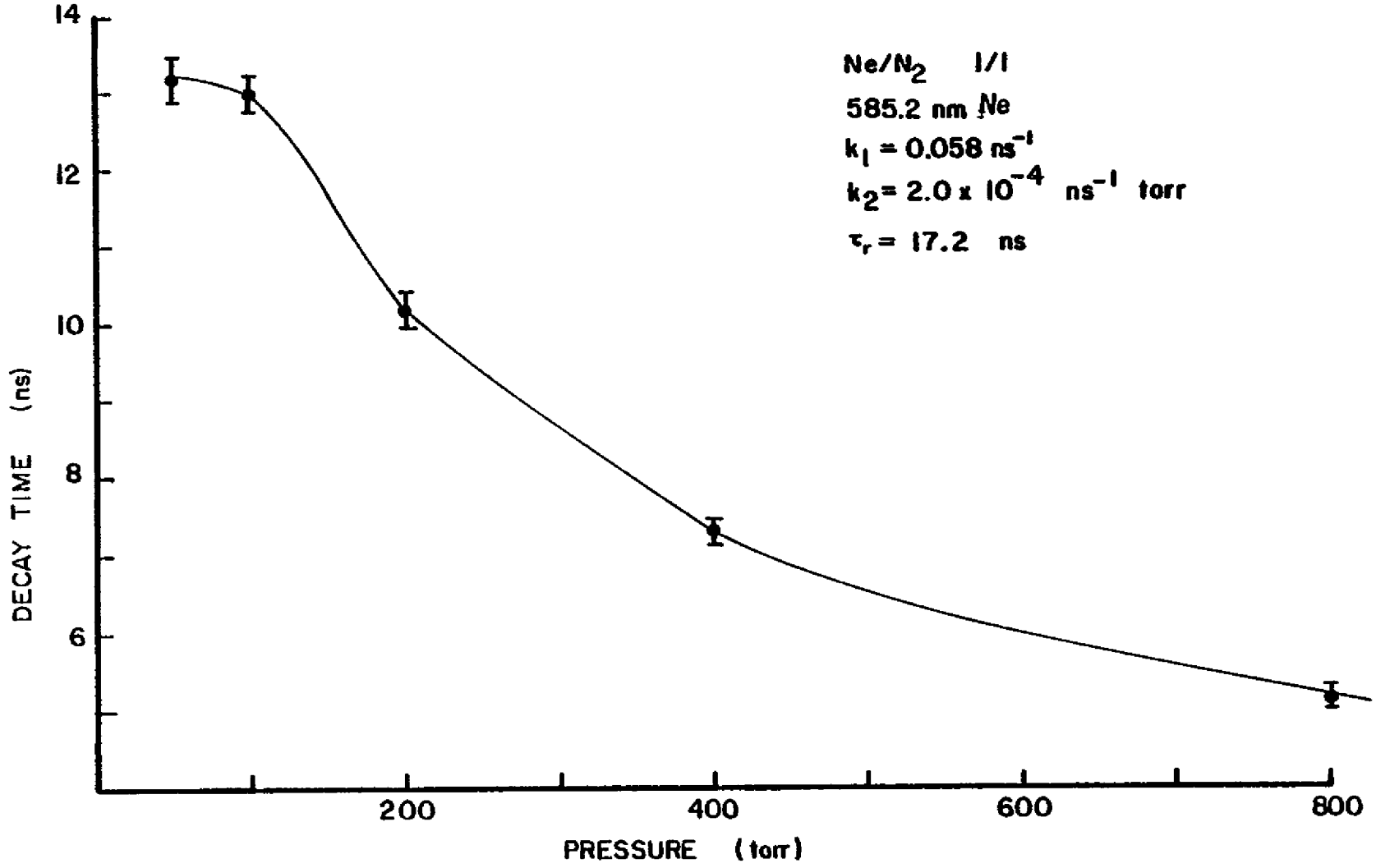

Figure 43. Decay Time Versus Pressure for 585.2 nm

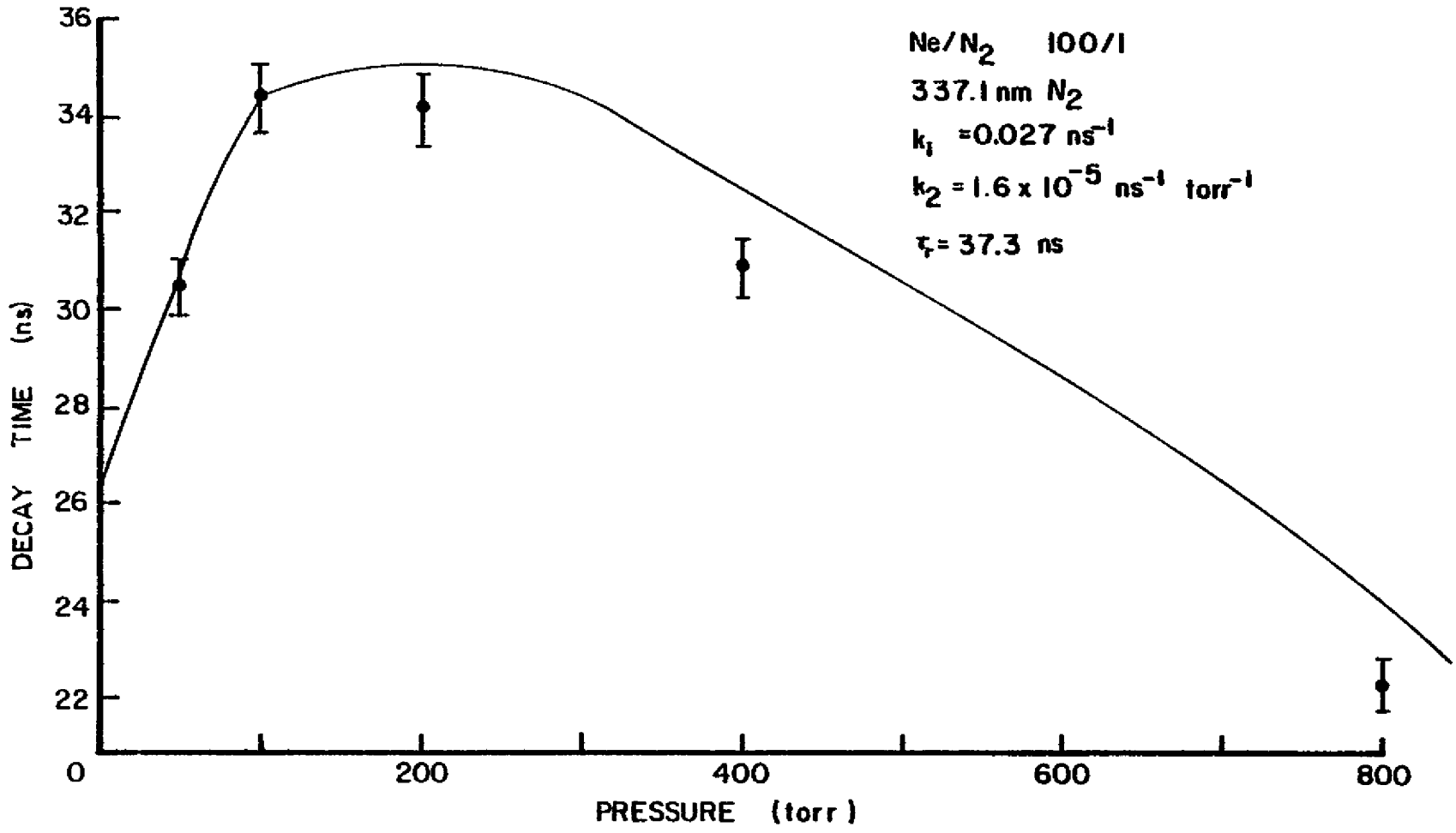

Figure 44. Decay Time Versus Pressure for 337.1 nm

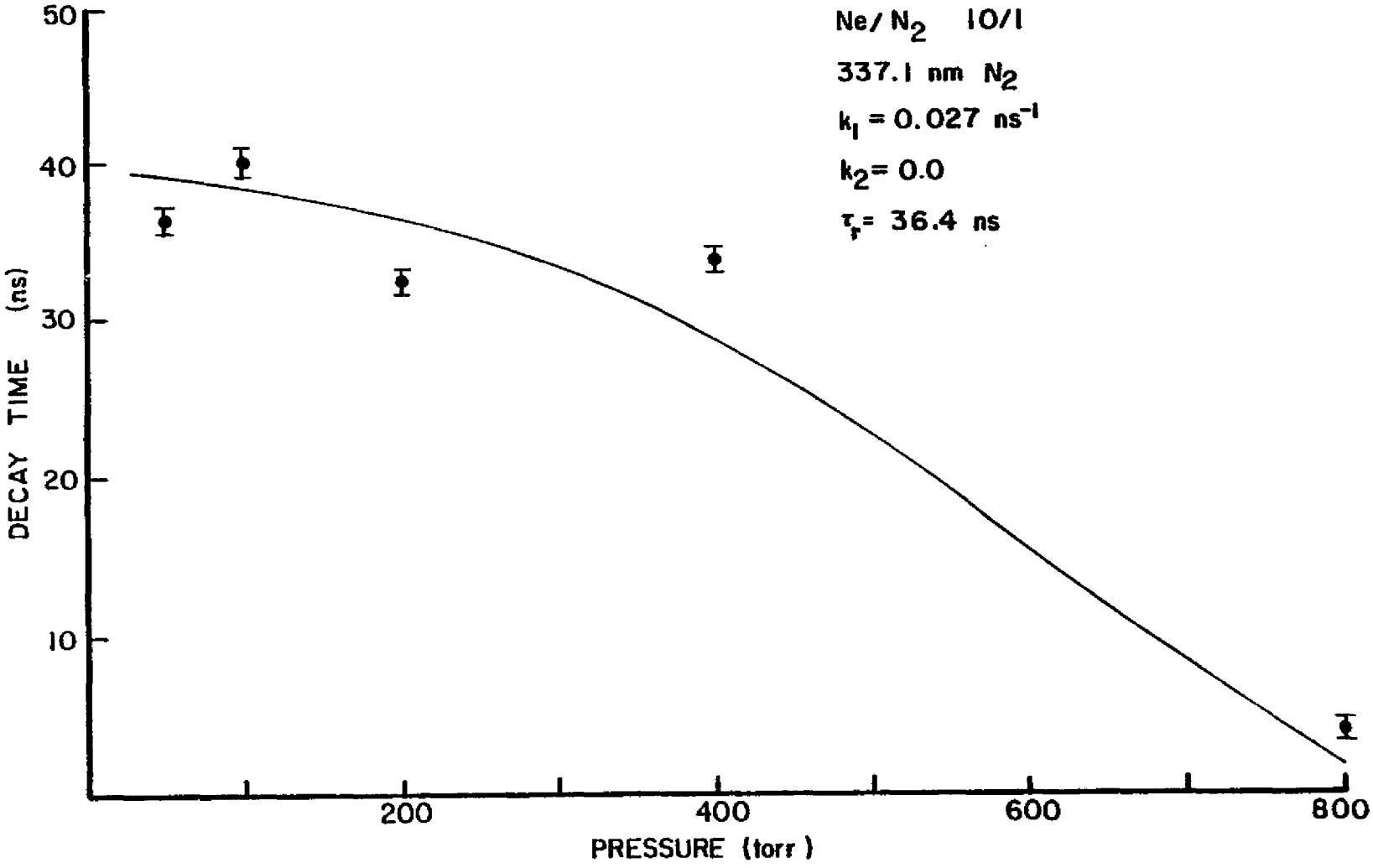

Figure 45. Decay Time Versus Pressure for 337.1 nm

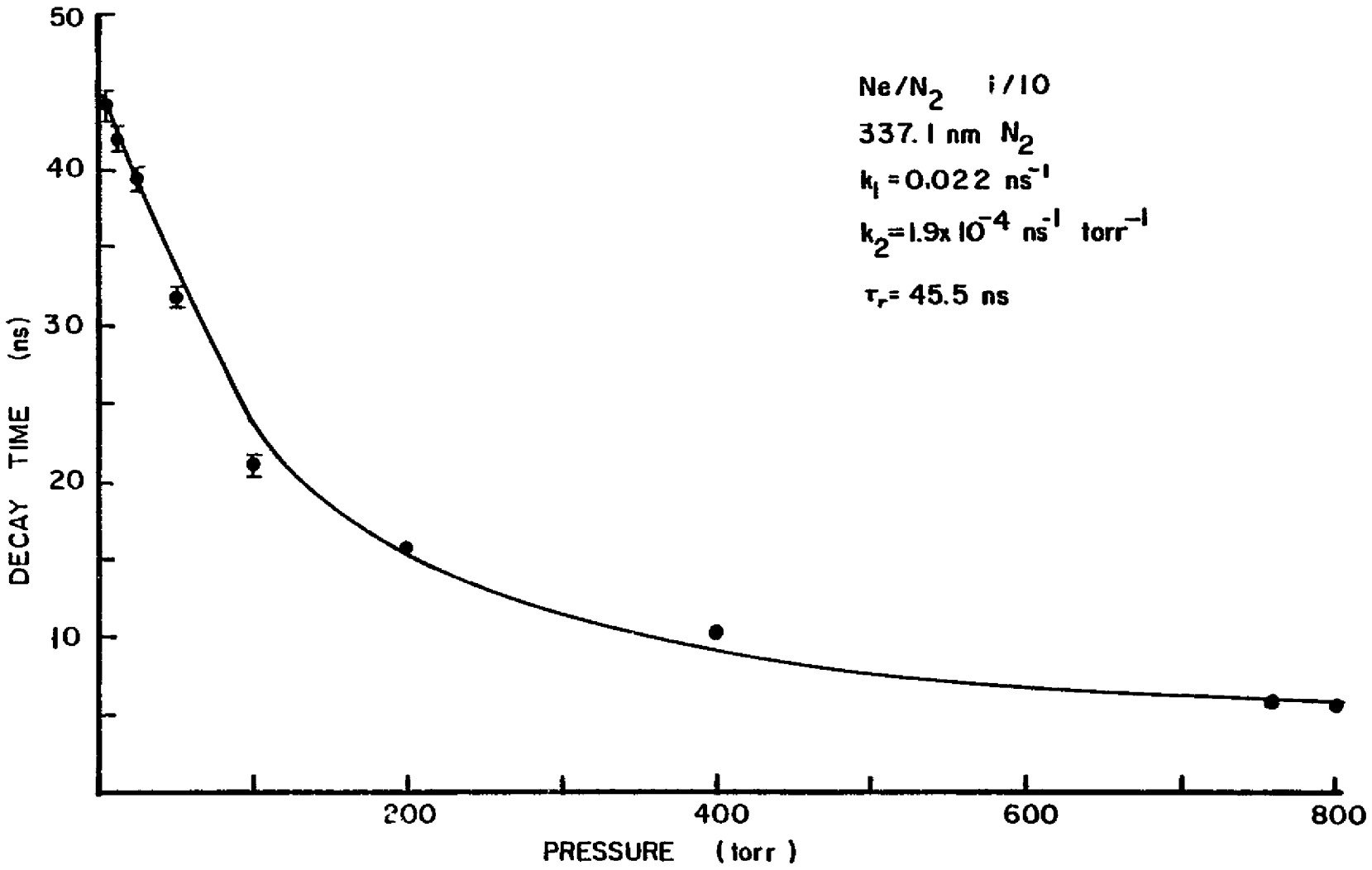

Figure 46. Decay Time Versus Pressure for 337.1 nm

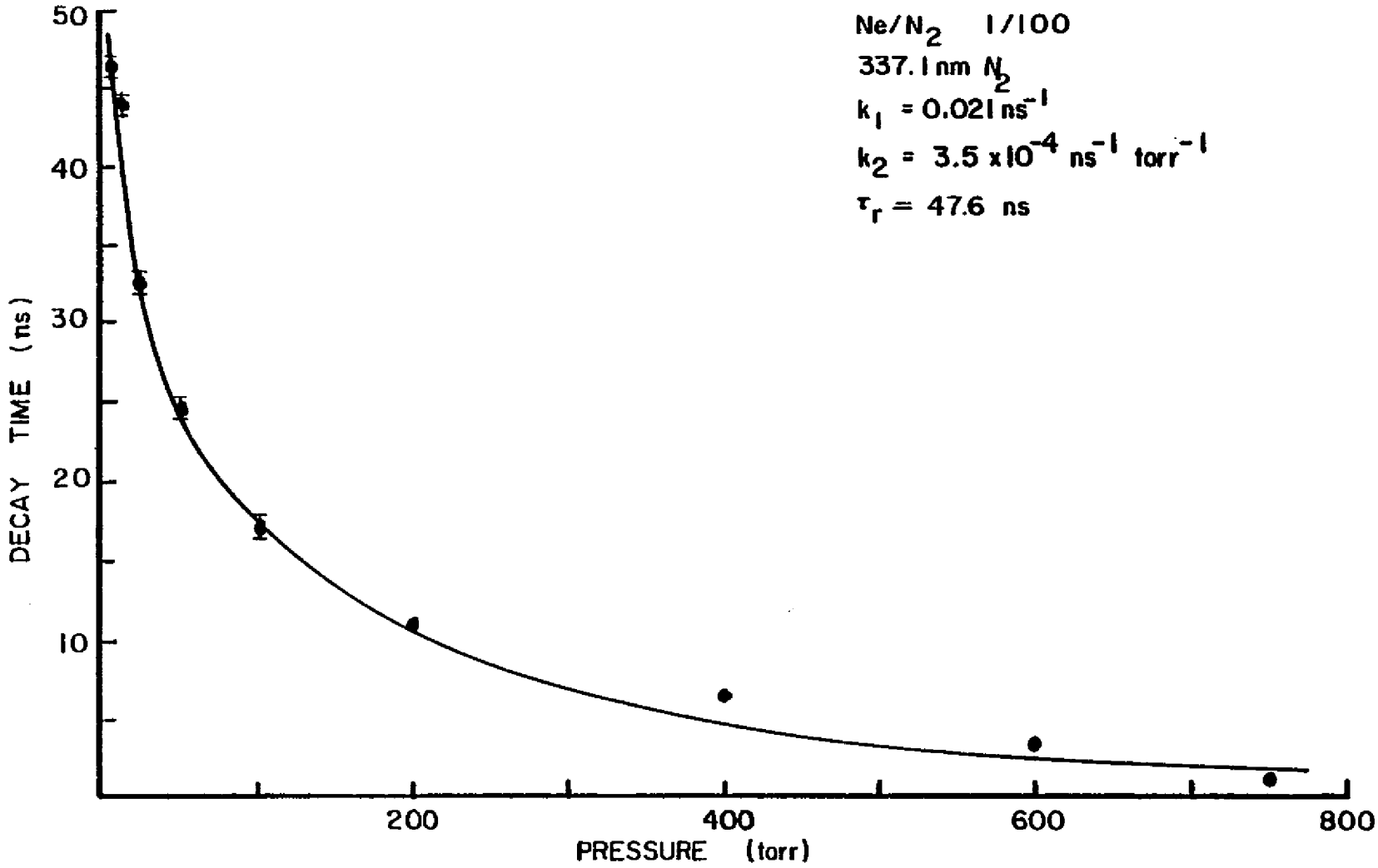

Figure 47. Decay Time Versus Pressure for 337.1 nm

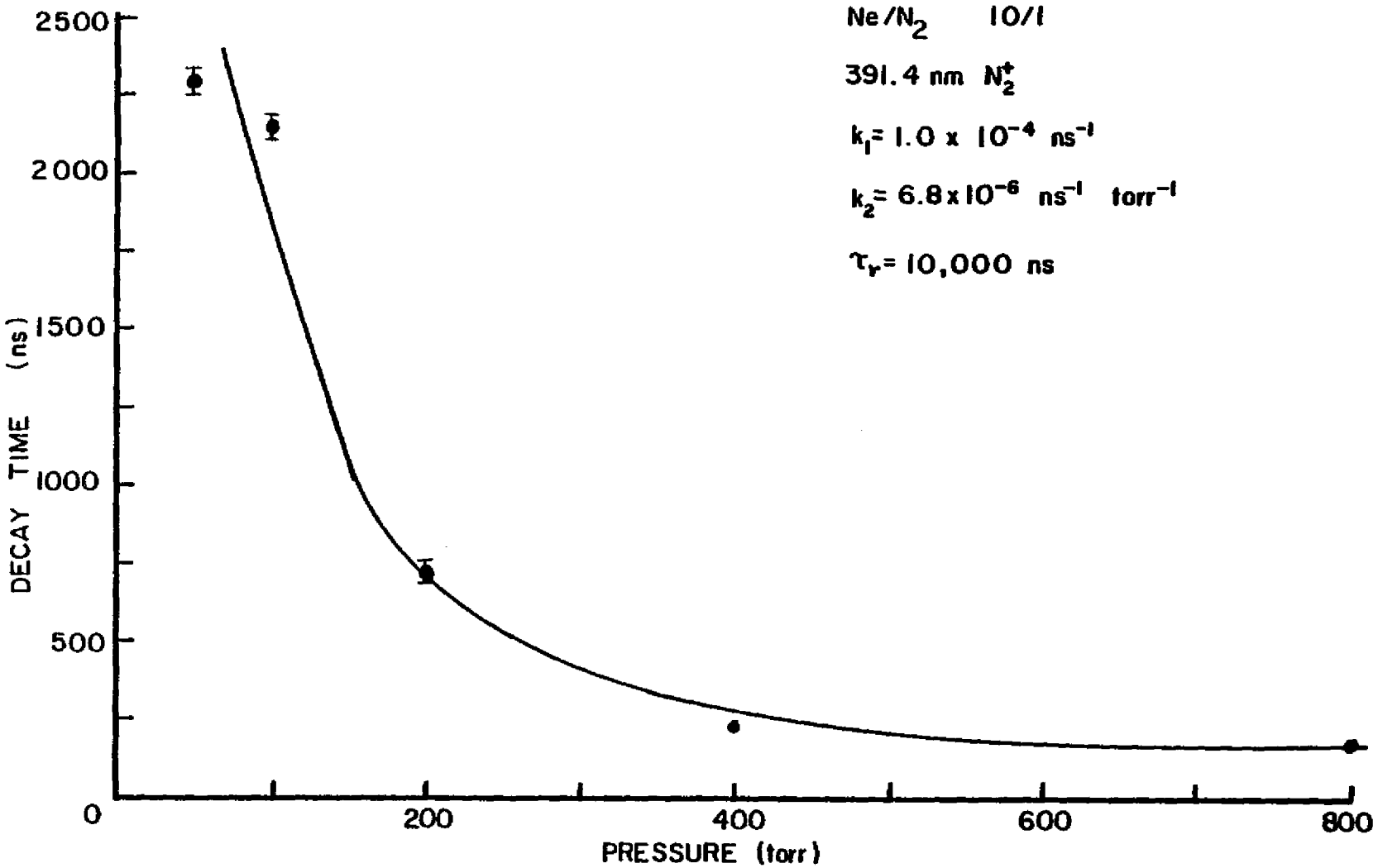

Figure 48. Decay Time Versus Pressure for 391.4 nm

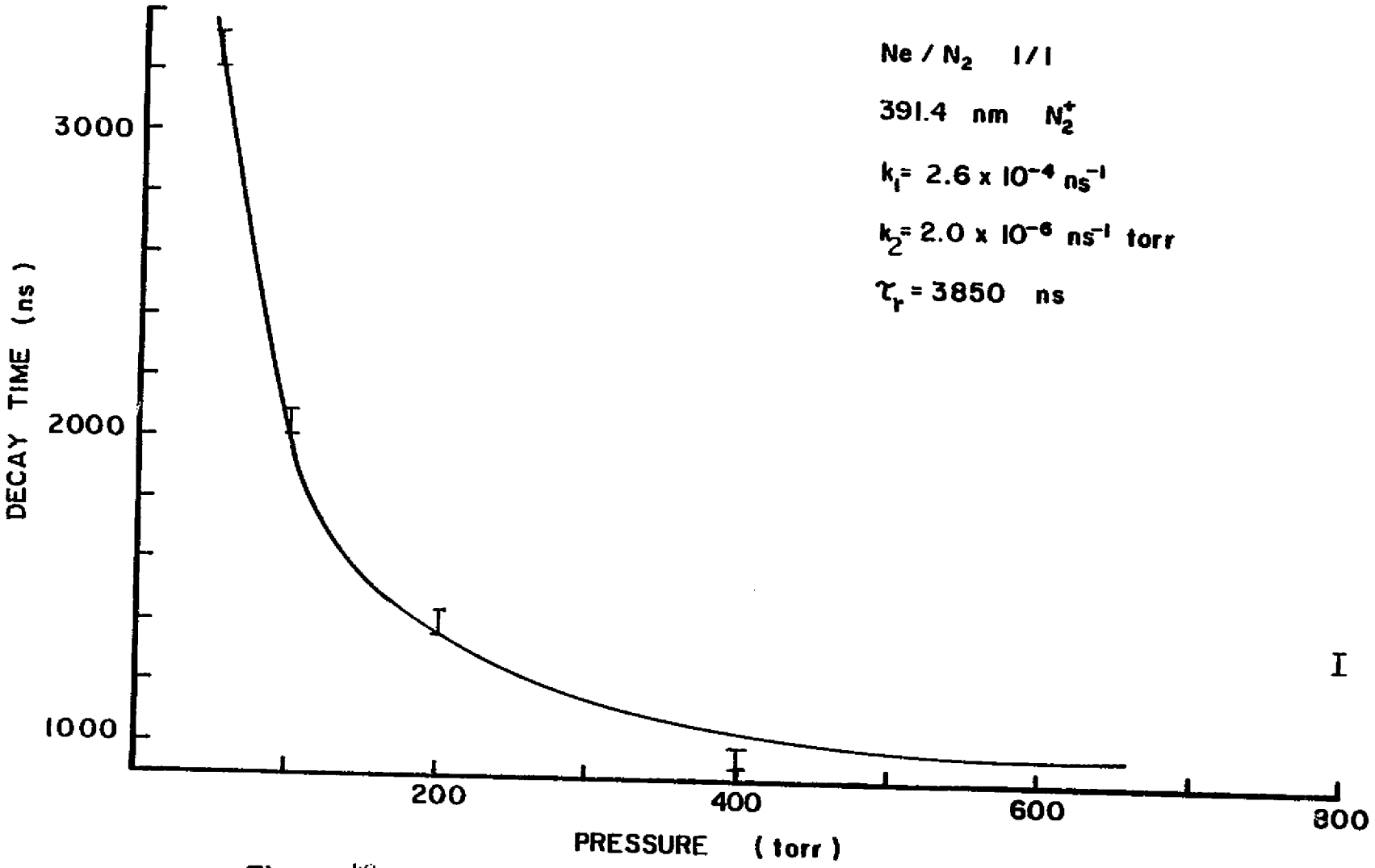

Figure 49. Decay Time Versus Pressure for 391.4 nm

Anomalous excitation of N_2^+ has been seen before in laser produced air plasmas, argon plasma jets, radio frequency plasma torches, and manganese seeded plasma jets, but has received no adequate explanation.

(3) Helium/Nitrogen Mixtures

For the helium/nitrogen mixtures the emission was dominated, just as in the case of electrical excitation, by the first negative bands due to the N_2^+ molecular ion. As the nitrogen concentration increased to 1%, the dominant band became the second positive system but the first negative was still visible. This behavior is to be compared with the case of electrical excitation in glow discharge where the 391.4 emission dominated to much higher concentrations of N_2. The persistence of the N_2^+ emission may be due to the electric field inhibiting recombination and, hence, keeping the population of N_2^+ elevated with respect to the fission fragment excited case. At 10% nitrogen, all observable emission was due to the neutral molecule. The effect of He on the relative intensity of the 391.4 nm line of N_2^+ was investigated as a function of total pressure for various mixture ratios. These results are indicated in Figure 50a The decay curves for 1/2% N_2 in helium, appear in Figure 50b. It is seen that there is a dramatic difference in results for total pressures of 800 torr and 100 torr. There was a lot more energy coming out of the gas as light, and it came out for a much longer time even though the energy deposited by the fission fragment was less for a gas that was mostly helium than for the heavier nitrogen. Figure 51 shows the change with pressure of the decay time for various mix ratios. As the amount of N_2 decreased, the lifetime of the N_2^+ level was increasingly determined by the helium metastable lifetime. As the amount of nitrogen increased, recombination took

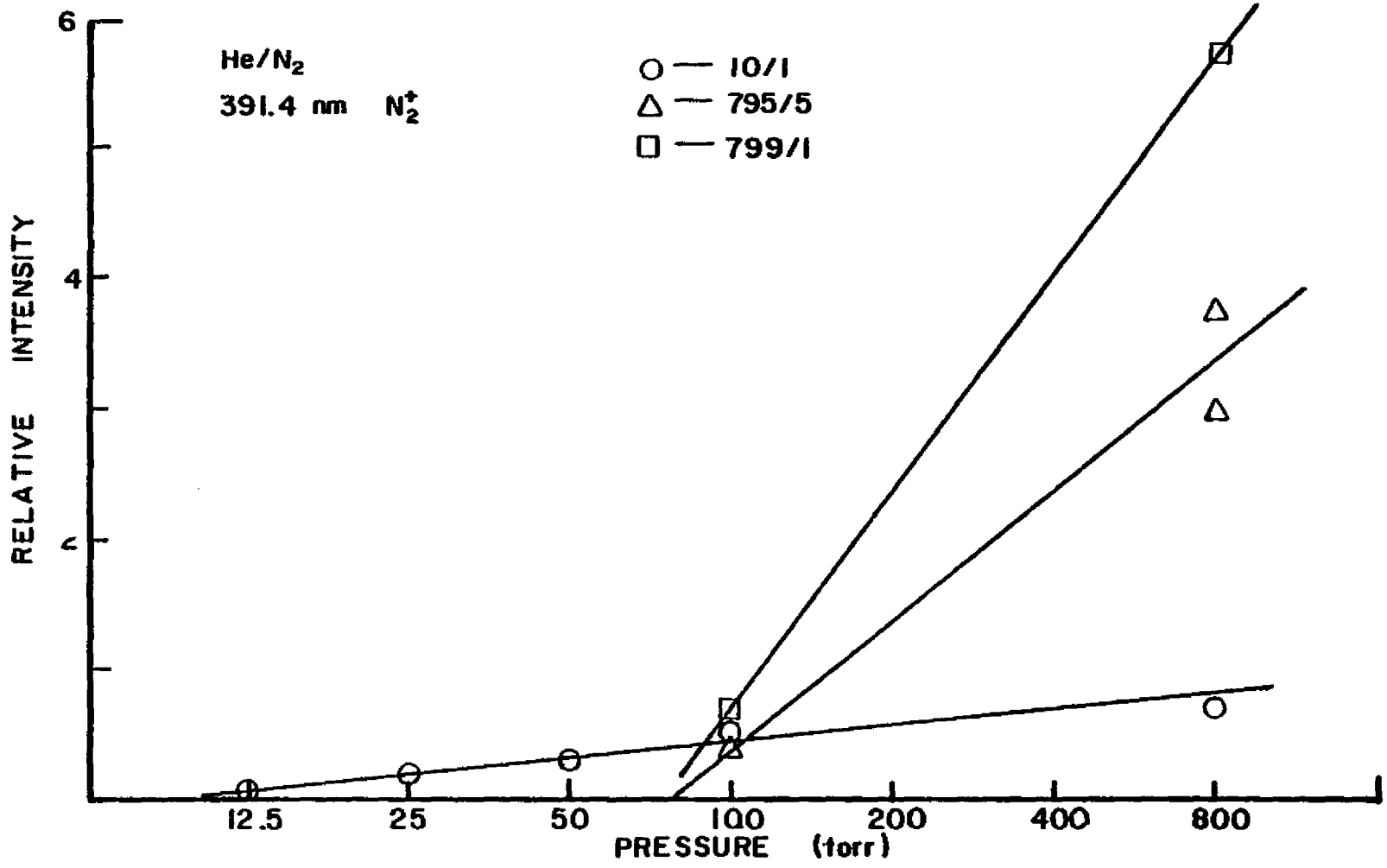

Figure 50a. Relative Intensity Versus Pressure for 391.4 nm

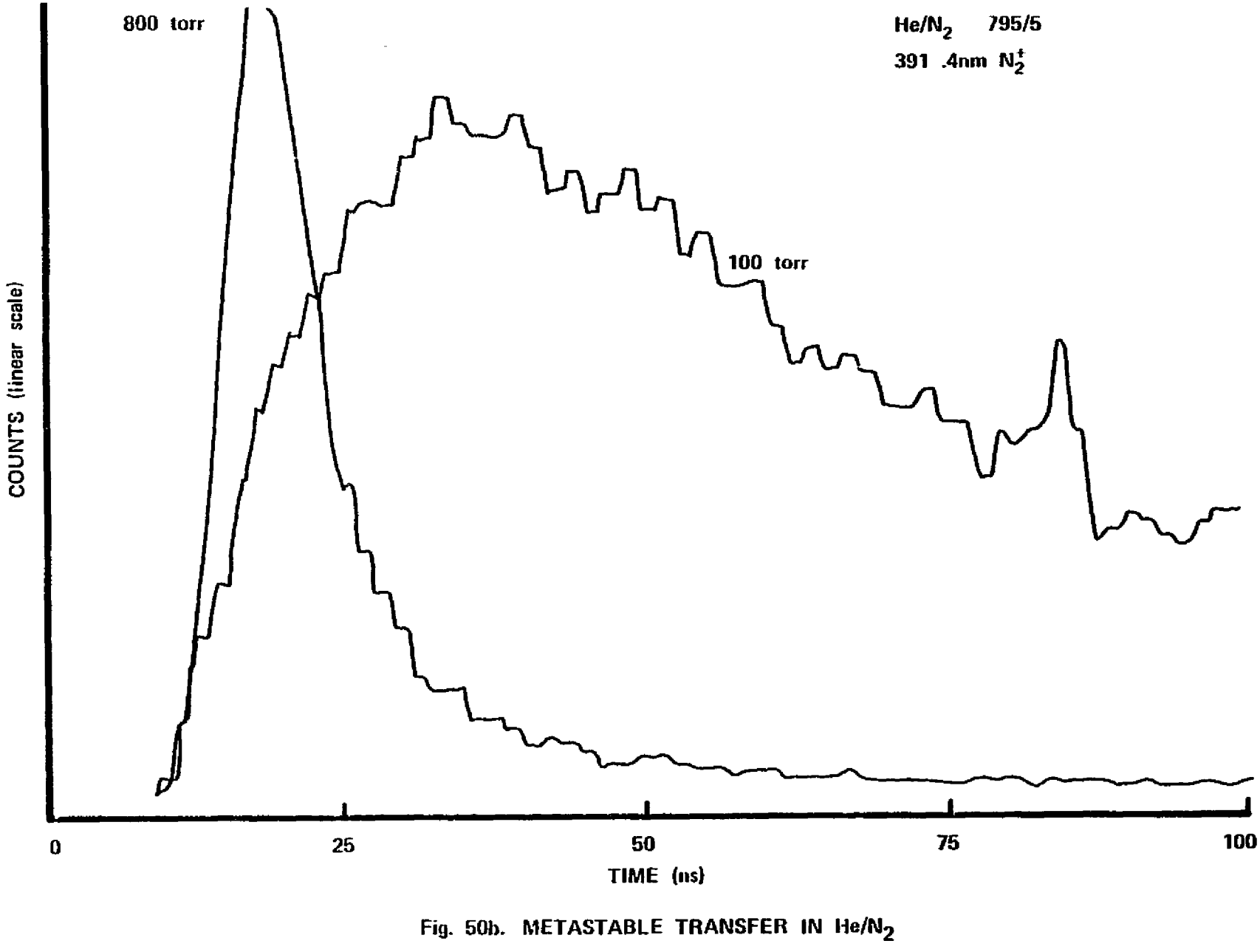

Fig. 50b. METASTABLE TRANSFER IN He/N_2

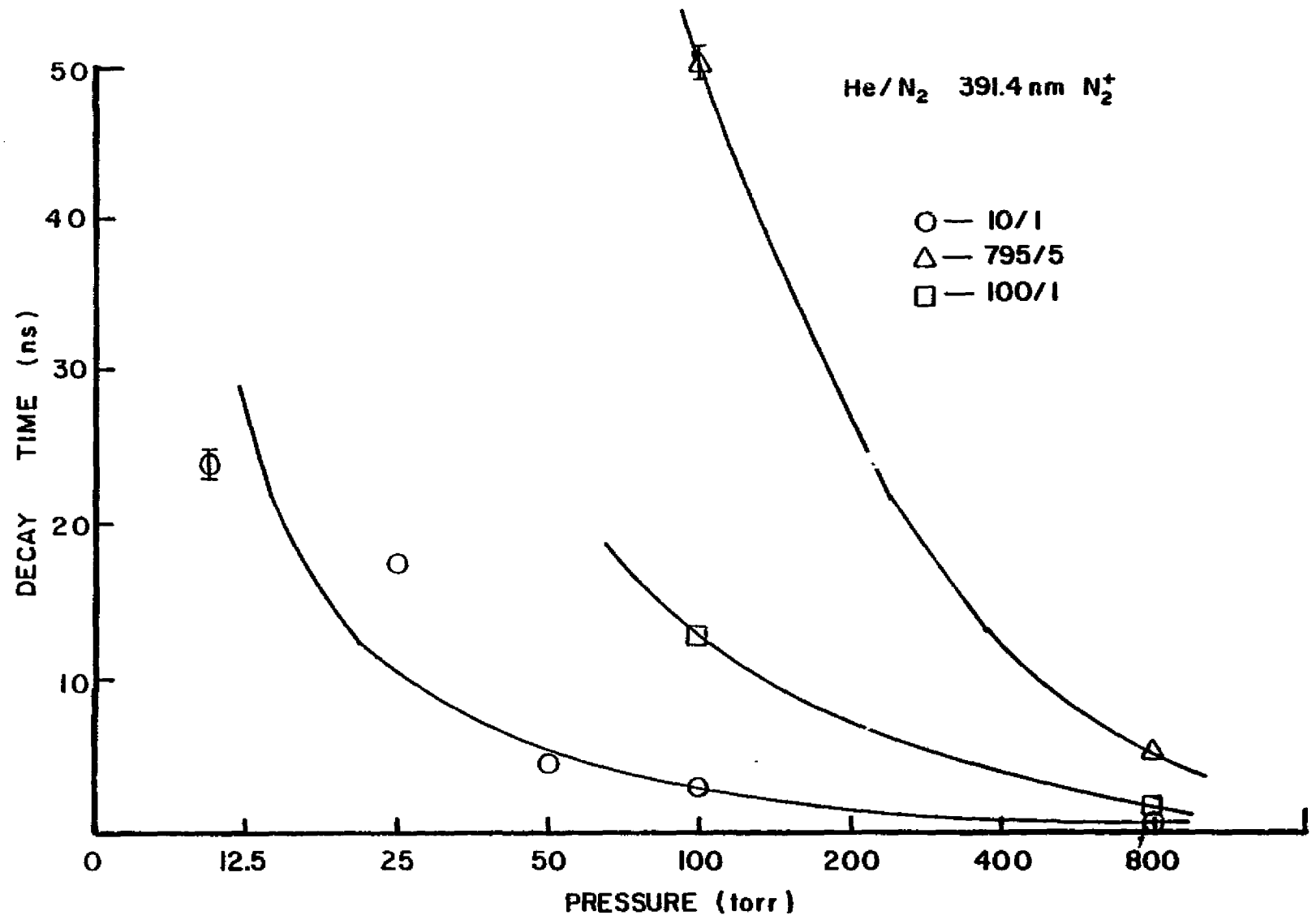

Figure 51. Decay Time Versus Pressure for 391.4 nm

place much more rapidly, causing an additional depletion of the level.

(4) Argon/Nitrogen

Because of the intense emission observed in the past from fission fragment excited mixtures of argon and nitrogen and also because of the interest in using argon as a cover gas in the gaseous core reactor, preliminary measurements were carried out on a 10 to 1 mixture of argon to nitrogen, the mixture that had been found previously to give the most light. Analysis of the decay curves (Figure 52) of the $C^3\pi_u$ level indicates two components, a fast and a slow one. Quantitatively the fast decay approaches 45 ns, the radiative lifetime of the $C^3\pi_u$ level, while the slow decay shows a zero pressure value of 600 ns. The phenomenon being observed is the fast initial decay of the directly excited nitrogen level and the slower metastable transfer from the argon 4^1P level with which it is in resonance. As the pressure drops, the collision frequency decreases and metastable transfer is no longer so important vis a vis direct excitation.

(5) Carbon Tetrafluoride

One of the peripheral interests in the optical emission of fission fragment excited gases had been the possibility of using a gaseous scintillator as an incore monitor of the power level in the LMFBR. Early studies by Pagano indicated that the fluorocarbon CF_4 had the dual advantage of being inert and having high luminosity. Pagano was not able to determine whether CF_4 or some dissociation product was causing the intense emission which he observed. Because of the difficulty of obtaining CF_4 (or Freon-14), only a few measurements were carried out. Spectral scans showed a broad continuum in the ultraviolet which had been previously observed by Walters,

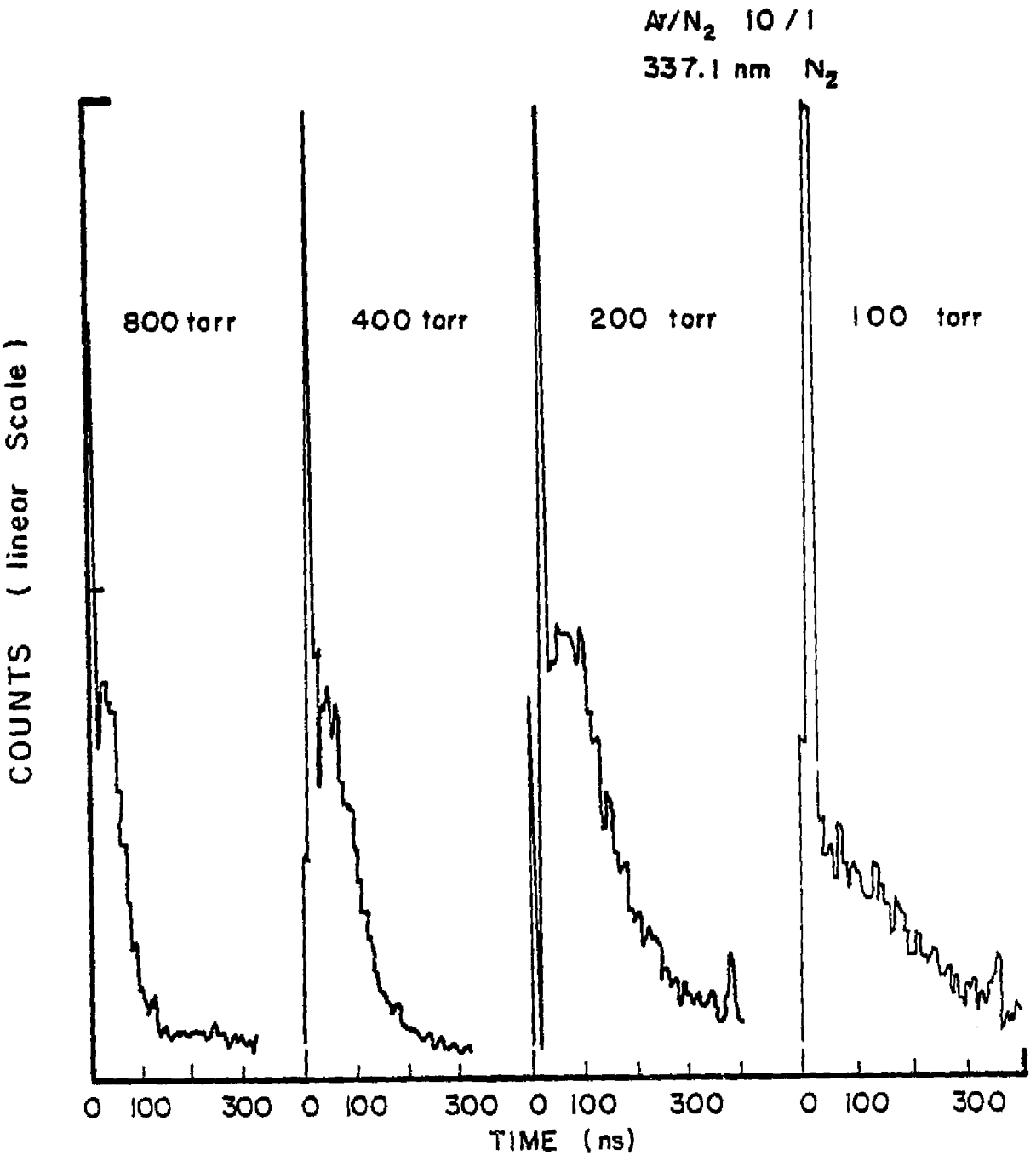

Figure 52. Fast and Slow Decay in Ar/N_2

C-8

A decay curve was made of the $C^3\pi_u$ level of the nitrogen impurity at 586 torr, and the decay time was a simple exponential with a 1/e time of 26.2 ns (Figure 53). This emission was much too weak to account for the intense total luminosity emission.

b. UF_6 Additive Studies (Low Concentrations)

In order to obtain a better understanding of the quenching mechanism present when UF_6 is added to a scintillating gas, the pressure dependent lifetimes of excited levels of Ar, N_2, and Xe in the pressure range 0-400 torr were measured in the pure gases and with 1% UF_6 added. Decay curves were collected using the delayed coincidence single photon counting system described above.

(1) Nitrogen

As mentioned in the previous section, the inverse lifetime versus pressure curve for the second positive system of N_2 has been found to be a straight line for pressures up to 1000 torr. Of particular interest in this study, therefore, was the effect of UF_6 on the excited level lifetime and on the change, if any, in the pressure dependence from the case of pure N_2.

A plot of inverse lifetime versus pressure for the 337.1 nm transition in UF_6 seeded nitrogen appears in Figure 54. Note the departure of the results from linearity for the UF_6 admixture.

(2) Argon

Figure 55 indicates the lifetime versus pressure data for the 810.3 nm ArI line for pure Ar and Ar with 1% UF_6. Two other ArI lines, 696.5 nm and 763.5 nm, were not detectable when 1% UF_6 was added to the Ar. Both were detectable, however, when pure Ar was in the chamber.

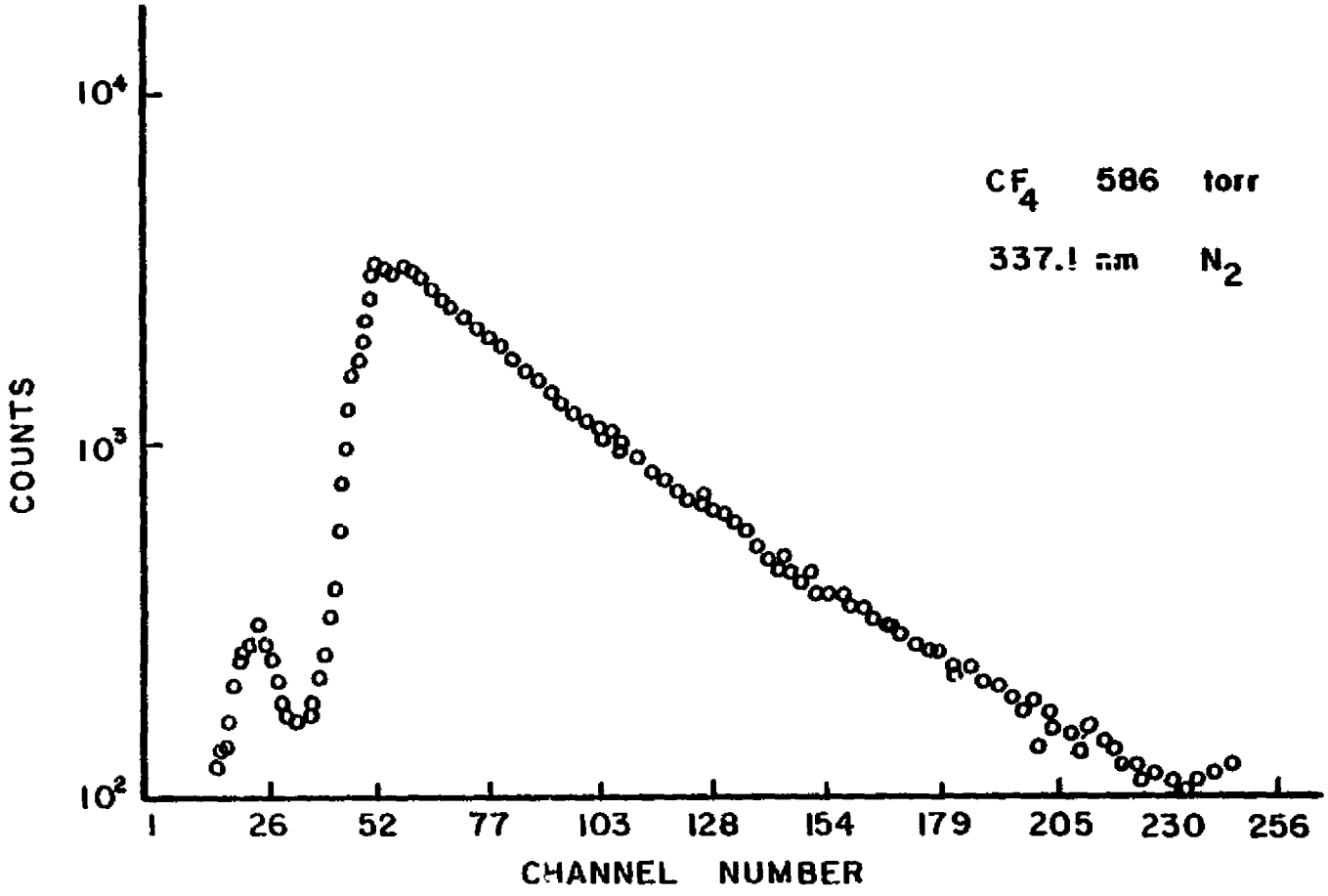

Figure 53. N_2 Impurity in CF_4

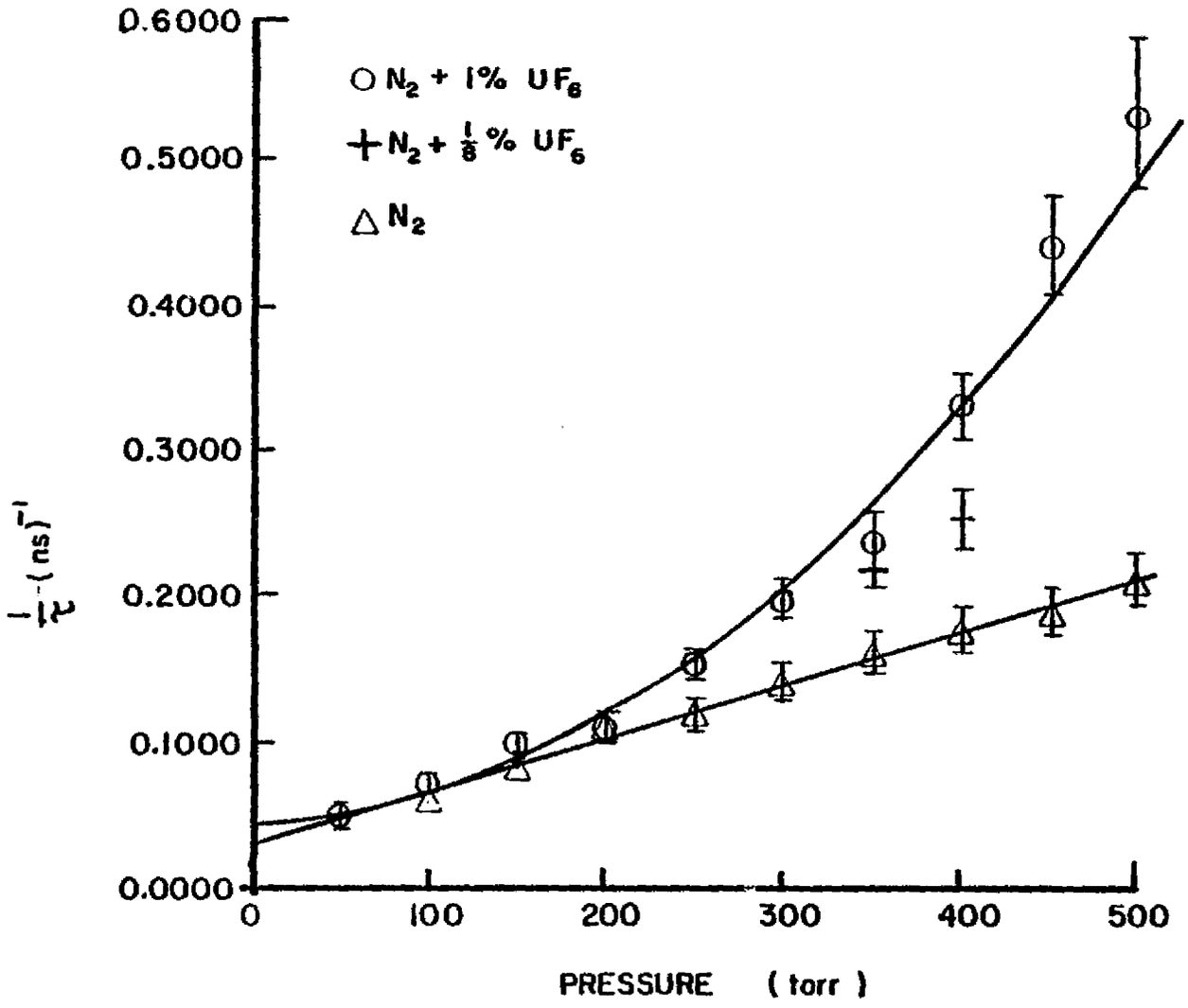

Figure 54. Results For 337.1 nm N_2 Line

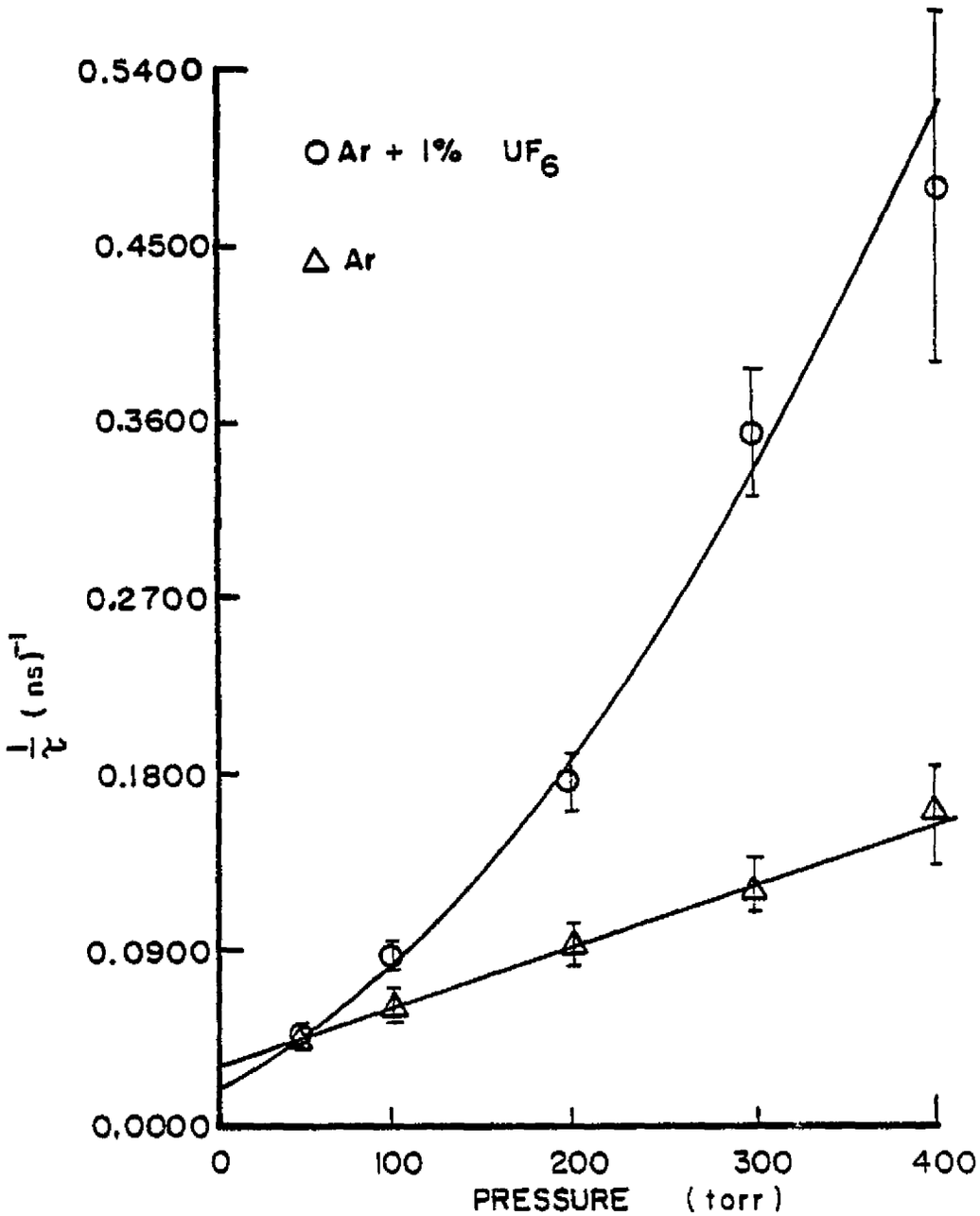

Figure 55. Results for 810.3 nm Ar I Line

(3) Xenon

The data for the 828.0 nm XeI line appear in Figure 56. When a mixture of Xe and 1% UF_6 was placed in the chamber, there was a tremendous decrease in the luminosity as compared to the pure xenon emission. The only two data points obtainable for this mixture are plotted on Figure 56. As can be seen by comparison with Figures 54 and 55, there is significant increase in the transition probability (decrease in the lifetime) at pressures well below those required for a similar increase (decrease) for N_2/UF_6 or Ar/UF_6 mixtures.

Summary of UF_6 Admixture Results

From Figures 54 and 55, it can be seen that even a small amount of UF_6 present in the scintillating gas (1%) causes two changes in the pressure dependent lifetime of the excited levels. First, a decrease in the lifetime is evident. This decrease with UF_6 present means there are additional deexcitation pathways for depopulating the upper states. A decrease in luminosity which accompanies the decrease in lifetime indicates that these pathways are nonradiative.

The second change is the manner in which the lifetime varies with pressure. For both Ar and N_2 there is a significant deviation from a linear relationship between the inverse lifetime and pressure when UF_6 is added. The linear relationship for the pure gas implies that the exciter level population obeys two-body collision kinetics. With UF_6 present, the sharp increase in the inverse lifetime as pressure is increased indicates that additional deexcitation processes are present. The parabolic fit of the inverse lifetime versus pressure data for N_2/UF_6 and Ar/UF_6 mixtures suggests that three-body collisions are significant. Other investigators have attributed

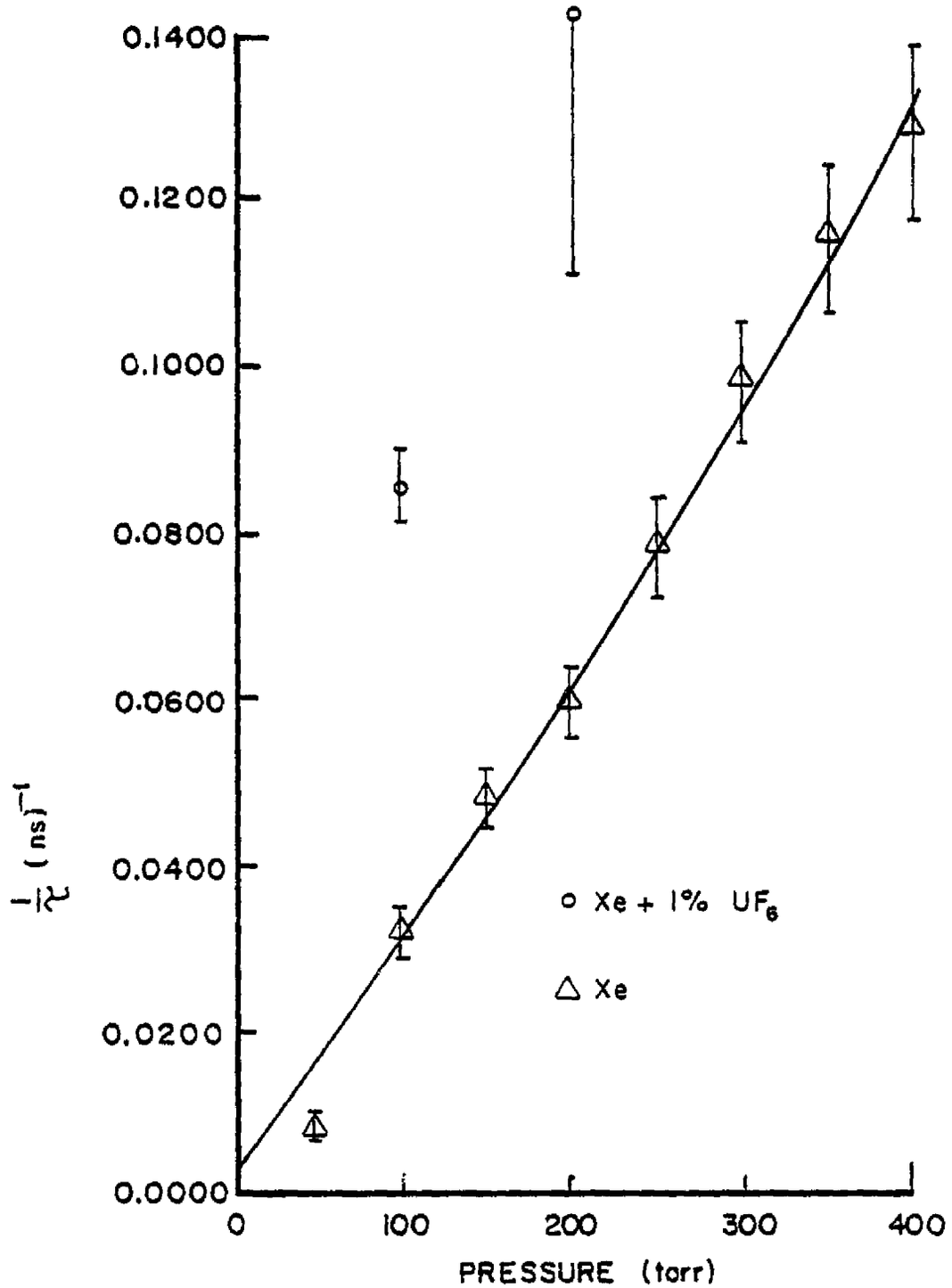

Figure 56. Results for 828.0 nm XeI Line

the quadratic behavior of inverse lifetime for the $^3P_2$ metastable level in argon to three-body collisions. It is of interest to note that those studies were conducted over the same range of pressures used in the present study.

The most severe decrease in lifetime caused by the addition of UF_6 occurred when Xe was the scintillating gas. As can be seen from Figure 56 the inverse lifetime more than doubled when 1% UF_6 was added even at total pressures as low as 100 torr. Based on the total number of events recorded in the MCA, the 828.0 nm line for pure xenon was the brightest line studied. When UF_6 was added, however, the transition was barely detectable. The total luminosity response was also severely degraded.

The decrease in lifetime caused by the presence of UF_6 becomes significant at different total pressures for the three scintillating gases studied. As can be seen by comparing Figures 54, 55, and 56, the pressure above which the effects of UF_6 are significant is lower for Ar than for N_2 and appears to be lowest for Xe. It seems to decrease as molecular weight of the scintillating gas increases. It should be noted, however, that there is no apparent correlation between this pressure and the atomic (molecular) diameter since the Ar atom has the smallest diameter of the three gases studied.

For 200 torr and lower pressures there does not appear to be a significant decrease in the excited level lifetime of the $C^3\pi_u$ level of N_2 with UF_6 present. Analyzing the data in two separate pressure regions suggests an alternative explanation for the inverse lifetime versus pressure behavior.

Figure 57 contains the data points for N_2 with 1% UF_6. Also shown in the figure is the straight line obtained from fitting the pure N_2 data. The two lines drawn through the N_2/UF_6 data resulted

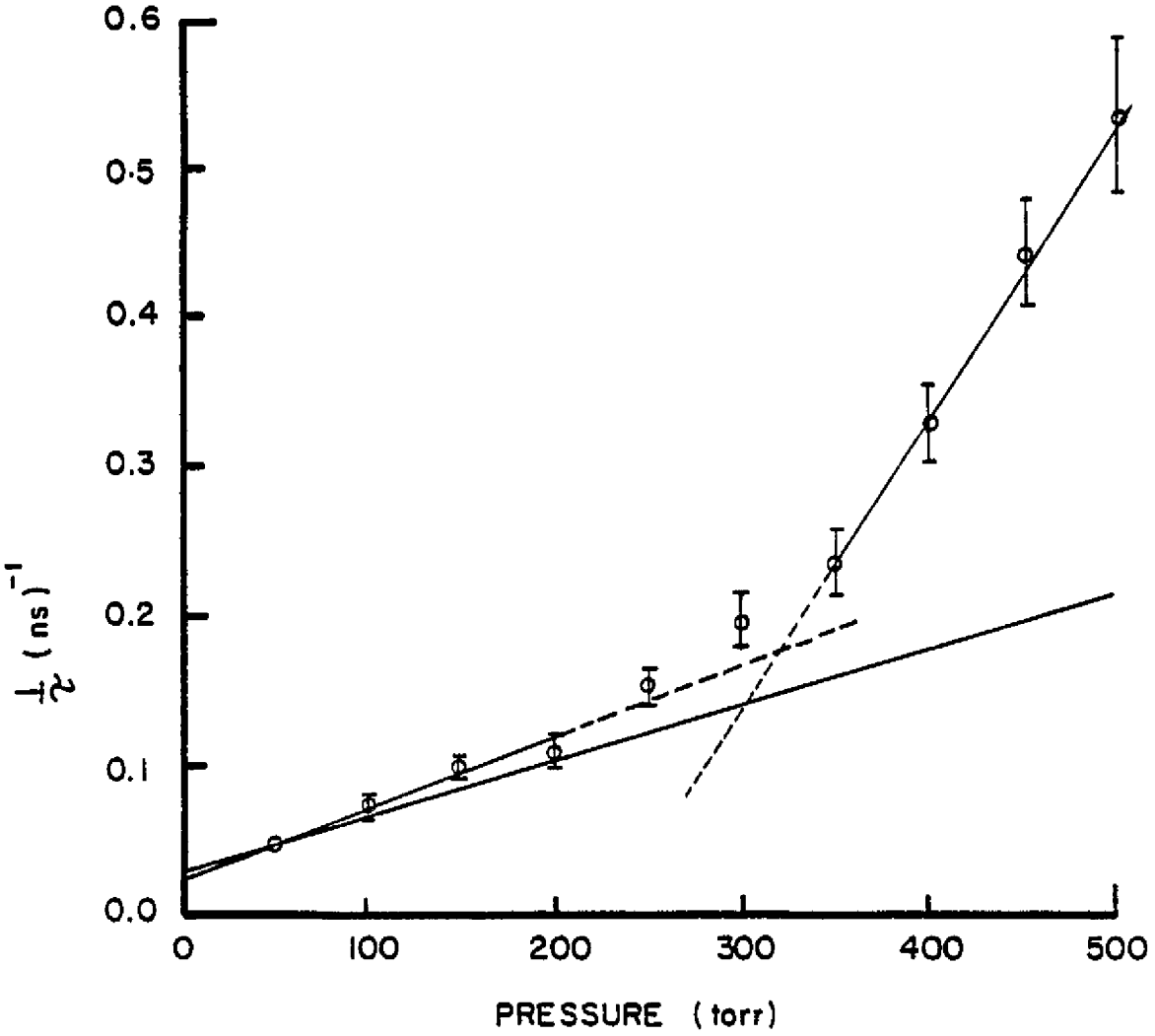

Figure 57. Results for 337.1 nm N_2 Line

from fitting the data using a linear least squares method over two separate regions--0 to 200 torr and 350 to 500 torr.

Using the low pressure fit, a value for the radiative lifetime can be calculated. The value obtained in this manner was 45 ± 14 ns. The value obtained from the pure N_2 data was determined as 39 ± 9 ns. These two are seen to be in good agreement. It is of interest to note that the radiative lifetime obtained from the parabolic fit of the N_2/UF_6 data was 23 ± 4 ns. It is expected that both the pure N_2 data and the N_2/UF_6 data should yield the same value for the radiative lifetime since this represents the lifetime for an isolated excited N_2 molecule.

Fitting the data over two separate pressure regions rather than with a continuous parabola implies that the process responsible for the additional depopulation of the excited levels is not present, or at least not significant until a "threshold" pressure is reached. For N_2 this "threshhold" appears to be between 200 and 300 torr. One possible explanation might be that with only 1% UF_6 collisions between excited N_2 molecules and UF_6 molecules do not become significant until the total pressure is increased above 200 torr. Above this pressure the two-body collision rate would then increase dramatically. More data, both at higher pressures and for different concentrations of UF_6, will have to be taken before a definite conclusion can be made regarding this behavior.

c. UF_6 Additive Studies (High Concentrations)

For this series of experiments the 337.1 nm transition in N_2 and the 810.3 nm transition in ArI were observed in the presence of 3% and 10% partial pressure of UF_6. The results are summarized below.

(1) Nitrogen

Figure 58 summarizes the effect of increasing concentrations of UF_6 in N_2. The physical significance of these results has been discussed earlier. As increased percentages of UF_6 are added, the value of the lifetime similarly decreases, thus, the inverse lifetime, or lambda, increases. Also note that at increased absolute concentrations of UF_6, that is, at higher concentrations and at higher pressures, the relative error in the data points is increased. This phenomenon exists because at higher concentrations, more light is attenuated by the optically thick UF_6 gas. For equivalent periods of counting, the light output, hence, the absolute count rate, is less at higher UF_6 concentrations and the relative error is increased for decreased absolute count rates.

(2) Argon

Figure 59 describes the pressure dependence of the 810.3 nm line in ArI with 10% UF_6. Pure Argon and 1% UF_6 in Argon data obtained by previous experimenters, was also included in the figure for comparison. Since the 10% UF_6 in Ar data did not appear to fit a straight line, a parabolic least squares fit was attempted. The results for the rate coefficients indicate the radiative lifetime to be 108.1 ns.

D. UF_6-CO_2 Laser-Reactor Studies

Uranium hexafluoride is a most important candidate for the volume power source of a nuclear-pumped laser. The advantages over the use of He^3, $n(He^3,p)T$, are an increased power density and self criticality. The disadvantages are the incompatibilities of UF_6 with laser gases. Therefore, it is imperative to determine what UF_6 will do to the chemical status as

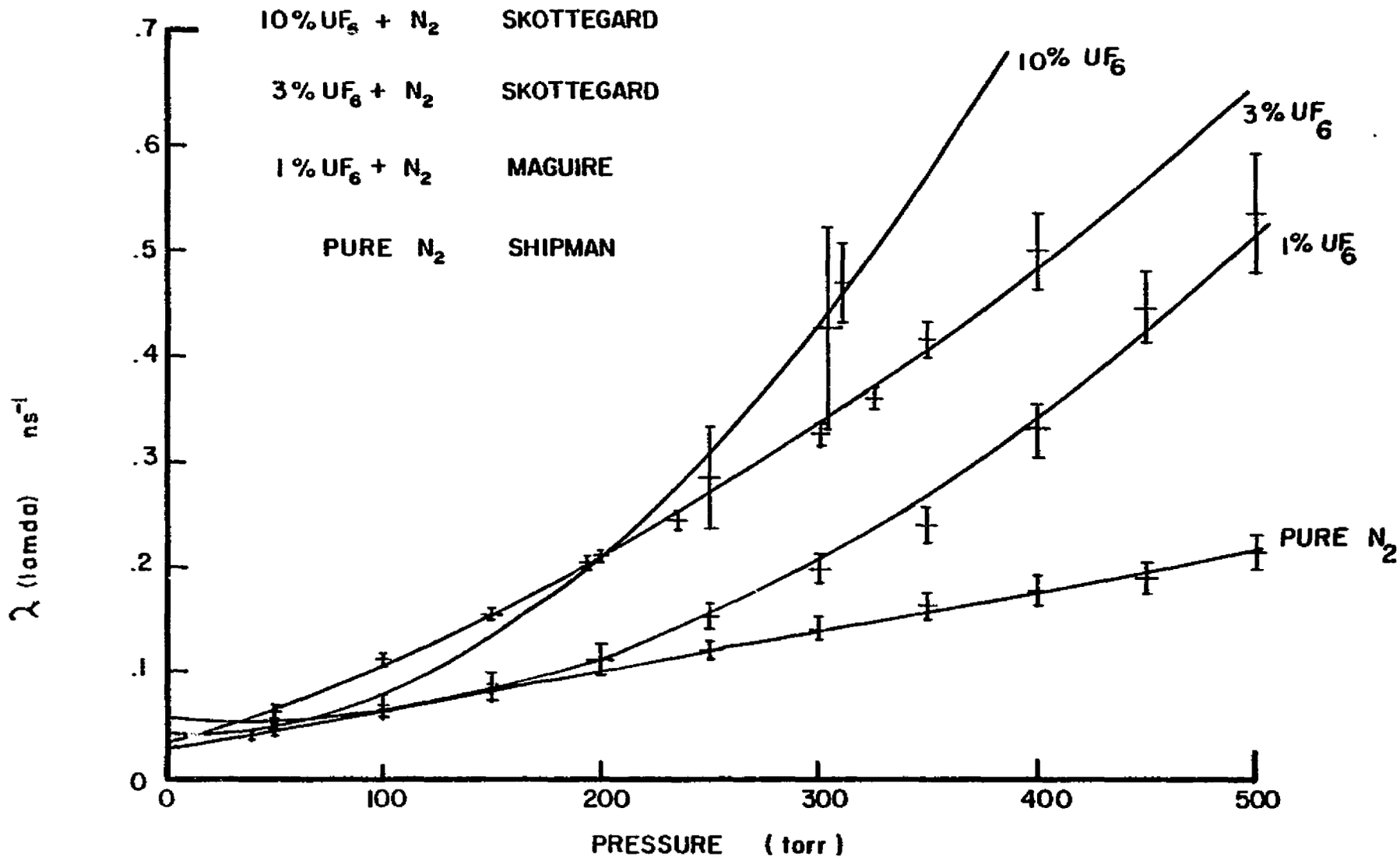

Figure 58. Effect of UF_6 Additive on N_2 Excited State Lifetime (337.1 nm).

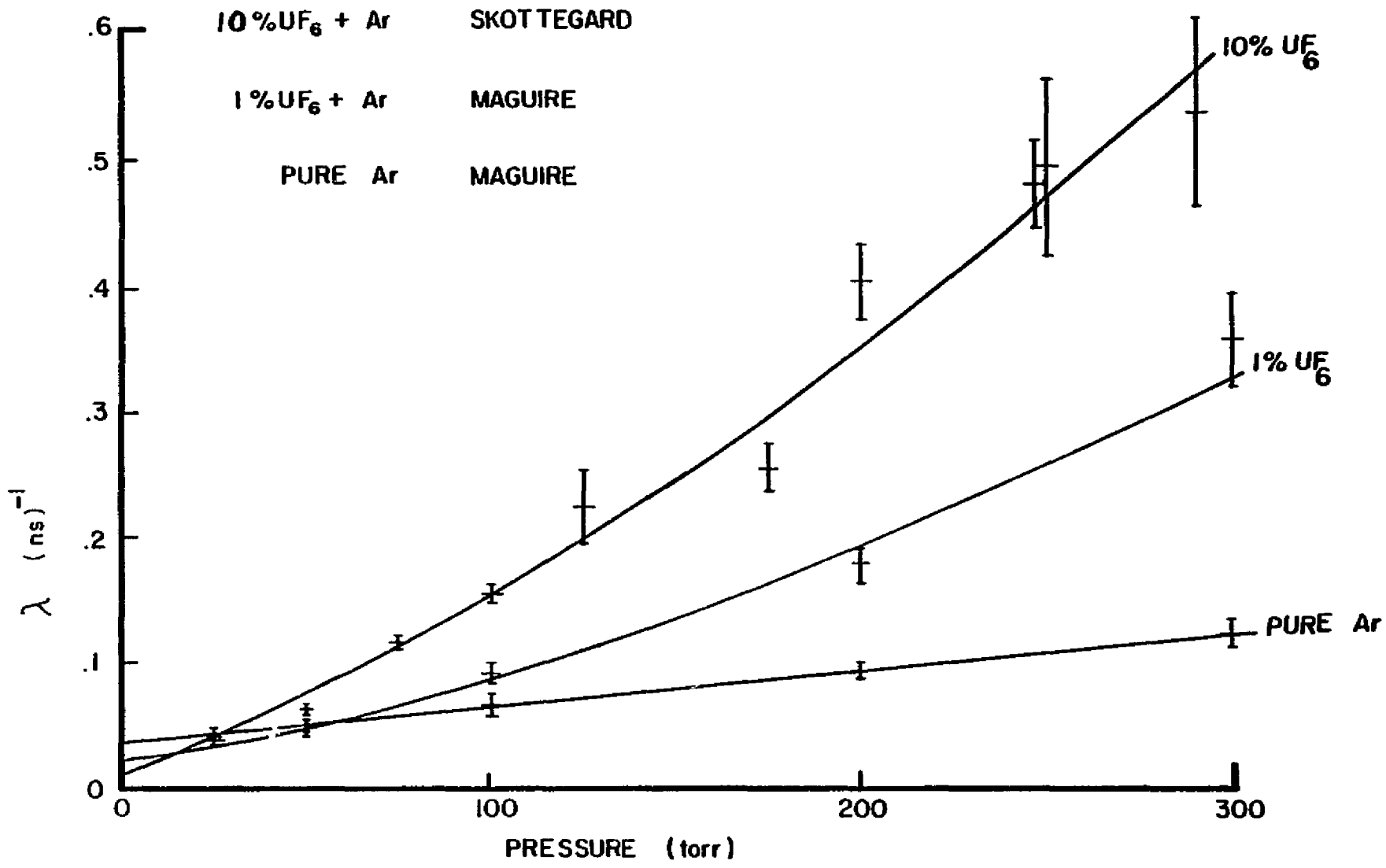

Figure 59. Effect of UF_6 Additive on ArI Excited State Lifetime (810.3 nm)

well as to the electronic status of the laser gas that is, will the gas sustain a population inversion. Then, once the status of the gas is understood, the examination of a suitable reactor configuration must be studied.

For this reason this section concerns itself with the addition of UF_6 into an operational CO_2 - discharge laser and the evaluation of a suitable gas-core lasing reactor. The object is the determination of partial pressure of UF_6 vs. the laser power output.

Then, once the UF_6 to (CO_2, He, N_2) ratio which still allows lasing was known, calculations were carried out to determine if such a laser-reactor system is practical.

The laser used is a statically filled, axially excited CO_2 laser. The gas mixture is 1:1:8, CO_2:N_2:He. The laser characteristics are:

16 mm pyrex bore

85 cm interelectrode distance

water cooling

NaCl windows - 6mm thick

10 meter radius hole coupled output mirror - gold on pyrex

Flat mirror - gold on pyrex

There were two major pieces of equipment used for data acquisition. A thermopile was used to determine the laser output power. A CO_2 spectrum analyzer was used to determine which vibrational and which rotational levels were lasing. With a static fill of 15 torr, the laser output was 5 watts at the 10.6μm transition. The partial pressure of the UF_6 was controlled by temperature. A quartz vial was used to contain the UF_6. A liquid nitrogen bath for temperature control was used to control the admixtures of up to 10% UF_6.

With a partial pressure up to 3% UF_6 the device did still continue to lase in the CW-Continuous Wave-Mode. (See figure 60.) With concentrations of 2% UF_6 or less the laser output was still a substantial fraction of the UF_6 free output. The total pressure of the discharge system was only 15 torr. This was due to the unstable discharge set up by the admixture of UF_6. The inability to go to higher pressures therefore was due to the electrical characteristics of the discharge and not the lasing characteristics.

The characteristics of CO_2 lasers are such that they can be lased at very high pressures. Therefore, with the determination of the ratio of tolerance at 3%, the study of a lasing gas-core was undertaken. The case studied here is a 4 meter diameter, 1 meter thick carbon reflected spherical reactor. At 3% UF_6 the total pressure is only 1.70 atm. for criticality. Figure 61 shows the total pressure for a critical system vs. the percent of UF_6. Table III is a listing of the experimental points taken.

Therefore, it is indicated that such a lasing reactor may be possible. The study of a higher pressure laser system such as a TEA laser would perhaps give a better feeling for the high pressure tolerance ratio. Once this data is known, high pressure systems could be tested.

E. Nuclear Pumped CW-Laser

1. Introduction

To show the feasibility of extracting power from a nuclear reactor in the form of laser light, it is mandatory to demonstrate that CW-laser action is possible. So far, the nuclear pumped laser that has been demonstrated used pulsed reactors having extremely high neutron fluxes as energy sources. Pulse length varied with different experiments but, in all cases, was a small fraction of a second. For engineering applications

TABLE III

CRITICALITY CALCULATIONS FOR UF_6/CO_2 LASER-REACTOR

ase	Percent Laser Gas	Kg of U^{233}	Pressure (atm) UF_6 (at 300 K)	Pressure (atm) Total
1	0.0	16.1	0.051	0.051
2	99.0	18.1	0.057	5.70
3	98.0	17.0	0.054	2.63
4	97.9	17.0	0.054	2.49
5	97.7	16.9	0.052	2.26
6	97.0	16.7	0.053	1.70

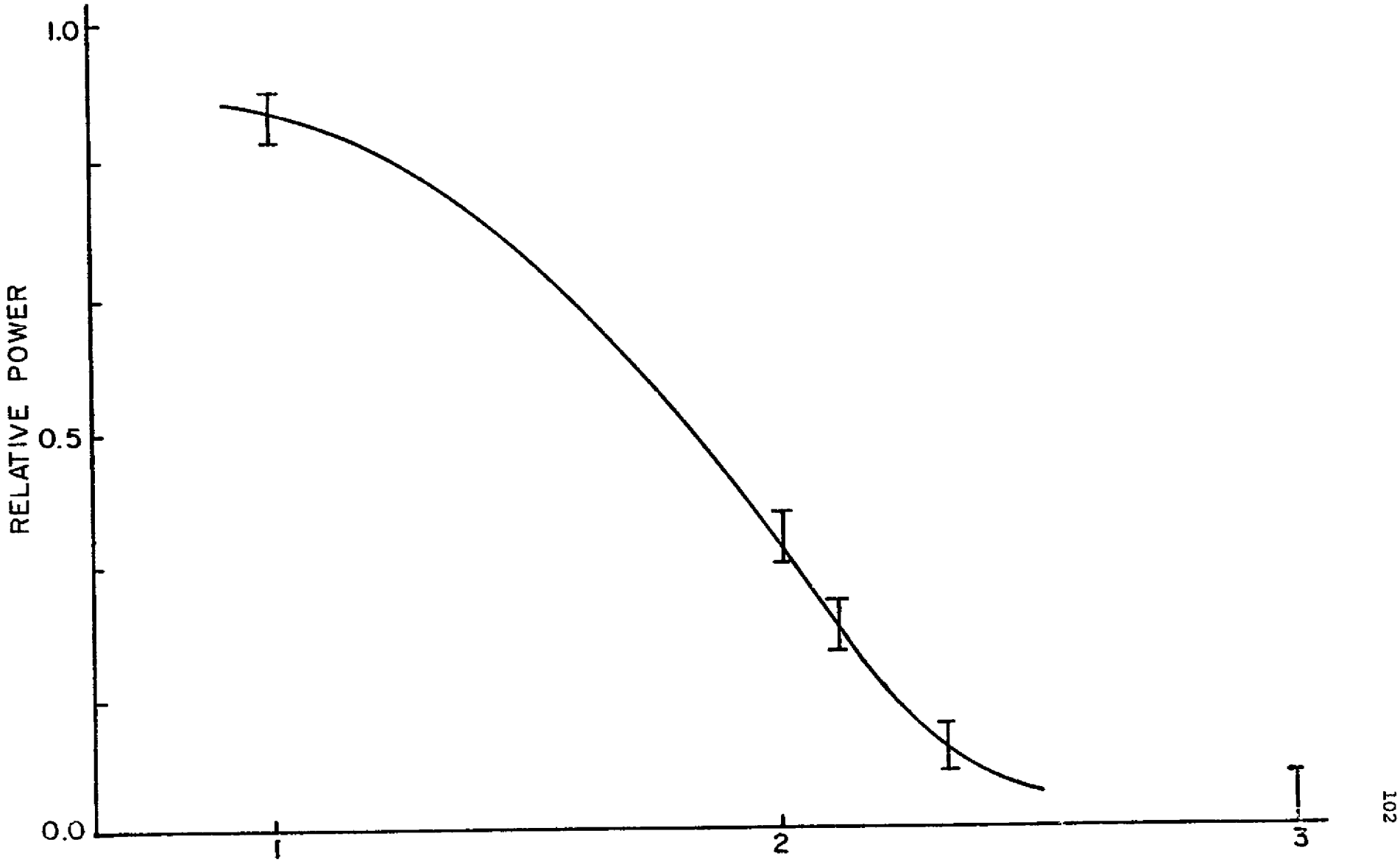

FIG. 60. LASER OUTPUT VS. UF_6 CONCENTRATION

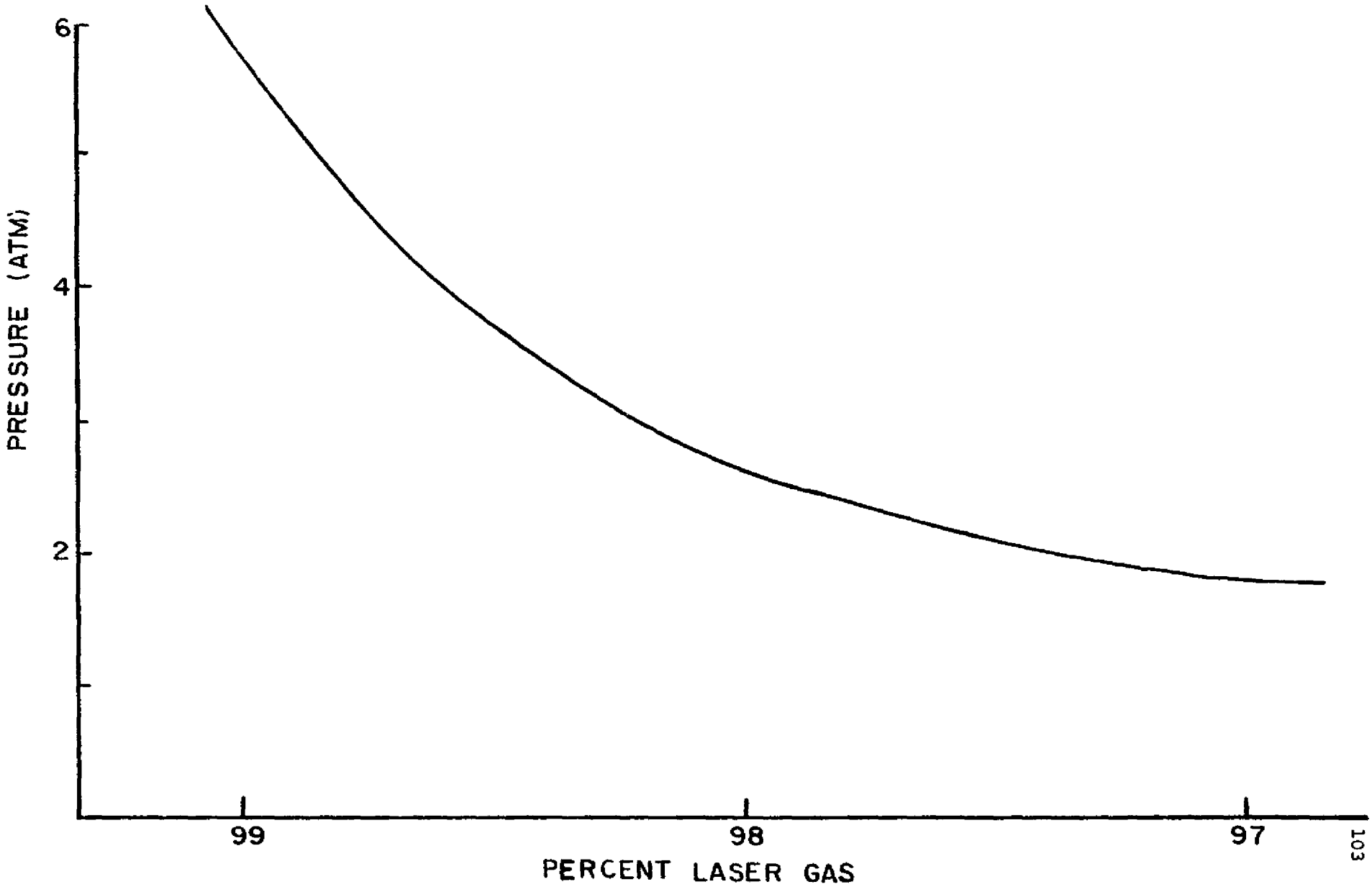

FIG. 61. GAS-CORE REACTOR PRESSURE VS. CONCENTRATION OF LASER GAS

of these pulsed lasers, a pulsed reactor with a high repetition rate would be required. Such reactors do not exist at present, although it is conceivable that they could be developed. However, it would be much easier if a steady state reactor, having a moderate neutron flux, could be used. The following describes the work done culminating in the actual CW nuclear pumped lasing of the He-Ne system.

2. Gain Measurements

The single pass gain experiments were carried out in two different reactors. The first, a medium flux tank type heavy-water reactor, located at the Georgia Institute of Technology, was used for the thermal neutron flux range from 1×10^{9} to 1×10^{14} n/cm^2-sec. The other reactor, an Argonaut type reactor located at the University of Florida, was used for lower thermal neutron fluxes ranging from 2×10^{5} to 2×10^{12} n/cm^2-sec. The overlap in ranges allowed comparison of the data taken at each reactor.

a. Medium Flux Reactor Gain Measurements

Figure 62 shows the experimental arrangement. A He-Ne amplifier was located in a throughport close to the reactor core. The amplifier consisted of a water-cooled stainless-steel tube, terminated by two sapphire windows. It was filled with a ^{3}He-Ne (5:1) mixture at a total pressure of 300 torr. At the entrance of the throughport, a commercially available .5mW He-Ne oscillator was located. The amplified laser beam was projected onto the entrance slit of a monochromator and detected by a photomultiplier tube. The resulting photocurrent was measured with a picoammeter and continuously displayed on an x-y plotter. In the throughport, a maximum neutron density of 1×10^{14} (corresponding to 5MW reactor power) was available for the ^{3}He(n,p)T reaction to excite the laser gas.

Figure 63 shows the results of the gain measurement. A peak

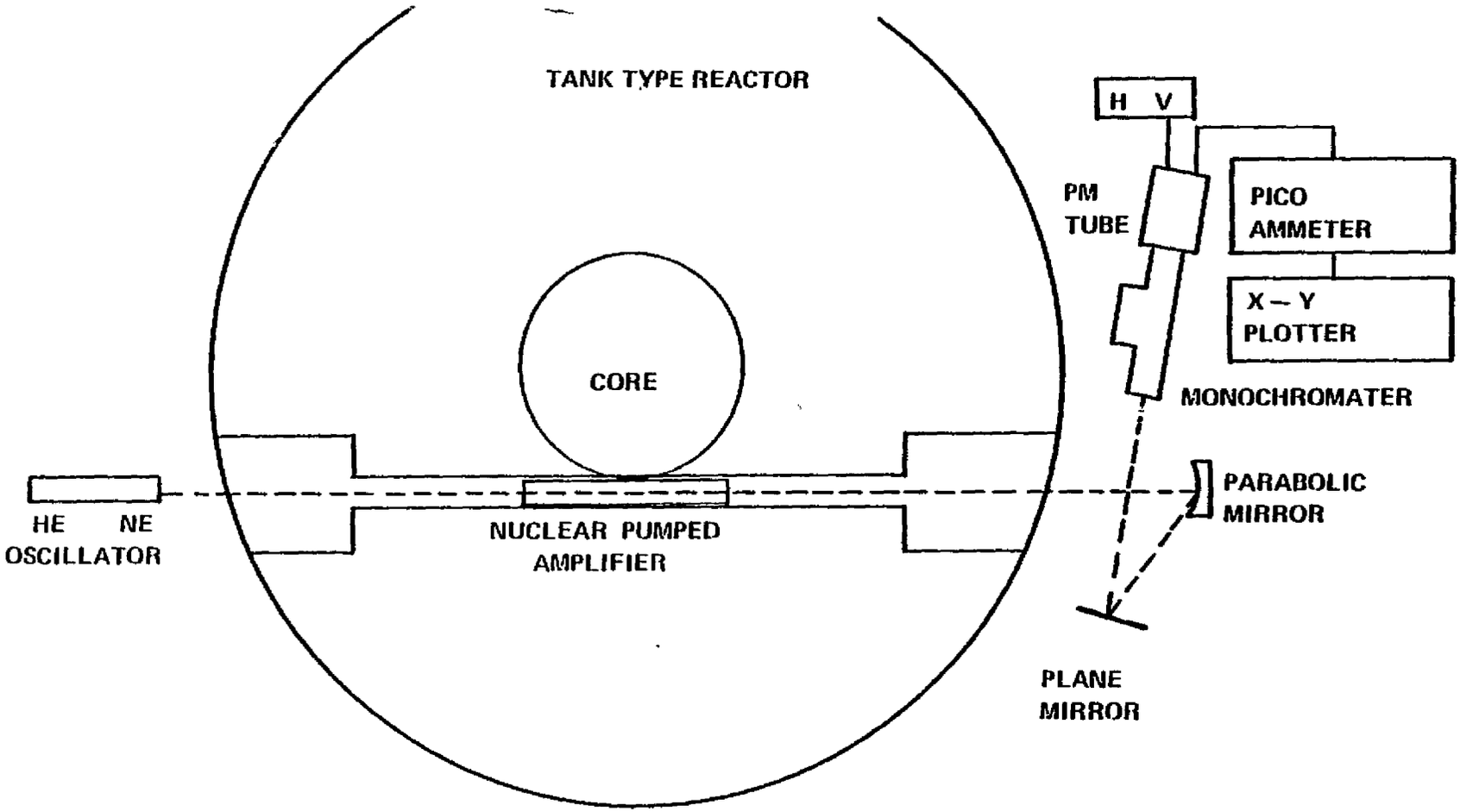

Fig. 62. EXPERIMENTAL ARRANGEMENT

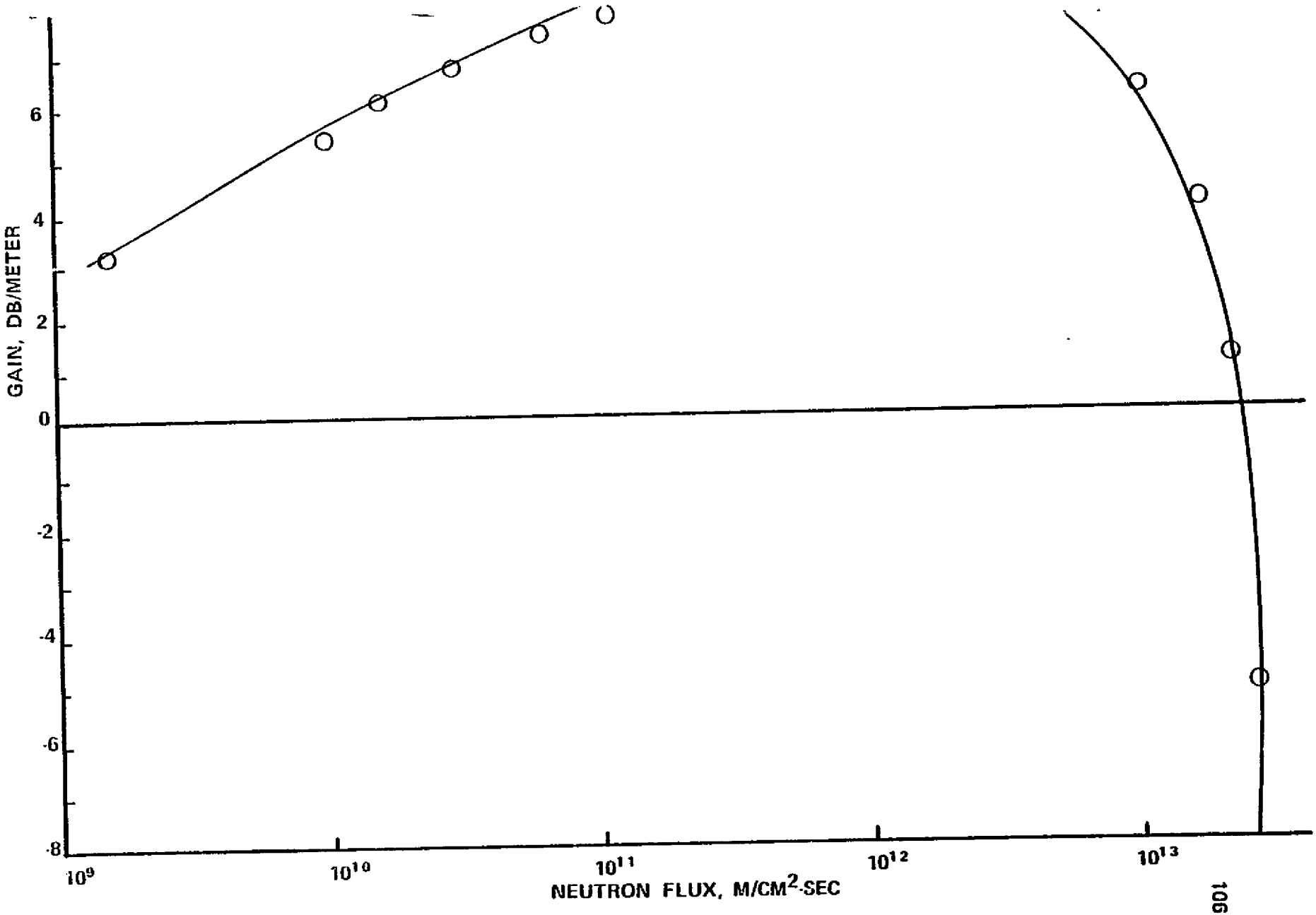

Fig. 63. RESULTS OF GAIN MEASUREMENTS

power gain of 8.84 dB/m for the neon $^3S_2 - {}^2P_4$ laser transition (λ = 6323.2Å) was observed. This maximum amplification was achieved at a neutron flux of 2 x 10^{12}n/cm^2-s. At higher neutron fluxes, the gain decreased and turned into absorption. This agrees with the electrically pumped case where at large discharge tube currents, the output falls off and eventually ceases due to overdriving the laser medium. This overdriving is a result of destruction of the He 2^1s metastables by collisions of the second kind with electrons.[4] These measurements can be compared to older results (Miley, et al.[5]) which concerned nuclear enhancement of an electrically excited pulsed He-Ne laser. The fact that their laser was electrically excited and operated at a lower gas pressure makes comparison difficult; however, the reason why no large gain was observed in this older work can be found in the fact that they were made at a neutron flux of n ≃ 10^{15}n/cm-sec, where, according to the present measurements, no gain can be expected.[5]

The power deposition in the laser amplifier was ~12 mW/cm^3 at peak gain, while <4 x 10^{-3} mW/cm^3 was extracted in the form of laser light. This results in an efficiency of about 0.03%.

b. Low Flux Reactor Gain Measurements

The first experiment indicated that the University of Florida training reactor, a low flux reactor (max 2 x 10^{12}n/cm^{2}sec) would be sufficient to continue the study of He-Ne.

A stainless steel capsule similar to that used previously, but uncooled, was inserted into the horizontal throughport of the reactor, see Figure 64. A commercial helium neon laser was used for the gain measurements. A beam splitter and a filter holder were inserted into the optical path.

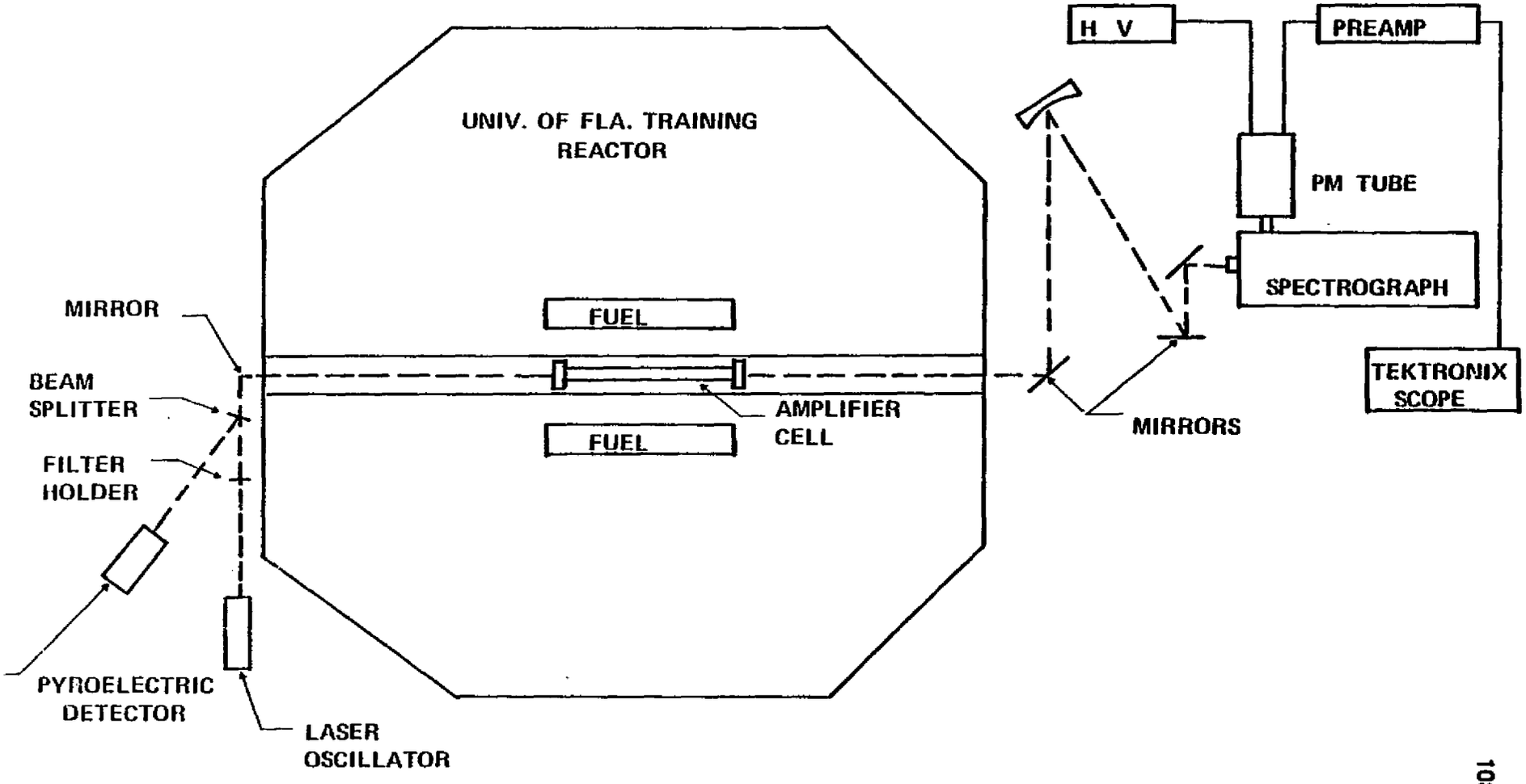

Fig. 64. HORIZONTAL THROUGHPORT AT UFTR

The beam splitter, used in conjunction with a pyroelectric detector, allowed checking of constancy of the input beam. The filter holder provided a means to insert various filters into the light beam. Therefore, it was possible to measure gain for various input intensities.

On the output side of the amplifier cell a series of mirrors were used to project the beam onto the slit of a one meter spectrometer tuned to the first order 6328Å laser wavelength, which ensured that only the 6328Å laser light would be detected by the photomultiplier tube. The photomultiplier output was amplified and fed into one channel (A) of a differential amplifier while the output of the pyroelectric detector was fed into the other channel (B) of this differential amplifier.

The differential amplifier technique was used as follows. With the reactor off (at zero power) the sensitivity of the two channels was adjusted so that in the absence of gain or absorption, the reference channel (B) cancels the output signal of the PM tube (A) exactly regardless of the amplitude of the laser probe input signal. In the presence of gain, the amplifier outputs a positive signal to the scope. Knowing the value of the input laser intensity and measuring this positive signal, gain is determined. By using this technique, the possibility that variations in the output of the probe laser being mistaken for gain is eliminated.

The probe laser used provided the opportunity for a second measurement technique independent of the differential amplifier. The laser had a high frequency noise component in its output. This component was also amplified in the gain cell. By measuring this noise component, one can calculate gain in the same way as the AC gain is found in a transistor circuit.

The results of these measurements can be seen in Figure 65. Both methods agreed within the experimental error.

These measurements agreed very well with the preliminary measurements made at the medium flux reactor. In addition, these measurements are now extended to lower flux levels.

Differences between the measurements done at the two different locations pertain to the neutron flux range between $6 \times 10^{11} n/cm^2 sec$ and $10^{13} n/cm^2 sec$. The uncooled laser tube shows a maximum gain at $6 \times 10^{11} n/cm^2 sec$ while the cooler laser tube shows the maximum gain at $1 \times 10^{12} n/cm^2 sec$. Since both measurements agree for the lower flux levels, it is suggested that the faster decrease of the gain curve for fluxes higher than $5 \times 10^{11} n/cm^2 sec$ for the uncooled tube is due to the fact that the tube is heated by the nuclear reactions which is detrimental to laser performance.

The reason that an attempt was made at all to use an uncooled tube is that the access port for the low flux reactor is only 2" in diameter, while the one for the medium flux reactor was 6" in diameter. It is difficult to reduce the complete instrument package to the smaller diameter. On the other hand, this reactor offers operational characteristics, which are better for the neutron flux range of interest than the one of the medium flux reactor which is designed to operate at $10^{13} n/cm^2 sec$, and higher.

In order to assure that small signal gain can be determined, it is necessary to measure gain for different input intensities. This was done with reactor power as parameter. Due to the heating effect, the reactor power was restricted to the region between 5 and 30 KW where heating does not produce a marked increase in the tube temperature.

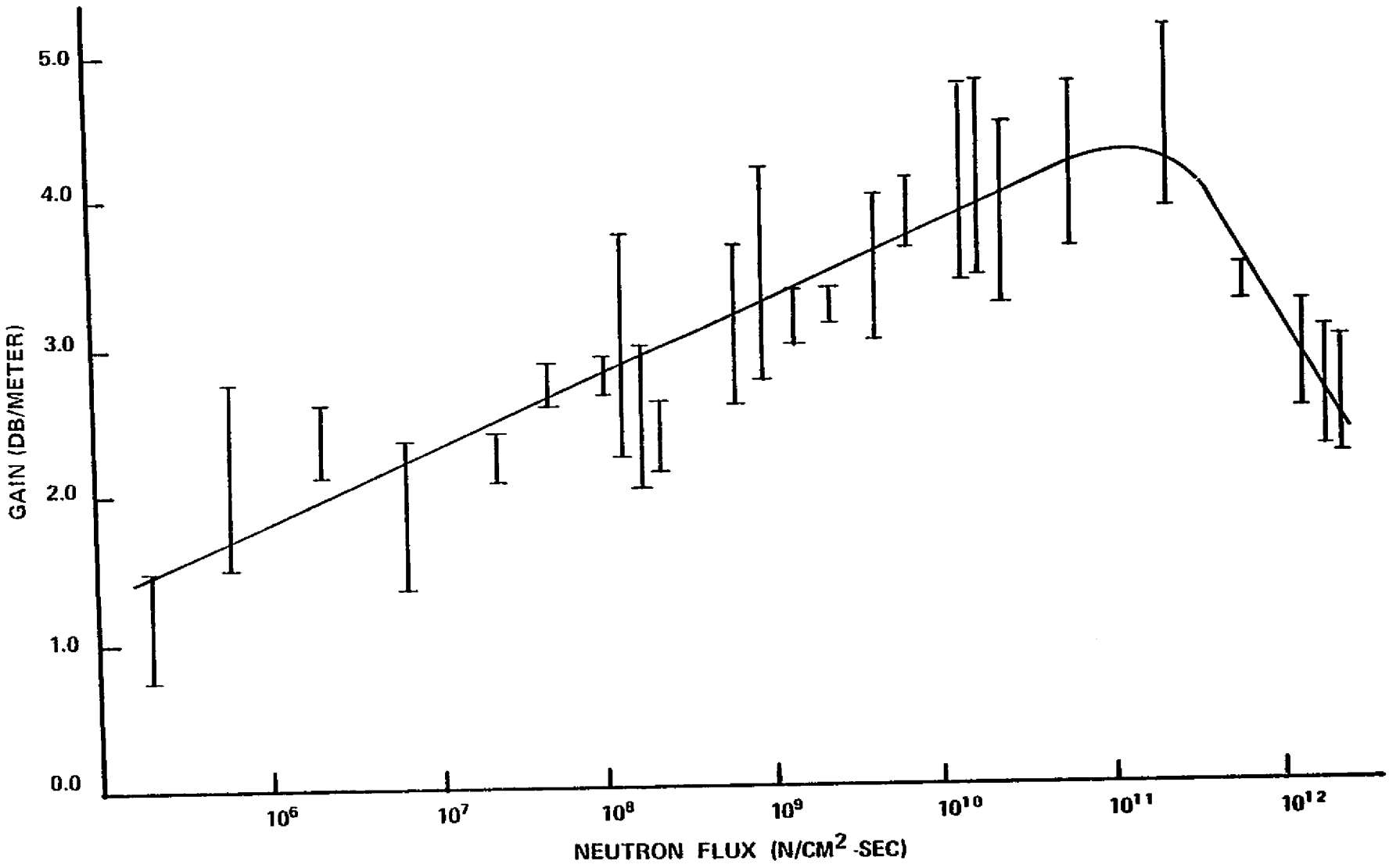

Fig. 65. RESULTS OF MEASUREMENTS AT UFTR

The results of these measurements are shown in Figure 66. As can be seen, the gain measured for small signals is, indeed, substantial (up to 800%), however, as a consequence, saturation is reached at fairly low input levels as well. Therefore, only low power laser output can be expected for a nuclear pumped He-Ne laser, which is in agreement with the situation of the discharge He-Ne laser.

3. Laser Experiment

To demonstrate lasing for a He-Ne nuclear pumped laser, an experiment as sketched in Figure 67 was set up.

The laser cavity designed to resonate at 6328Å, used a corner cube reflector and a 20 m-radius, dielectric output mirror.

The corner cube was used in order to reduce the alignment problems for incore reactor experimentation. It was felt that due to the extremely high single pass gain, a corner cube reflector, instead of a regular laser mirror, could be tolerated. The cavity has a single pass loss of 51% which is unusually high for laser cavities, yet still should be sufficient to support lasing according to the single pass gain measurements.

This proved, indeed, to be the case and Figure 68 shows the laser output as a function of reactor power.

The threshold for lasing is at a neutron flux level of $2 \times 10^{11} n/cm^2$-sec. After threshold, the plot of laser output vs. reactor power shows a 45° slope. After a short time at full reactor power, lasing ceased due to the heating of the capsule as predicted in the gain measurements.

4. Checks for Lasing

First, a wavelength scan with the spectrometer was performed to insure that the observed phenomena is, indeed, a spectrum line and not a portion of a continuum. Optical materials, like sapphire, which is used

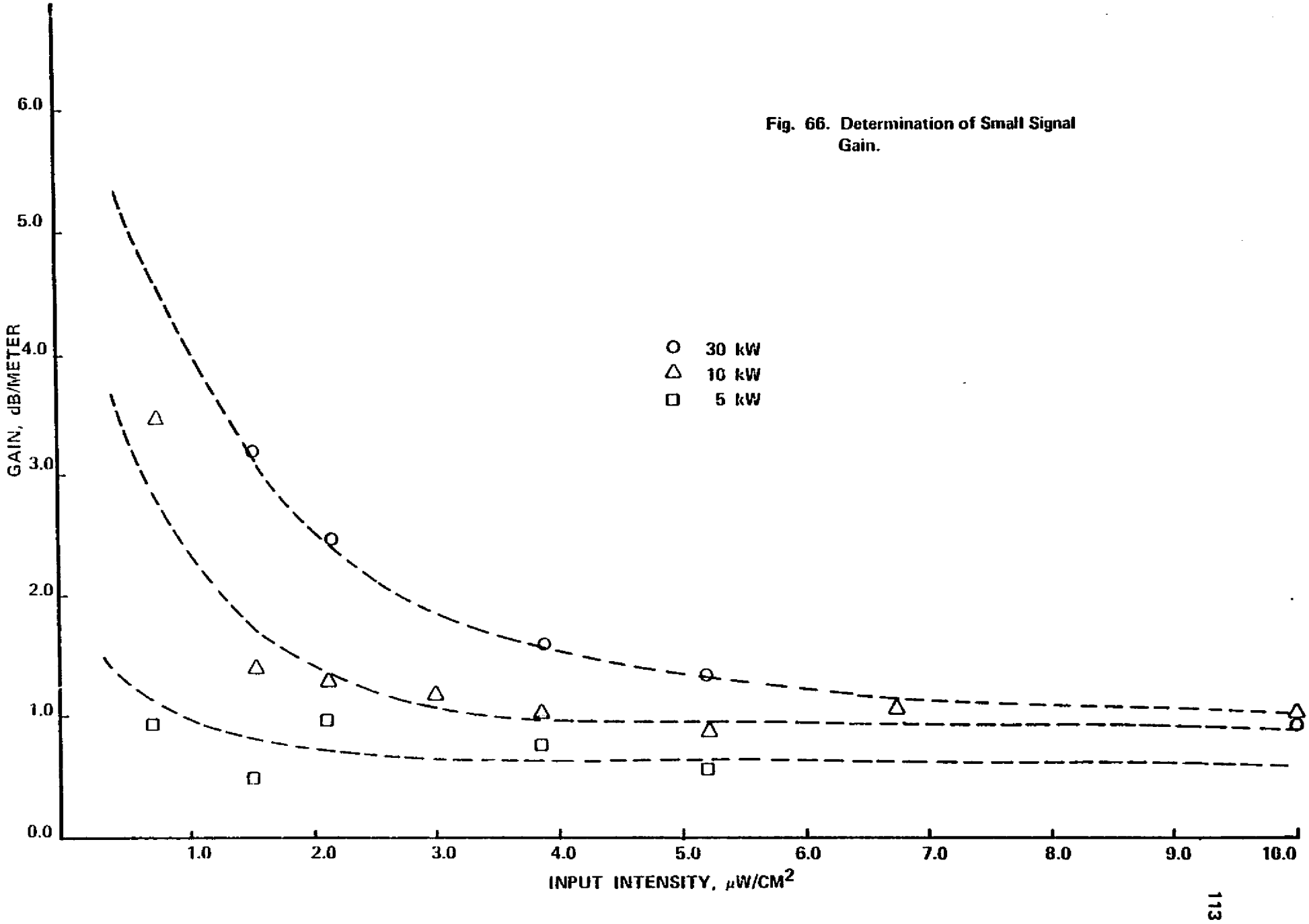

Fig. 66. Determination of Small Signal Gain.

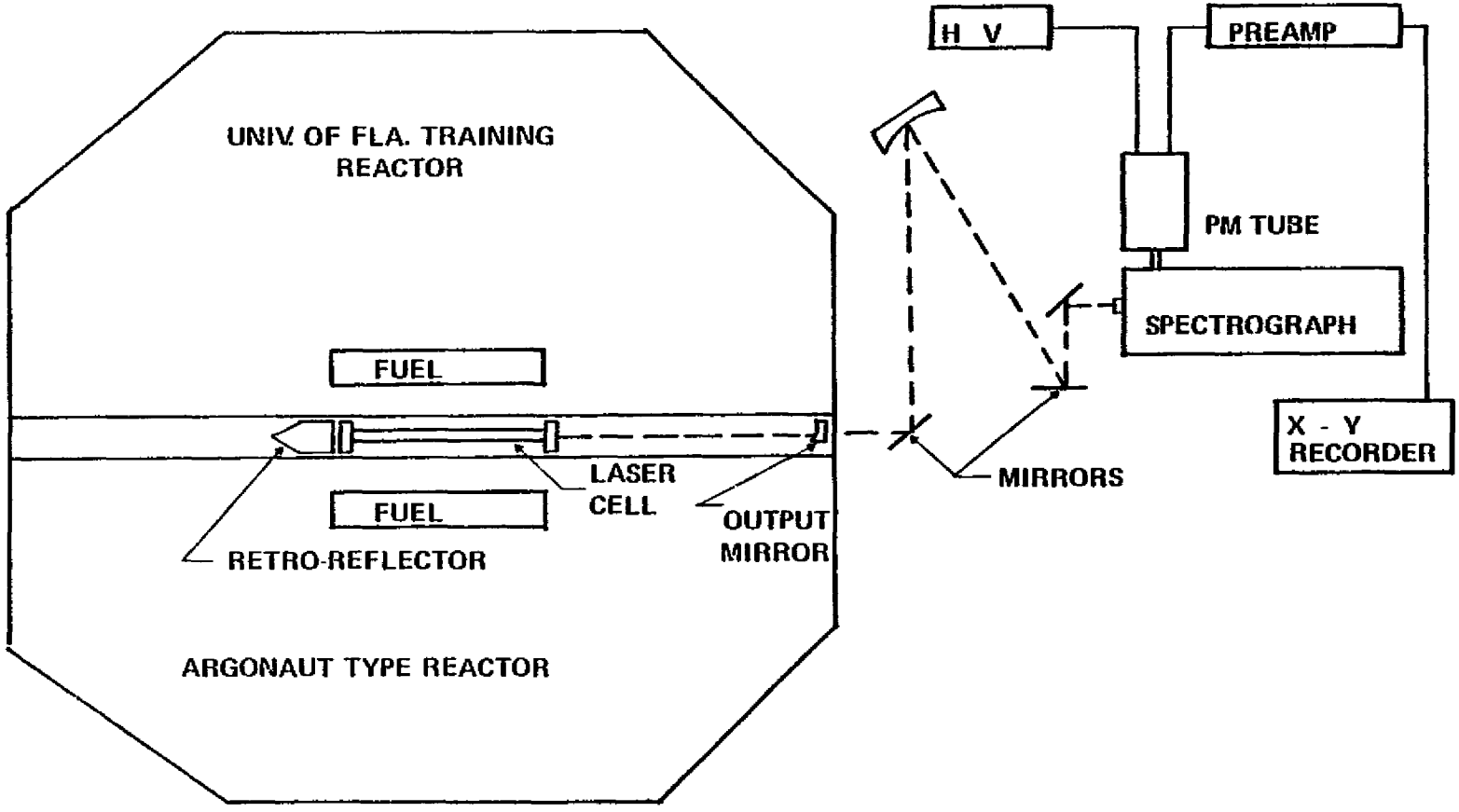

Fig. 67. LASER EXPERIMENT

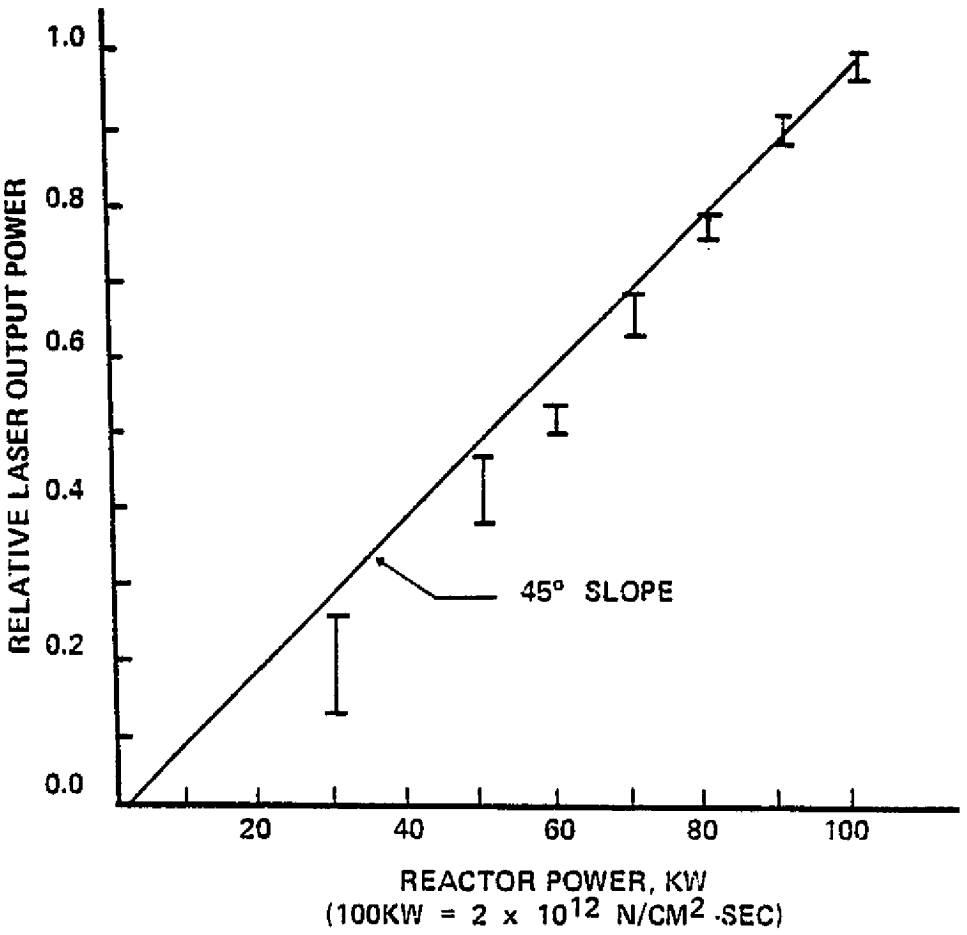

Fig. 68. LASER OUTPUT VERSUS REACTOR POWER

as window material in the present tube, luminesce under influence of nuclear radiation.[5] This radiation output is also proportional to reactor power and could produce a similar plot as Figure 68. However, the sapphire luminescence peaks at blue wavelengths and is continuous radiation. Detection of a red line would discard the possibility that sapphire light was observed.

The wavelength scan showed several red lines, one being at 6328Å, the wavelength the spectrometer was detecting when the data of Figure 68 were obtained.

The intensity ratios of these lines were measured, the 6328Å line being, of course, the strongest.

The next check for lasing was to spoil the resonant cavity and repeat the wavelength scan. Under these conditions, only spontaneous light output can be expected. In other words, the intensity ratios of the observed red lines should change with respect to the intensity of the 6328Å line, since in the previous scan this line was the only lasing line.

This turned out to be the case and the ratio of spontaneous to stimulated output was found to be $\frac{I_{stim}}{I_{spon}} \simeq 60$. There is substantial error of measurement attached to this value, since the spontaneous intensity of the 6328Å line is, indeed, very weak, since it is like most laser lines, a weak spectrum line. However, the error is less than a factor of 60 and there is, undoubtedly, an output of stimulated emitted radiation.

IV. SURVEY OF ACCOMPLISHMENTS

A. Ph.D Degrees Generated Under Both Grants

NAME	TITLE OF DISSERTATION
R. Randol	"Determination of High-Pressure, Uranium Plasma Properties"
H. Rhoads	"Direct Nuclear Excitation of a CO_2 Laser"
R. Walters	"Excitation and Ionization of Gases by Fission Fragments"
J. Mack	"Investigation of Uranium Plasma Emission from 1050 to 6000 Å"
J. Fuller	"Infrared Laser Emission from a Helium-Xenon Mixture Using Fission Fragment Excitations"
J. Davis	"Kinetic and Experimental Study of Argon and Argon-Nitrogen Mixtures Excited by Fission Fragments"
R. Davie	"Spectroscopy of Fission Fragment Excited Atmospheric Pressure Argon and Xenon Plasmas"
B. Carter	"CW Nuclear Pumping of the Helium Neon System"
B. Schnitzler	"Measurement of Total Pressure from Molten Uranium Using a Liquid-Wall Furnace"

B. Masters Degrees Generated Under Both Grants

NAME	TITLE OF THESIS OR PROJECT
R. Randol	"A Short-Time Spectroscopic Technique for Vacuum Ultra-Violet Plasma Diagnostics"
J. Mack	"Temperature Profile Determination of a Uranium Plasma in a Helium Atmosphere"
J. Fuller	"Measurements on a Repetitively Pulsed, High-Power CO_2 Laser"
J. Davis	"Generation of Uranium Plasma with a Sliding Spark"
B. Schnitzler	"Spectroscopy of a Constricted Sliding Spark Discharge"
D. Sterritt	"A Study of the Thermodynamic Properties of Uranium Hexafluoride"
D. J. Baker	"Preliminary Heat Transfer Calculations for the Liquid Wall Furnace"

J. Spector	"Absorption Coefficient of Uranium Hexafluoride Measured by a Ballistic Piston Compressor"
B. Miller	"A Thermodynamic Study of Rapid Compression of Uranium Hexafluoride Gas"
R. Paternoster	"Radioactive Waste Disposal by Nuclear Transmutation in a UF_6 Gaseous-Core Reactor"
B. Carter	"A Preliminary Experiment on CW Nuclear Pumping of He-Ne"
C. Winship	"Experimental Design and Construction of a He^3-Ne Nuclear Pumped Laser System"
E. Holtzclaw	"Fission Fragment Emission from Uranium Foils"
R. Lee	"Optical Emission from Fission Fragment Excited Ar-N_2 Gas Mixtures"
C. Skottegard	"Electric Field and UF_6 Effects on the Scintillation Lifetimes of Nitrogen, Argon, Helium, and CO_2 Gas Mixtures.
R. Hansen	"Liquid Reactor Laser Research"
R. Borland	"The Homogeneous Gas Core Reactor Applied to Nuclear Pumped Lasers"

C. High Honors Projects

NAME	TITLE OF PROJECT
C. Skottegard	"A Safety Analysis Report for the Extended MCFIG"
B. Miller	"Preliminary Feasibility Study of a Nuclear Piston Engine"

D. Publications Generated Under Both Grants

1. Book Edited

Uranium Plasmas, NASA SP-236, Library of Congress Catalog Card Number 70-608314, available through U. S. Government Printing Office, Washington, D. C., K. Thom and R. T. Schneider, 1971.

2. Periodicals

"Radiation from a Uranium Plasma," R. T. Schneider, C. D. Kylstra, A. G. Randol, III, and M. J. Ohanian, ANS Transactions, 12, 3 (1969).

"Measurement of Temperature and Partial Pressure of a Uranium Plasma," A. G. Randol, III, G. R. Shipman, and R. T. Schneider, Applied Spectroscopy, 24, 253-258 (1970).

"Temperature Measurement on a Uranium Plasma," R. G. Shipman, J. M. Mack, and R. T. Schneider, Applied Spectroscopy, 23, 671 (1969).

"Measurement of the Emission Coefficient of a Uranium Plasma," R. T. Schneider, A. G. Randol, III, C. D. Kylstra, and M. J. Ohanian, ANS Transactions, 12, 413 (1969).

"Experimental Determination of the Boiling Point of Uranium," A. G. Randol, III, R. T. Schneider, and C. Kylstra, ANS Transactions, 12, 541 (1969).

"Boiling Point of Uranium," A. G. Randol, R. T. Schneider, and C. D. Kylstra, page 181-195 in "Research on Uranium Plasmas," NASA SP-236, U.S. Government Printing Office (1971).

"Spectroscopic Study of a Uranium Arc Plasma," H. D. Campbell, C. D. Kylstra, A. G. Randol, III, and R. T. Schneider, page 187-195 in "Research on Uranium Plasmas," NASA SP-236, U.S. Government Printing Office (1971).

"Generation of a Fissioning Plasma," C. D. Kylstra and R. T. Schneider, page 205-209 in "Research on Uranium Plasmas," NASA SP-236, U.S. Government Printing Office (1971).

"Enhancement of Laser Output by Nuclear Reactions," page 397-400 in "Research on Uranium Plasmas," NASA SP-236, U.S. Government Printing Office (1971).

"Nuclear Pumped Gas Lasers," K. Thom and R. T. Schneider, AIAA Journal, 10, 400-406 (1972).

"Excitation and Ionization of a CO_2-Laser by Nuclear Reaction Products," H. S. Rhoads and R. T. Schneider, Bull. of the Amer. Phys. Soc., Ser II, 17, 400 (1972).

"Plasma Properties of a D.C. Uranium Arc," J. M. Mack, Jr., J. L. Usher, H. D. Campbell, and R. T. Schneider, Bull. of the Amer. Phys. Soc., Ser. II, 17, 383 (1972).

"Uranium Plasma Emission Coefficient in the Visible and Near U.V.," J. M. Mack, Jr., J. L. Usher, H. D. Campbell, and R. T. Schneider, 2nd Symposium on Uranium Plasmas: Research and Applications. Published by AIAA, New York (1971), p. 105.

"CO_2 Laser Experiments Using Nuclear Reactions as the Ionization Source," H. S. Rhoads, F. Allario, and R. T. Schneider, 2nd Symposium on Uranium Plasmas: Research and Applications. Published by AIAA, New York (1971), p. 53.

"Generation of a Uranium Plasma at Near Gaseous Core Reactor Conditions," J. F. Davis, III, B. G. Schnitzler, and R. T. Schneider, 2nd Symposium on Uranium Plasmas: Research and Applications. Published by AIAA, New York (1971), p. 110.

"Ballistic Piston Fissioning Plasma Experiment," B. E. Miller, K. Thom, G. T. Lalos, and R. T. Schneider, 2nd Symposium on Uranium Plasmas: Research and Applications. Published by AIAA, New York (1971), p. 78.

"Nuclear Enhancement of CO_2 Laser Output," H. S. Rhoads and R. T. Schneider, ANS Transactions, 14, 429 (1971).

"Nuclear Pumped Lasers," K. Thom and R. T. Schneider, The Indian and Eastern Engineer, 114, 155-162 (1972).

"On the Emission Coefficient of Uranium Plasmas," R. T. Schneider, H. D. Campbell, and J. M. Mack, Nuclear Technology, 20, 15-26 (1973).

"Electron Energy Distribution Function of Fission Fragment Excited Gases," R. A. Walters and R. T. Schneider, ANS Transactions, 17, 1 (1973).

"Pressure Dependence of Helium Line Intensities Excited by Fission Fragments," R. R. Paternoster, R. A. Walters, and R. T. Schneider, ANS Transactions, 17, 2 (1973).

"Population Inversions in Fission Fragment Excited Helium," G. R. Shipman, R. A. Walters, and R. T. Schneider, ANS Transactions, 17, 3 (1973).

"Enhancement of CO_2-Laser Output by Nuclear Radiation," J. F. Davis, R. T. Schneider, and G. R. Shipman, ANS Transactions, 17, 4 (1973).

"Emission Coefficient Investigation of Uranium Plasmas," J. M. Mack, R. T. Schneider, and H. D. Campbell, ANS Transactions, 17, 7 (1973).

"Measurement of the Ratio of Specific Heats of UF_6," D. E. Sterritt, G. T. Lalos, and R. T. Schneider, ANS Transactions, 17, 191 (1973).

"Nuclear Waste Disposal Utilizing a Gaseous-Core Reactor," R. Paternoster, M. J. Ohanian, R. T. Schneider, and K. Thom, ANS Transactions, 19, 203 (1974).

"Nuclear Pumped Gas Lasers," in Laser Interaction and Related Phenomena; Volume 3A, page 85-107, Edited by H. J. Schwartz and H. Hora, Plenum Press, New York and London (1974).

"Specific Heat Ratios of UF_6 Measured with a Ballistic Piston Compressor," D. E. Sterritt, G. T. Lalos, and R. T. Schneider, Nuclear Technology, 25, 150-164 (1974).

"Fission Fragment Exictation of Atmospheric Pressure Argon and Argon-Nitrogen Mixtures," R. N. Davie, J. F. Davis, and R. T. Schneider, ANS Transactions, 22, 149 (1975).

"Direct Nuclear Pumping of a Helium Xenon Laser," H. H. Helmick, J. L. Fuller, and R. T. Schneider, Appl. Phys. Lett., 26, 6, 327 (1975).

"Fissioning Uranium Plasmas and Nuclear Pumped Lasers," R. T. Schneider and K. Thom, Nuclear Technology, 27, 34-50 (1975).

"The Nuclear Laser Story," New Scientist, Volume 67, Number 956, page 13-15, (1975).

"Observations on the Luminescence of α-Al_2O_3 (Synthetic Sapphire) in a Reactor Environment," R. N. Davie, J. F. Davis, and R. T. Schneider, Nuclear Technology, 31, 276-278 (1976).

"Physics and Potentials of Fissioning Plasmas for Space Power and Propulsion," K. Thom, F. C. Schwenk, and R. T. Schneider, Astronautica Acta, 3, 505-516 (1976).

"Optical Radiation of Fission Fragment Excited UF_6 and Ar-N_2-UF_6 Mixtures," R. N. Davie, G. Albrecht, E. E. Carroll, and R. T. Schneider, ANS Transactions, 23, 518 (1976).

"Population Inversions Observed in Fission Fragment Excited Xenon," R. N. Davie, J. F. Davis, and R. T. Schneider, ANS Transactions, 23, 520 (1976).

"Gaseous Fuel Reactor Research," K. Thom and R. T. Schneider, IEEE Transactions, Vol. P.S.-5, No. 4, 259-272 (1977).

"Measurement Methods for Fission Fragment-Generated Plasmas," R. T. Schneider, ANS Transactions, 26, 530-531 (1977).

"Effects of UF_6 on N_2 and Argon-Excited State Lifetimes," T. C. Maguire, E. E. Carroll, Jr., and R. T. Schneider, ANS Transactions, 27, 927 (1977).

"Results of an Experiment Demonstrating a Nuclear-Pumped CW-Laser," B. D. Carter, M. J. Rowe, and R. T. Schneider, ANS Transactions, 27, 928 (1977).

"Parametric Study of Reactor Configurations Exhibiting Minimal Transuranic Production," B. G. Schnitzler, and R. T. Schneider, ANS Transactions, 27, 929 (1977).

"Gaseous-Fuel Nuclear Reactor Research for Multi-megawatt Power in Space K. Thom, H. H. Helmick, and R. T. Schneider, Astronautica Acta, in print.

"Nuclear Pumped Lasers: A Progress Report," Physics in Technology, (London, England), March, 1978.

3. Invited Papers

"Spectroscopic Diagnostics of a Uranium Plasma," Seventeenth Symposium on Spectroscopy, (Jan. 8-10, 1969), Gainesville, Florida.

"Radiation Transfer Study on a Uranium Plasma," Fifth Annual Southeastern Seminar on Thermal Sciences, (April 21-22, 1969), Gainesville, Florida.

"Nuclear Pumped Lasers," 10th Anniversary Meeting of the Society of Engineering Science, (November 5-7, 1973), Raleigh, N.C.

"Fissioning Plasmas and Nuclear Pumped Lasers," 25th Anniversary Meeting of the American Nuclear Society, (1975), Philadelphia, Pennsylvania.

"Direct Conversion of Nuclear Energy into Laser Light," 1973 IEEE International Conference on Plasma Science, (May 24-26, 1976), Austin, Texas.

"Lasers from Fission," Nuclear Pumped Laser Workshop, (April 6-8, 1975), Naval Postgraduate School, Monterey, California.

"Measurement Methods for Fission Fragment-Generated Plasmas," American Nuclear Society, 1977 Annual Meeting, (June 12-16, 1977), New York.

"Measurement Techniques for Plasmas Excited by Nuclear Radiation," Workshop on Nuclear Radiation Induced Plasmas and Direct Nuclear Pumped Lasers, (Aug. 1-12, 1977), Miami University, Oxford, Ohio.

"Measurement Techniques for Nuclear Excited Plasmas," First International Symposium on Fission Induced Plasmas and Nuclear Pumped Lasers, (May 23-25, 1978), Paris, France.

"Radiation Induced Plasma Diagnostics," Workshop on Nuclear Radiation Induced Plasmas and Direct Nuclear Pumped Lasers, (August 1-11, 1977), Miami University, Oxford, Ohio.

"Nuclear Pumped Lasers," Annual Meeting of the American Physical Society, (Jan. 1979).

4. International Conferences

"Plasma Diagnostics of a Uranium Plasma," C. D. Kylstra, H. D. Campbell, and R. T. Schneider, International Conference on Gas Discharges, (September 15-18, 1970), London, U.K.

"Absolute Intensity Measurements on a Uranium Arc in the Vacuum-Ultraviolet Region," J. M. Mack, H. D. Campbell, and R. T. Schneider, 25th Annual Gaseous Electronics Conference, (October 17-20), London, Ontario.

"Fission Fragment Produced Plasmas," R. A. Walters and R. T. Schneider, 25th Annual Gaseous Electronics Conference, (October 17-20, 1972), London, Ontario.

"Spectroscopic Analysis of Plasmas Produced by Fission Fragments," R. A. Walters and R. T. Schneider, International Conference on Nuclear Solutions to World Energy Problems, (Nov. 12-16, 1972), Washington, D. C.

"Fissioning Uranium Plasmas," K. Thom and R. T. Schneider, Symposium on Applications of Nuclear Data in Science and Technology, International Atomic Energy Agency, (March 12-16, 1973), Paris.

"On the Feasibility of Nuclear Pumping of Gas Lasers," Laser Interactions and Related Plasma Phenomena. Third Workshop held at RPI, (August 13-17, 1973), Troy, New York.

"Physics and Potentials of Fissioning Plasmas for Space Power Propulsion," K. Thom, F. Z. Schwenk, and R. T. Schneider, International Astronautical Federation, XXVth Congress, (Sept. 30-Oct. 5, 1974), Amsterdam.

"Experimental Measurement of the Thermodynamic Properties of Hot Highly Compressed Gases," G. T. Lalos, D. E. Sterritt, and R. T. Schneider, 4th International Conference on Chemical Thermodynamics, (Aug. 26-30, 1975), Monpellier, France.

"Lasers from Fission (Gaseous Core Reactors and Nuclear Pumped Lasers for Space Power Generation and Transmission)," K. Thom, H. H. Helmick, and R. T. Schneider, Proceedings of the XXVI International Astronautical Congress, (1975), Lisbon, 1975, Pergamon Press - Oxford and New York, 1976.

"Optical Radiation from a Fissioning Gas," G. Albrecht, E. E. Carroll, R. N. Davie, and R. T. Schneider, 1976 IEEE International Conference on Plasma Science, (May 24-26).

"Development of an Experiment for the Generation of a Fissioning High Pressure Gas," D. E. Sterritt, G. T. Lalos, and R. T. Schneider, 1976 IEEE International Conference on Plasma Science, (May 24-26).

"Gaseous-Fuel Nuclear Reactor Research for Multimegawatt Power in Space," K. Thom, H. H. Helmick, and R. T. Schneider, XXVIII International Astronautical Congress, (Sept. 25-Oct. 1, 1977), Prague CSR.

"Optical Radiation from a Fissioning Gas," R. N. Davie, G. E. Albrecht, E. E. Carroll, and R. T. Schneider, 1976 IEEE International Conference on Plasma Science, (May 24-26).

"The Gas Core Reactor Concept - An Alternative to Existing Reactor Concepts," B. G. Schnitzler and R. T. Schneider, Miami International Conference on Alternative Energy Sources, (Dec. 5-7, 1977), Miami Beach, Florida.

"CW-He-Ne Nuclear Pumped Lasers," D. Carter and R. T. Schneider, First International Symposium on Fission Induced Plasmas and Nuclear Pumped Lasers," (May 23-25, 1978), Orsay, France.

"Electronic State Populations of (n,p) Excited He^3," J. W. Griffin, L. D. Luker, and R. T. Schneider, 1978 IEEE International Conference on Plasma Science, (May 15-17), Monterey, Cal.

5. National Meetings

"Spectroscopic Measurements on a High Pressure Uranium Arc," G. R. Shipman, A. G. Randol, III, and R. T. Schneider, 20th Annual Mid-American Symposium on Spectroscopy, (May 12-15, 1969), Chicago, Ill.

"Radiation from a Uranium Plasma," R. T. Schneider, C. D. Kylstra, A. G. Randol, III, and M. J. Ohanian, American Nuclear Society 15th Annual Meeting, (June 15-19, 1969), Seattle, Wash.

"Temperature Measurements on a Uranium Plasma," G. R. Shipman, J. M. Mack, and R. T. Schneider, 8th National Meeting, Society for Applied Spectroscopy, (Oct. 6-10, 1969), Anaheim, CA.

"Experimental Determination of the Boiling Point of Uranium," A. G. Randol, III, R. T. Schneider, and C. D. Kylstra, Trans. Am. Nuc. Soc., 12, 2 413 (1969), San Francisco, CA.

"Measurement of the Emission Coefficient of a Uranium Plasma," R. T. Schneider, A. G. Randoll, III, C. D. Kylstra, and M. J. Ohanian, American Nuclear Society Winter Meeting, (Nov. 30-Dec. 5, 1969), San Francisco, CA.

"Properties of a Uranium Plasma," H. D. Campbell, C. D. Kylstra, and R. T. Schneider, 8th Aerospace Science Meeting, (Jan 19-27, 1970), AIAA New York.

"Boiling Point of Uranium," A. G. Randol, III, C. D. Kylstra, and R. T. Schneider, Symposium on Research on Uranium Plasmas and Their Technological Application, (Jan. 7-10, 1970), Gainesville, FL,

"Spectroscopic Study of a Uranium Arc Plasma," H. D. Campbell, C. D. Kylstra, A. G. Randol, III, and R. T. Schneider, Symposium on Research on Uranium Plasmas and Their Technological Application, (Jan. 7-10, 1970), Gainesville, FL.

"Enhancement of Laser Output by Nuclear Reactions," F. Allario, R.A. Lucht, R. Hess, Symposium on Research on Uranium Plasmas and Their Technological Application, (Jan. 7-10, 1970), Gainesville, FL.

"Generation of a Fissioning Plasma," C. D. Kylstra and R. T. Schneider, Symposium on Research on Uranium Plasmas and Their Technological Application, (Jan. 7-10, 1970), Gainesville, FL.

"Uranium Plasma Emission Coefficients," C. D. Kylstra, H. D. Campbell, and R. T. Schneider, AIAA 6th Propulsion Joint Specialist Conference, (June 15-19, 1970), San Diego, CA.

"Nuclear Pumped Gas Lasers," K. Thom and R. T. Schneider, AIAA 9th Aerospace Science Meeting, (Jan. 25-27, 1971), New York.

"A New Gas Scintillation Detector for Fast Reactors," J. Handschuh, R. A. Walters, E. E. Carroll, and R. T. Schneider, IEEE Nuclear Science Sumposium, (Dec. 6-8, 1972), Miami, Florida.

"Recent Experimental Results Concerning Nuclear Pumped Gas Lasers," R. A. Walters, R. R. Paternoster, and R. T. Schneider, SPIE 17th Annual Meeting and Display, (Aug. 27-29, 1973), San Diego, CA.

"Application of Gas Core Reactors for Transmutation of Nuclear Waste," B. G. Schnitzler, and R. T. Schneider, Third Symposium on Uranium Plasmas, (June 10-12, 1976), Princeton University.

"Energy Flow in Argon and Argon-n_2 Mixtures Excited by Fission Fragments," J. F. Davis, R. N. Davie, and R. T. Schneider, Third Symposium on Uranium Plasmas, (June 10-12, 1976), Princeton University.

"Thermodynamic Properties and Nucleonics of High Pressure Subcritical UF_6-He Gas Volume Irradiated by an External Source," D. E. Sterritt, G. T. Lalos, and R. T. Schneider, Third Symposium on Uranium Plasmas, (June 10-12, 1976), Princeton University.

"Nuclear Pumped Gas Lasers," K. Thom and R. T. Schneider, Third Symposium on Uranium Plasmas, (June 10-12, 1976), Princeton University.

"A Spectroscopic Study of a Fissioning Gas," R. N. Davie, G. Albrecht., E. E. Carroll, and R. T. Schneider, Third Symposium on Uranium Plasmas, (June 10-12, 1976), Princeton University.

"Nuclear Pumped He-Ne Laser," Optical Society of America, Fall Meeting Florida Section, (Nov. 4-5, 1977), Coral Gables, Fla.

"Parametric Study of Reactor Configurations Exhibiting Minimal Transuranic Isotrope Production," B. Schnitzler and R. T. Schneider, ANS 1977 Winter Meeting, (Nov. 27-Dec. 2, 1977), San Francisco.

"Effects of UF_6 on N_2 and Argon Excited States Lifetimes," E. E. Carroll, T. Maguire, and R. T. Schneider, ANS 1977 Winter Meeting, (Nov. 27-Dec. 2, 1977), San Francisco, CA.

"Results of an Experiment Demonstrating a Nuclear Pumped CW-Laser," D. Carter, M. Rowe, and R. T. Schneider, ANS 1977 Winter Meeting, (Nov. 27-Dec. 2, 1977), San Francisco.

"Nuclear Pumped Laser Reactors," ANS Annual Meeting, (June, 1979), Atlanta, Ga.

REFERENCES

1. G. R. Shipman, "Delayed Coincidence Spectroscopy of Fission Fragment Excited Gases," Ph.D Dissertation, Department of Nuclear Engineering Sciences, University of Florida, 1976.

2. T. C. Maguire, "Effects of UF_6 on the Excited Level Lifetimes of Nitrogen, Argon, and Xenon," Masters Project, Department of Nuclear Engineering Sciences, University of Florida, 1978.

3. C. Skottegard, "Electric Field and UF_6 Impurity Effects on the Scintillation Lifetimes of Fission Fragment Excited Nitrogen, Helium, Argon, and CO_2 Gas Mixtures," Masters Project, Department of Nuclear Engineering Sciences, University of Florida, 1978.

4. A. E. Siegman, An Introduction to Lasers and Masers, New York: Mc-Graw Hill Book Company, 1971.

5. J. C. Guyot, G. H. Miley, J. T. Verdeyen, and T. Ganely, "On Gas Laser Pumping via Nuclear Radiation," Trans. Symp. Research on Uranium Plasmas and Their Technological Applications, NASA SP-236 (1970).